NEW DESIGNS AND ANALYTICAL MODELING OF PIEZOCERAMIC POLYMER COMPOSITES

Period January 15, 1996 to January 14, 1997

Final Report

OFFICE OF NAVAL RESEARCH
Contract No.: N00014-96-1-0357
P.R. No.: 96PR02867-00

Submitted by: Q.M. Zhang
Associate Professor of Electrical Engineering
Materials Research Laboratory
The Pennsylvania State University
University Park, PA 16802

PENNSTATE

REPORT DOCUMENTATION PAGE

Form Approved
OMB No. 0704-0188

1. AGENCY USE ONLY (Leave blank)	2. REPORT DATE	3. REPORT TYPE AND DATES COVERED
	2/10/97	Final Technical Report 01/15/96-01/14/97

4. TITLE AND SUBTITLE

New Design and Analytical Modeling of Piezocomposite Polymer Composites

5. FUNDING NUMBERS

6. AUTHOR(S)

Qiming Zhang

7. PERFORMING ORGANIZATION NAME(S) AND ADDRESS(ES)

Materials Research Laboratory and
Electrical Engineering Department
The Pennsylvania State University
University Park, PA 16802

8. PERFORMING ORGANIZATION REPORT NUMBER

9. SPONSORING/MONITORING AGENCY NAME(S) AND ADDRESS(ES)

Wallace A. Smith
ONR 332
Office of Naval Research
Ballston Centre Tower One
800 North Quincy St.
Arlington, VA
22217-5660

10. SPONSORING/MONITORING AGENCY REPORT NUMBER

11. SUPPLEMENTARY NOTES

12a. DISTRIBUTION/AVAILABILITY STATEMENT

Distribution is unlimited

12b. DISTRIBUTION CODE

13. ABSTRACT (Maximum 200 words)

In this program, a dynamic model has been developed which yields nearly exact solution to the field quantities in a 2-2 piezocomposite and in some special 1-3 piezocomposite. In the model, we avoided the approximations made in the earlier works and hence, can address the dynamic response of piezocomposites, such as the frequency of various modes, the mode coupling, the electromechanical coupling factor, the vibration profiles of composites under different external driving conditions and medium, etc. in a realistic and consistent manner. Especially, the model can directly address the issue of the effect of the thickness of a composite plate on the ultrasonic response of a composite transducer. For example, it is shown that for a composite plate, as long as the thickness resonance is below that of the lowest lateral mode, there is always a frequency near the thickness resonance where the vibration of profile of a composite is uniform. The effect of the aspect ratio is on the frequency bandwidth in which the polymer and ceramic vibrate in unison. The prediction based on the model on the lateral modes is also far beyond the earlier models and is in excellent accord with the experimental observation. The input acoustic impedance of a piezocomposite was also analyzed and experimentally investigated since it is related to the design of the matching and backing. From the results, it is shown that the thickness of the matching layer should be less than the conventional $\lambda/4$. The effect of the acoustic loss of the polymer matrix is treated and it is shown that it has a strong effect on the dispersion curves in a composite, especially on the modes related to the lateral periodic structure

14. SUBJECT TERMS

Transducer Materials, Piezocomposite, Structure-Property Relation, Acoustic Modes

15. NUMBER OF PAGES

16. PRICE CODE

17. SECURITY CLASSIFICATION OF REPORT	18. SECURITY CLASSIFICATION OF THIS PAGE	19. SECURITY CLASSIFICATION OF ABSTRACT	20. LIMITATION OF ABSTRACT
Unclassified	Unclassified	Unclassified	Unlimited

Table of Contents

I. Introduction

To produce a high performance ultrasonic transducer requires the transducer material, which performs the energy conversion between the mechanical form and electrical form, to have a high electromechanical coupling factor, broad operation frequency bandwidth, and adjustable acoustic impedance which can be tuned to match that of the medium. With single phase piezoelectric materials, it is difficult to simultaneously meet all the requirements. Piezoceramic polymer composite materials, which combine the high electromechanical activity of piezoceramics and the low acoustic impedance of polymeric materials, have provided new opportunities to meet these requirements.[1,2] Since their inception in the seventies, the piezoceramic polymer composites have become one of the most important transducer materials and are being widely used in many areas such as medical imaging, nondestructive evaluation of materials, and underwater vision, etc.

Being a diphasic material, the properties of a piezo-composite can be tailored over a wide range by adjusting the material properties and geometric shapes of constituent phases.[3,4] It has also been observed that the properties of a composite vary with frequency.[5] The challenge of understanding the seemingly complex relationship between the performance of a composite and the properties of its constituents and the great opportunities provided by these materials have stimulated, in the past two decades, extensive investigations, both experimental and theoretical, on this class of materials.

The classic work of Newnham et al.,[6] which classified piezocomposite materials according to the connectivity of the constituent phases, has greatly facilitated the analysis of the composites as the connectivity is one of the key parameters in determining the performance of a composite. For composites with 1-3 and 2-2 connectivities, both analytical and finite element modeling have been carried out which have provided useful guidelines in the design of composite transducers.[7-13] The isostrain models developed by Smith et al.[3] and Hashimoto et al.[4] linked the material parameters of the constituents to the effective piezoelectric properties of 1-3 and 2-2 composites respectively and predicted that the thickness coupling factor k_t of a composite can approach the longitudinal coupling factor k_{33}^{l} of the piezoceramic rod and k_{33}^{w} of the plate respectively, which is in good agreement with experiments for composites with a high aspect ratio t/d, where t is the thickness and d is the periodicity of the composites. Auld et al., using the Floquet theory, investigated wave propagation in both the 2-2 and 1-3 composites and showed that due to the periodic structure of these composites, there exist pass bands and stop bands, similar to the band structure in a crystal solid, and that there are piezoelectric resonances associated with the stop band edge resonances.[7-10] For the design of composite transducers, the recognition of the existence of these modes and the precise prediction of their frequencies are of prime importance since quite often, it is the interference of these modes with

the thickness mode of a composite that deteriorates the performance, especially at high frequency operations. Craciun et al. examined the coupling between these lateral modes and thickness mode using a phenomenological approach and the results provided qualitative understanding between the coupling of the two modes and the material properties.[11] The results from these investigations have played important roles in the development of ultrasonic composite transducers. However, due to the approximations used in the analysis, there are severe limitations. For instance, various features related to the dynamic behavior of a composite transducer were not treated in a consistent manner, and the effect of finite thickness of a composite on the material properties, that has been shown to be crucial in determining the performance of a piezocomposite, cannot be treated in these analyses. To address these realistic issues of a composite material, finite element analysis has been employed by many authors.[12-15] For example, the dispersion curves have been evaluated for various modes in a composite and the dependence of the electromechanical coupling factor on the ceramic volume content and the ceramic rod shape was investigated.

For a piezoceramic polymer composite, it has to be recognized that it is the ceramic phase which performs the energy conversion between the electric and mechanical forms and the polymer phase merely acts as a carrier which transfers acoustic energy between the piezoceramic and the external medium. Hence, if the elastic coupling between the two constituents is not very effective, even if the material exhibits a perfect acoustic impedance matching with the medium and the electromechanical coupling factor is large, the electromechanical performance of the material is still poor. These observations clearly indicate that in modeling piezoceramic polymer composites, one cannot simply use an effective medium approach and has to take into account explicitly this internal degree of freedom.

The objective of this program is to develop a realistic model which can address these practical issues and to conduct systematic experimental study to verify the model results and to provide new insight into composite materials for both underwater and ultrasonic transducer applications.

Through this program, an analytical model on the dynamic problem of a piezocomposite material with the 2-2 connectivity and 1-3 connectivity has been developed.[16-18] In the model, we avoided the approximations made in the earlier works and hence, can address the dynamic responses of 2-2 piezocomposites, such as the frequencies of various modes, the mode coupling, the electromechanical coupling factor, the vibration profiles of composites under different external driving conditions, etc., in a realistic and consistent manner.

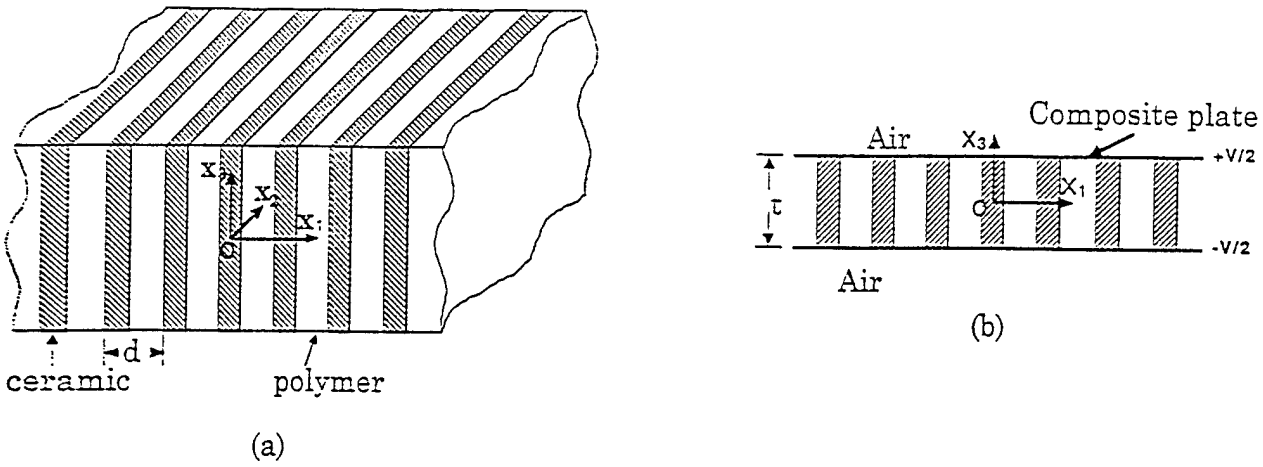

Figure 1. (a) Schematic drawing of a 2-2 piezoceramic polymer composite which is unbounded in all three orthogonal directions. The period of the composite is d. (b) Schematic drawing of a 2-2 piezoceramic polymer composite plate with a thickness t situated in air. An external voltage is applied to the composite.

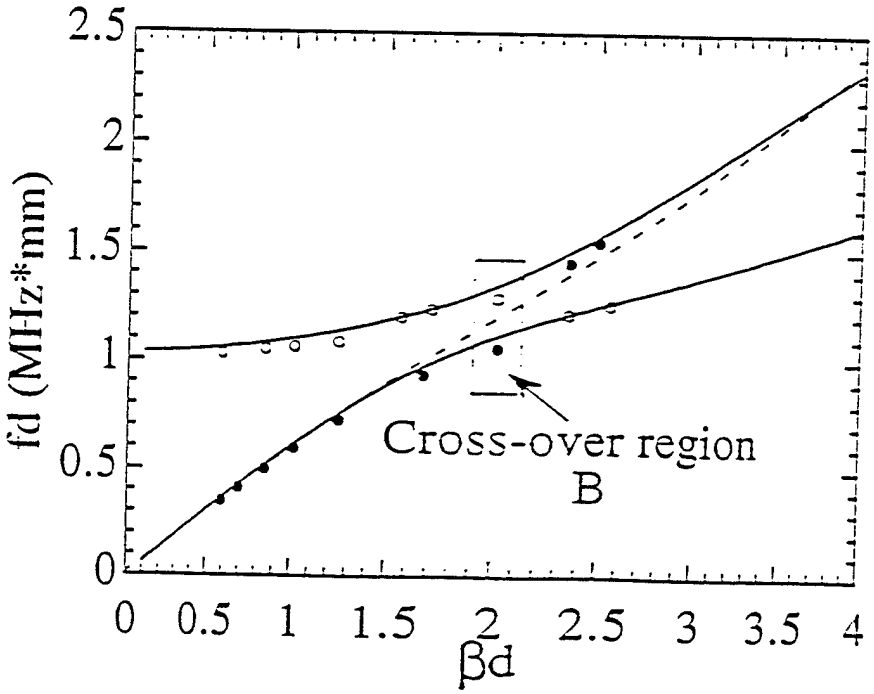

Figure 2. The first and second branches of the dispersion curves (solid lines) and the experimentally measured thickness mode (solid circles) and lateral mode (open circles) for a 2-2 composite made of PZT-5H and Spurr epoxy with 44% ceramic content. After the crossover region, the thickness mode jumps to the second branch. The criterion for the thickness mode is that it is the one with the larger effective coupling factor.

For example, one of the misconceptions in the early studies of the dynamic behavior of piezocomposites is the direct linkage between the non-uniform surface vibration profile in a composite and the aspect ratio of the ceramic plate (in 2-2 composites) or rod (in 1-3 composites). Based on the model results, it will be shown, which was verified by experiment, that for a composite plate, as long as the thickness resonance frequency is below that of the lateral mode, there is always a frequency near the thickness resonance where the vibration profile of the composite is uniform. The influence of the aspect ratio is on the frequency bandwidth in which the polymer and ceramic vibrate in unison.

Our results also show that there exist a series of modes associated with the periodic structure of the composite, which is beyond the stop-band edge resonance prediction. In 1-3 composites, the experimental results indicate that the nature of these modes is far more complicated than the simple picture of stop-band edge resonance. Further theoretical modeling is clearly needed in this area since these modes play a crucial role for a broadband transducer.

The approach taken here to solve the vibration problem in a finite thickness composite plate is based on the method of partial wave expansion where various elastic and electric fields are expended in terms of the eigenmodes of the structure as shown in figure 1(a) and the coefficients for each eigen-mode are determined by the boundary conditions at $x_3 = t/2$ (figure 1(b)).

In this program, we also examined how the material properties at the two sides of the interface, i.e., the properties of a piezoceramic polymer composite and a uniform medium, either a liquid or a solid, influence the wave transmission and reflection at the interface and the acoustic energy transfer inside the composite. These are directly related to the design of the matching layer and backing for a composite transducer. From the results, it is shown that the thickness of the matching layer should be less than the conventional $\lambda/4$. It is also shown that the input acoustic impedance of a composite depends strongly on the frequency and the elastic properties of the medium which the composite is in contact with.

This report is organized as the following. In the section II, the results on the dynamic behavior of a 2-2 composite transducer are presented. We will first present the details of derivation of the eigenfunctions for a 2-2 piezoceramic polymer composite. Based on the results, the wave propagation in an unbounded 2-2 composite is analyzed. For finite thickness composites, various features of a piezocomposite plate under an external driving electric field in both air and water media are treated. The response behavior of the composite plate under external pressure is also treated. Experiments were conducted to provide comparison with the theoretical results. From the results, we will show explicitly how the aspect ratio t/d influences the transduction performance of a composite plate.

In the section III, the acoustic impedance and the wave propagation at the interface between a 2-2 composite and an acoustic medium, either a solid or a fluid are analyzed. The general formula used to treat the wave propagation at the interface is briefly presented and the results for the fluid-composite interface are derived. The definition of the input acoustic impedance of the composite at the interface is also discussed. The wave propagation at a interface between a solid and a piezocomposite is analyzed. The issues related to the anti-reflection quarter wave matching layer at a composite-medium interface are examined. And a brief summary and discussion are presented at the end of the section.

In the section IV, the results on 1-3 composites are presented. The effect of the loss in the elastic properties in the polymer phase is considered and it was found that due to the acoustic loss, the dispersion curve for the lateral mode in the composite shows marked change. The experimental results related to the lateral modes are also presented.

A summary will be presented on the section V.

II. Dynamic Behavior of a Finite Thickness 2-2 Piezoceramic-Polymer Composite Plate:

2.1 General Solution of the Waves in a 2-2 Piezocomposite:

Shown in figure 1(a) is a schematic drawing of a 2-2 composite (unbounded in the x_3-direction), where plates of piezoceramic and polymer form a parallel array. The coordinate system is chosen such that the x_3-axis is along the ceramic poling direction, the x_1-axis is perpendicular to the ceramic polymer interface, and x_2-axis is in the plane of the plates. For a typical 2-2 composite, the dimensions in the x_1- and x_2-directions are much larger than the period d and thickness t. In the treatment here, they can be taken as infinite without much error in the results. Under these conditions, the composite is clamped in the x_2-direction so that $S_2=0$, where S_2 is the strain in the x_2-direction, and the problem becomes a two dimensional one with no dependence on the x_2-coordinate.

The governing equations for the dynamics of a 2-2 composite are[19-21]

$$\frac{\partial T_1}{\partial x_1}+\frac{\partial T_5}{\partial x_3}=\rho\frac{\partial^2 u_1}{\partial t^2}$$
$$\frac{\partial T_5}{\partial x_1}+\frac{\partial T_3}{\partial x_3}=\rho\frac{\partial^2 u_3}{\partial t^2} \qquad (1)$$

$$\frac{\partial D_1}{\partial x_1} + \frac{\partial D_3}{\partial x_3} = 0$$

The symbols adopted in this paper are summarized here: T_i and S_i are the stress and strain tensor components, where the Voigt notation is used, u_i is the elastic displacement vector, ρ is the density, and D_i is the electric displacement vector, E_i is the electric field. The relevant material coefficients are: e_{ij} is the piezoelectric coefficient, c_{ij} is the elastic stiffness, and ε_i is the dielectric permittivity. Equation (1) holds for both the polymer and ceramic phases.

The constitutive equations, relating stress T, strain S, electric displacement D, and electric field E, are

$$[T] = [c^E][S] - [e_t][E] \qquad (2\,a)$$

$$[D] = [e][S] + [\varepsilon^S][E] \qquad (2\,b)$$

For the polymer phase, e_{ki} in the equation (2) are zero. The superscripts E and S indicate that the coefficients are under the constant E field and constant strain conditions, respectively. Here $[e_t]$ is the transposed [e] array. Under the quasi-electrostatic approximation, the electric field E can be expressed as

$$\vec{E} = -\nabla\Phi \qquad (3)$$

where Φ is the electrical potential.

Combining eqs. (1), (2), and (3) yields three second order differential equations, governing the elastic displacement u_1, u_3, and electric potential Φ in the ceramic plate, respectively:

$$\begin{aligned} &c_{44}^E u_{3,11} + (c_{13}^E + c_{44}^E)u_{1.13} + c_{33}^E u_{3,33} + (e_{33}\Phi_{,33} + e_{15}\Phi_{,11}) = \rho\ddot{u}_3 \\ &c_{11}^E u_{1,11} + (c_{13}^E + c_{44}^E)u_{3,13} + c_{44}^E u_{1,33} + (e_{31} + e_{15})\Phi_{,13} = \rho\ddot{u}_1 \\ &e_{15}u_{3,11} + (e_{15} + e_{31})u_{1,13} + e_{33}u_{3,33} - (\varepsilon_{33}^S\Phi_{,33} + \varepsilon_{11}^S\Phi_{,11}) = 0 \end{aligned} \qquad (4)$$

For the polymer phase, e_{ij} in eq. (4) should be taken to zero.

For an unbounded composite, the solutions to eq. (4) have the form

$$\begin{aligned} u_3 &= A\exp(j(hx_1 + \beta x_3 - \omega t)) \\ u_1 &= B\exp(j(hx_1 + \beta x_3 - \omega t)) \\ \Phi &= C\exp(j(hx_1 + \beta x_3 - \omega t)) \end{aligned} \qquad (5)$$

where A, B, and C are three constants, ω is the angular frequency, h and β are the wave vector components in the x_1- and x_3- directions, respectively.

Substituting eq. (5) into (4) yields three homogeneous equations with the undetermined constants A, B, and C,

$$[M_{ij}][A_i] = 0 \qquad (6)$$

where $[A_i]=[A, B, C]^T$ and

$$[M_{ij}]=\begin{pmatrix} c_{33}^E\beta^2+c_{44}^E h^2-\rho\omega^2 & (c_{13}^E+c_{44}^E)h\beta & e_{33}\beta^2+e_{15}h^2 \\ (c_{13}^E+c_{44}^E)h\beta & c_{11}^E h^2+c_{44}^E\beta^2-\rho\omega^2 & (e_{15}+e_{31})h\beta \\ e_{33}\beta^2+e_{15}h^2 & (e_{15}+e_{31})h\beta & -(\varepsilon_{11}^S h^2+\varepsilon_{33}^S\beta^2) \end{pmatrix} \qquad (7)$$

The condition for a nontrivial solution is such that the determinant of the coefficient matrix vanishes, i.e.,

$$|M_{ij}|=0 \qquad (8)$$

Equation (8) is a cubic equation of h^2. For a given ω and β, eq. (8), in general, has three roots of h^2, denoted as h_1^c, h_2^c and h_3^c, corresponding to the quasi-electromagnetic, quasi-longitudinal, and quasi-shear waves in the piezoelectric plate, respectively. For each h_i^c, the ratio among A, B, and C can be determined from eq. (6). Since we are concerned only with the waves in the x_3 direction which correspond to piezo-active modes in a finite thickness composite plate, the general solutions become

$$\begin{aligned} u_3^c &= \sum_i R_i^c f_i^c \cos(h_i^c x_1)\sin(\beta x_3) \\ u_1^c &= \sum_i R_i^c g_i^c \sin(h_i^c x_1)\cos(\beta x_3) \\ \Phi^c &= \sum_i R_i^c t_i^c \cos(h_i^c x_1)\sin(\beta x_3) \end{aligned} \qquad (9)$$

where i runs from 1 to 3. f_i, g_i and t_i are the cofactors of $A_{k1}(i)$, $A_{k2}(i)$, and $A_{k3}(i)$ of the determinant (8) (where h is replaced by h_i^c for i=1, 2, and 3, respectively). The $\exp(-j\omega t)$ term in eq. (9) is omitted.

Following the similar procedure, the solutions for the polymer phase can be obtained (the center of the polymer plate is at $x_1 = d/2$)

$$\begin{aligned} u_3^P &= \sum_i R_i^P f_i^P \cos(h_i^P (x_1-\frac{d}{2}))\sin(\beta x_3) \\ u_1^P &= \sum_i R_i^P g_i^P \sin(h_i^P (x_1-\frac{d}{2}))\cos(\beta x_3) \\ \Phi^P &= C^P \cosh(\beta(x_1-\frac{d}{2}))\sin(\beta x_3) \end{aligned} \qquad (10)$$

where i =1, 2. f_i^P and g_i^P are the cofactors of $A_{k1}(i)$, $A_{k2}(i)$ of the determinant (8) with all the material parameters replaced by those of the polymer phase, and

$$(h_1^p)^2 = (k_L^p)^2 - \beta^2 \text{ and } (h_2^p)^2 = (k_T^p)^2 - \beta^2$$

where $k_L^P = \frac{\omega}{v_L^P}$, $k_T^P = \frac{\omega}{v_T^P}$, v_L^P and v_T^P are the longitudinal and shear wave velocities of the polymer phase, respectively.

The expressions of the stresses and the electric displacement in the ceramic plate can be obtained by substituting eq. (9) into eq. (2):

$$T_1^C = \sum_i T_{11}^C(i) R_i^C \cos(h_i^C x_1)\cos(\beta x_3)$$

$$T_3^C = \sum_i T_{33}^C(i) R_i^C \cos(h_i^C x_1)\cos(\beta x_3) \qquad (11)$$

$$T_5^C = \sum_i T_{31}^C(i) R_i^C \sin(h_i^C x_1)\sin(\beta x_3)$$

where

$$\begin{aligned} T_{11}^C(i) &= c_{11}^E h_i^C g_i^C + (c_{13}^E f_i^C + e_{31} t_i^C)\beta \\ T_{33}^C(i) &= c_{13}^E h_i^C g_i^C + (c_{33}^E f_i^C + e_{33} t_i^C)\beta \\ T_{31}^C(i) &= -c_{44}^E(\beta g_i^C + h_i^C f_i^C) - e_{15} h_i^C t_i^C \end{aligned} \qquad (12)$$

where i=1, 2, 3 for ceramic phase. The electric displacements are:

$$D_1^C = \sum_i D_1^C(i) R_i^C \sin(h_i^C x_1)\sin(\beta x_3) \qquad (13a)$$

$$D_3^C = \sum_i D_3^C(i) R_i^C \cos(h_i^C x_1)\cos(\beta x_3) \qquad (13b)$$

where $D_1^C(i) = -e_{15}(\beta g_i^C + h_i^C f_i^C) + \varepsilon_{11}^S h_i^C t_i^C$ and $D_3^C(i) = e_{31} h_i^C g_i^C + e_{33}\beta f_i^C - \varepsilon_{33}^C \beta\, t_i^C$. Similar expressions can be obtained for the polymer plate. For instance, the electric displacements are:

$$D_1^P = -\varepsilon_{11}^P \beta C^P \sinh(\beta(x_1 - \frac{d}{2}))\sin(\beta x_3) \qquad (14c)$$

$$D_3^P = -\varepsilon_{11}^P \beta C^P \cosh(\beta(x_1 - \frac{d}{2}))\cos(\beta x_3) \qquad (14d)$$

Making use of the boundary conditions at the ceramic polymer interface ($x_1 = \nu d/2$, where ν is the volume fraction of the ceramic in a composite), which are

$$u_1^C = u_1^P,\ u_3^C = u_3^P,\ T_1^C = T_1^P \text{ and } T_5^C = T_5^P \qquad (15a)$$

and $\Phi^C = \Phi^P$ and $D_1^C = D_1^P$ (15b)

R_i^c, R_j^P and C^P (i =1, 2, 3 and j=1, 2) can be determined. Expanding Eqs. (15) in terms of eqs. (9), (10), (11), (13) and (14) yields the following six homogeneous linear equations:

$$\begin{pmatrix} K_{11} & K_{12} & K_{13} & K_{14} & K_{15} & 0 \\ K_{21} & K_{22} & K_{23} & K_{24} & K_{25} & 0 \\ K_{31} & K_{32} & K_{33} & K_{34} & K_{35} & 0 \\ K_{41} & K_{42} & K_{43} & K_{44} & K_{45} & 0 \\ 0 & 0 & K_{53} & K_{54} & K_{55} & K_{56} \\ 0 & 0 & K_{63} & K_{64} & K_{65} & K_{66} \end{pmatrix} \begin{pmatrix} R_1^P \\ R_2^P \\ R_1^C \\ R_2^C \\ R_3^C \\ C^P \end{pmatrix} = 0 \qquad (16)$$

where the matrix elements K_{ij} are functions of β, ω, d, ν, and the material parameters of both the polymer and piezoceramic. The condition that the determinant

$$|K_{ij}| = 0 \qquad (17)$$

yields the relationship between ω and β, the dispersion relations in the composite. For each pair of ω and β, the relationships among R_i^C, R_j^P and C^P can be obtained. Hence, the various stress, strain, electric field distributions in the composite can be determined.

2.2. Dispersion Curves. Modes and Mode Coupling of a 2-2 Piezocomposite:

Eq. (17) allows us to determine the relationship between β and ω, the dispersion curves, for a composite if the materials parameters of piezoceramic and polymer and the geometric parameters, such as d and ν, are known. Eq. (17) is a transcendental function which cannot be solved analytically. A computer code was developed and the dispersion curves were evaluated numerically.

Shown in figure 2 (the solid curves) are the two lowest branches of the dispersion curves for a 2-2 composite made of PZT-5H piezoceramic and Spurr epoxy with the ceramic volume fraction of 44%.[22] For all the composites discussed in this paper, except otherwise specified, PZT-5H piezoceramic and Spurr epoxy are used as the constituents. The parameters of PZT-5H and Spurr epoxy are presented in Table I. The general trend of the dispersion curves in figure 2 resembles that of the symmetric Lamb waves in a plate.[19] As will be shown later, at small βd limit, the first branch corresponds to the longitudinal wave propagation along the x_3-direction, that is, u_3 is the dominant displacement which is more or less uniform and in phase in the x_1-direction, and its phase velocity is the effective longitudinal wave velocity of the composite. The second branch corresponds to the lateral resonance which arises from the periodic structure of the composite, that is, it is a stationary shear wave along the x_1-direction, and it can be shown that the displacement u_3 of the polymer phase is much larger than that of the ceramic phase and the phase difference between them is 180°. Hence, it can be related to the so called stop-band edge resonance as predicted by Auld et al.[7,8]

Table I. The material properties of PZT-5H and Spurr epoxy used for the 2-2 composites in the investigation.

PZT-5H: e_{33} = 23.09 C/m^2, e_{31} = - 6.603 C/m^2, e_{15} = 17.0 C/m^2, c_{11} = 12.72*10^{10} N/m^2, c_{44} = 2.3*10^{10} N/m^2, c_{33} = 11.74*10^{10} N/m^2, c_{13} = 8.47*10^{10} N/m^2, K_{11} = 1700, K_{33} = 1470, ρ = 7500 kg/m^3.

Spurr epoxy: c_{11} = 5.4*10^9 N/m^2, c_{44} = 1.3*10^9 N/m^2, ρ = 1100 kg/m^3.

Under the assumption that the wave length λ in the x_3-direction ($\beta = 2\pi/\lambda$) is equal to two times the composite thickness t (the condition for the thickness resonance), the theoretical dispersion curves can be compared with the experimental results, obtained from composites with different thickness. At low βd on the dispersion curves, where d is the period of the composite, the frequency of the fundamental thickness mode from the experiment falls on the first branch as marked by the black dots, and the frequency of the first lateral mode falls on the second branch as marked by the open circles. After the crossover region B, the modes interchange the positions on the dispersion curves where the thickness mode is in the second branch while there is a weak resonance at a frequency below the thickness mode and it falls on the first branch. Here, the thickness mode is defined as the one with higher electromechanical coupling factor. The mode on the first branch gradually diminishes at high βd values. The result is presented in figure 2. Clearly, there is an excellent accord between the theoretically derived resonance frequencies and experimentally observed ones.

Shown in figures 3(a) and figure 3(b) are the 3-dimensional dispersion curves for 2-2 composites with 15% and 44% ceramic volume fraction, respectively. Obviously, there are imaginary and complex branches of the dispersion curves. The modes on these branches are non-propagating modes (imaginary branches) and attenuated modes (complex branches), respectively. These modes do not exist in an unbounded composite, however, they are important in the vibration problems of finite thickness plates as well as in semi-infinite mediums, where they correspond to the evanescent waves at the surface which will be discussed later in the paper.

Figure 4 presents the effect of the stiffness of the polymer phase on the dispersion curves of a 2-2 composite with 30% ceramic content where PZT-5H is used as the piezoceramic phase. It is apparent that the frequency position of the second branch is very sensitive to properties of the polymer phase. This is quite understandable since as will be shown later, the frequency position of this branch is directly related to the shear velocity of the polymer matrix for composites at this ceramic content. The lower the shear wave velocity of the polymer phase is, the lower the frequency of the second branch will be. Therefore, for a transducer operated at high frequencies, in order to avoid the interference from the lateral modes, a polymer matrix with a high shear velocity should be utilized even

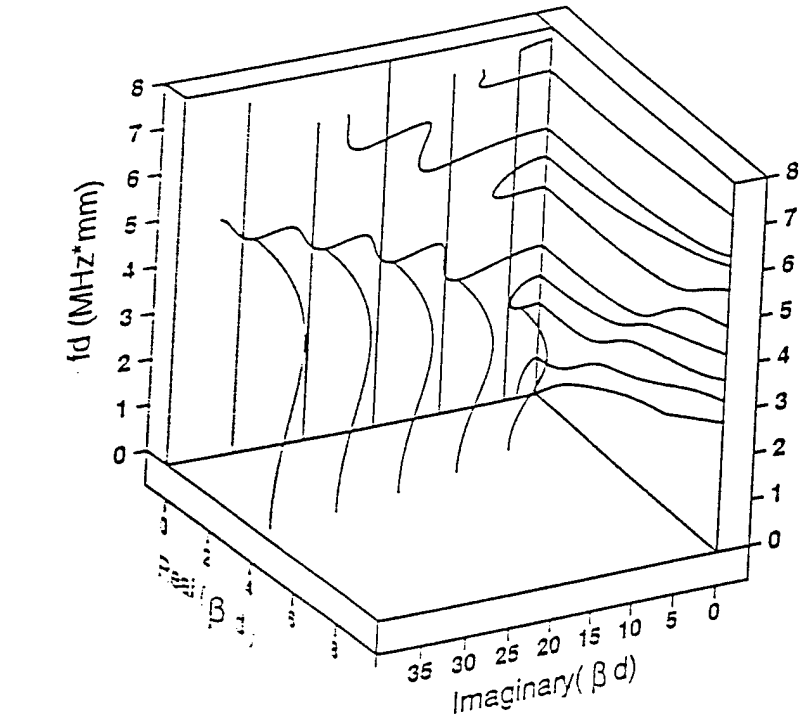

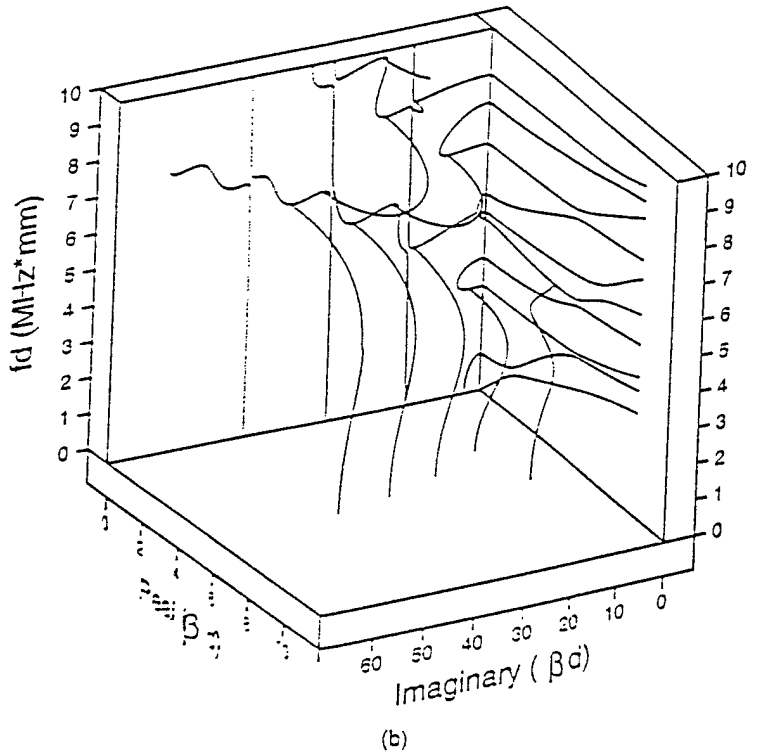

Figure 3. The dispersion curves for a 2-2 composite (figure 1(a))made of PZT-5H and Spurr epoxy for (a) 15% ceramic volume content and (b) 44% ceramic volume content.

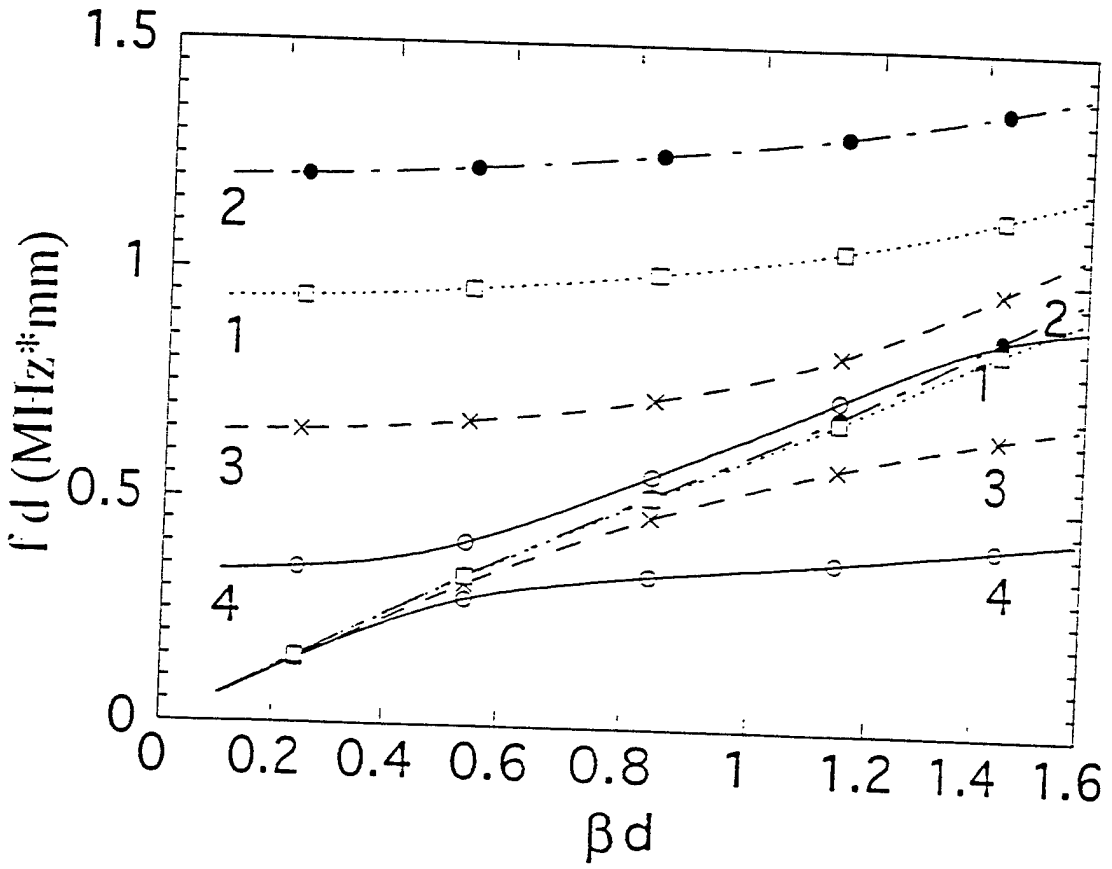

Figure 4. The effect of the properties of the polymer matrix on the dispersion curves of 2-2 composites with PZT-5H ceramic, derived from the model. The properties of the polymer phase are: curve 1: c_{11}= 7.72*10^9 N/m^2, c_{44}= 1.588*10^9 N/m^2, ρ = 1160 kg/m^3; curve 2: c_{11}= 1.3634*10^{10} N/m^2, c_{44}= 3.432*10^9 N/m^2, ρ = 1610 kg/m^3; curve 3: c_{11}= 3.173*10^9 N/m^2, c_{44}= 0.696*10^9 N/m^2, ρ = 1060 kg/m^3; curve 4: c_{11}= 1.622*10^9 N/m^2, c_{44}= 1.646*10^8 N/m^2, ρ = 890 kg/m^3.

though the thickness coupling factor k_t of this composite may be reduced as a result of the stiffer polymer matrix.[3,4]

In order to further elucidate the origins of these resonant modes, it is instructive to make a comparison between the dispersion curves of a composite and those of single piezoceramic and polymer plates with appropriate boundary conditions.[23] In general, in piezoceramic polymer composites, the elastic stiffness of the piezoceramic is more than one order of magnitude higher than that of the polymer. It is reasonable to assume that the piezoceramic plates in a 2-2 composite are stress free at the ceramic-polymer interface, that is, the stress components T_1 and T_5 are zero at the interface. Similarly, the polymer plates can be approximated as under the fixed boundary conditions, that is, u_1 and u_3 are zero at the interface. Under these assumptions, the dispersion curves of both single ceramic and single polymer plates are calculated for the plates with different widths corresponding to 2-2 composites with different ceramic volume fractions. The results are presented in figures 5(a), 5(b), and 5(c) corresponding to 2-2 composites with 15%, 44% and 80% ceramic content, respectively. In these figures, the solid lines are the dispersion curves of the 2-2 composites, the dashed lines are those of the ceramic plate, and doted lines are the dispersion curves of the polymer plate.

The results from these figures reveal that there are many resemblance between the dispersion curves of 2-2 composites and the dispersion curves of the single ceramic and single polymer plates with appropriate boundary conditions. For instance, at small βd, the first branch in the dispersion curves of the 2-2 composites with 44% and 80% ceramic volume content is very close to the first branch of the ceramic plate. On the other hand, for 2-2 composites with low ceramic volume content, a large difference between these two is found for the first branch. These results are consistent with those from Smith et al. and from Hashimoto et al. based on an effective medium model.[3,4] For the second branch which corresponds to the lateral resonant mode in a composite plate, at low and medium ceramic volume content, it is close to the first branch of the polymer plate which frequency at small βd is equal to $V_T^P / 2d_P$ where V_T^P and d_P are shear wave velocity and width of the polymer plate, respectively. However, for composites with high ceramic volume content such as the one shown here (80%), the second branch is related to the longitudinal resonance of the ceramic plate along the width (or x_1-) direction while the shear resonance associated with the polymer plate lies on the third branch of the dispersion curves.

Obviously, the coupling between the two phases through the interface boundary conditions will influence the dispersion curves of the waves in the two phases. It is well known that the dispersion curves for the uncoupled waves are split at their crossover points when coupling is introduced.[11] Far from the crossover region, the coupled wave dispersion curves should nearly coincide with those of

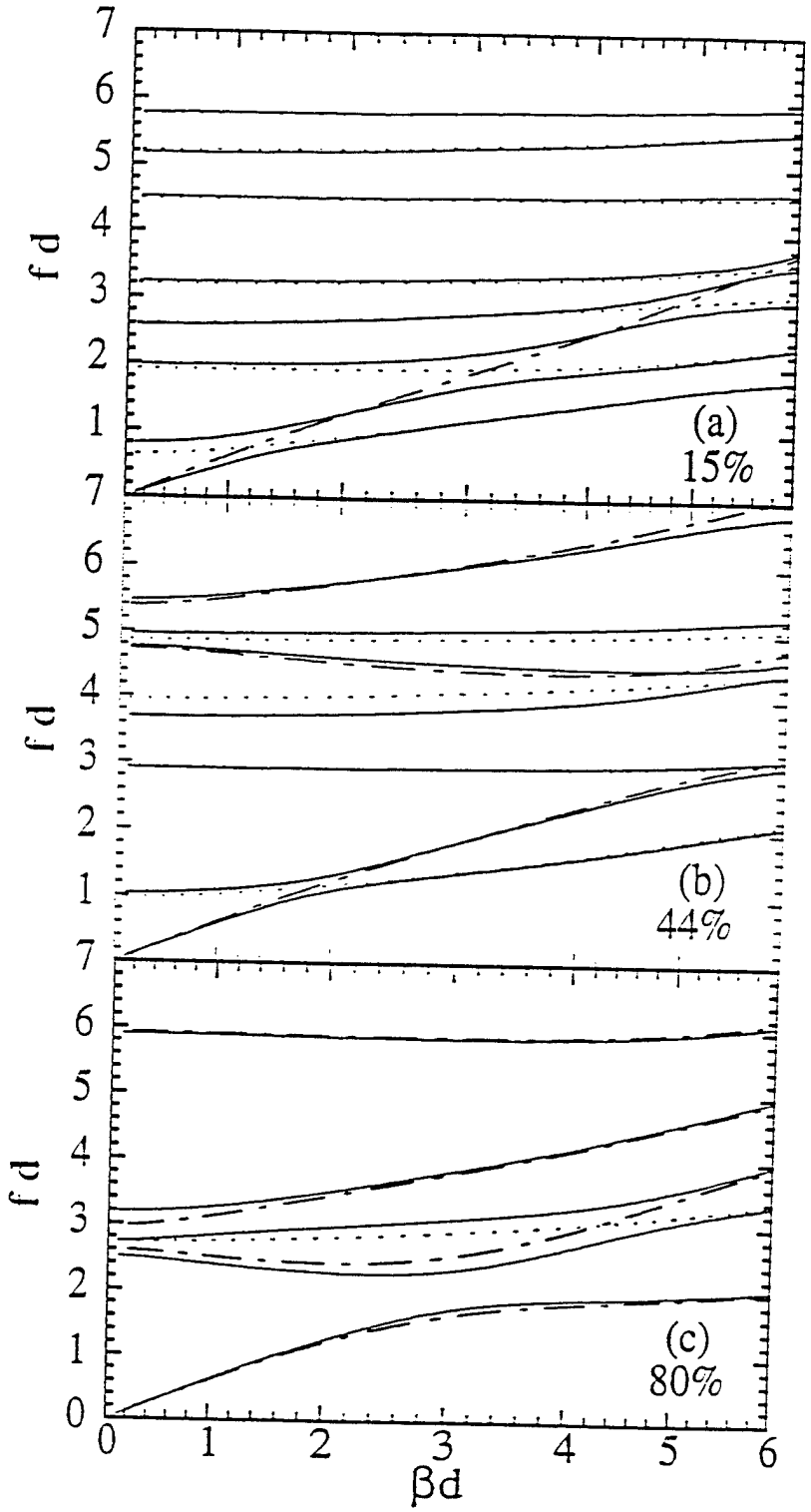

Figure 5. Comparison of the dispersion curves in 2-2 composites with those in a single piezoceramic plate and a polymer plate for composites with (a) 15% ceramic content; (b) 44% ceramic; and (c) 80% ceramic content. PZT-5H is used as the piezoceramic and Spurr epoxy as the polymer phase.

the uncoupled waves. If the coupling is very strong as for the 15% and 44% piezocomposites, the coupled waves exhibit large departure from the uncoupled curves in the crossover region, which is clearly shown in figure 5(a) and figure 5(b). While for the composite with 80% ceramic content, the coupling between the first and the second branches is through the coupling of P wave and SV wave in the ceramic plate where the interface does not have a significant effect on it.

2.3. Vibration of a Finite Thickness Composite Plate under an Electric Field in Air:

In the previous section, the properties of guided wave propagation in laminated 2-2 piezocomposites have been analyzed. In spite of the fact that many effective parameters of the material can be derived by this simple method, one key issue in the design of a composite transducer, i.e., the influence of the aspect ratio of the ceramic plates (or the unit cell) in a composite on the performance of the transducer cannot be addressed. In this section, we will treat the vibration problem of a finite thickness composite plate under an external driving electric field and situated in air. From the analysis, one can obtain detailed information on how the surface vibration profile changes with frequency and its dependence on the aspect ratio of the ceramic plate (or the unit cell dimension), the possible resonant modes in a composite transducer, and the dependence of the electromechanical coupling factor on the aspect ratio of the ceramic plate, etc. We will also show that as long as the thickness resonance frequency is below the lateral mode frequency, the aspect ratio will not have a direct effect on the vibration uniformity of a composite near the thickness resonance. The influence is on the bandwidth in which the ceramic and polymer vibrate with nearly same amplitude and phase.

A composite plate with a thickness t is drawn schematically in figure 1(b). For the problem treated here, the two free surfaces of the composite plate are electroded with conducting material and an AC electric field of a frequency f is applied between the two electrodes.

It is well known that there exist no simple solutions for the vibration problem of a finite thickness plate such as the piezocomposite treated here. One of the most frequently used approximation methods is to expand the elastic and electric fields in a material in terms of the eigenfunctions in an unbounded one.[21] Different techniques such as the variational technique and the method of least squares can be used to determine the expansion coefficients. For the composite plate treated here, we found that the variational technique is more appropriate in treating the boundary problem than the method of least squares because of the large difference in the vibration amplitudes between the two phases in the composite.

For the ceramic phase in the composite plate, the elastic displacements u_3 and u_1, and the electric potential Φ are expended in terms of the eigenfunctions derived:

$$u_3^C = \sum_{n=1}^{m}\sum_{i=1}^{3} R_{ni}^C f_{ni}^C \cos(h_{ni}^C x_1)\sin(\beta_n x_3)A_n$$

$$u_1^C = \sum_{n=1}^{m}\sum_{i=1}^{3} R_{ni}^C g_{ni}^C \sin(h_{ni}^C x_1)\cos(\beta_n x_3)A_n + CR_0^C \sin(h_{01}^C x_1) \qquad (18)$$

$$\Phi^C = \sum_{n=1}^{m}\sum_{i=1}^{3} R_{ni}^C t_{ni}^C \cos(h_{ni}^C x_1)\sin(\beta_n x_3)A_n + Cx_3$$

Similarly, for the polymer phase in the composite plate:

$$u_3^P = \sum_{n=1}^{m}\sum_{i=1}^{2} R_{ni}^P f_{ni}^P \cos(h_{ni}^P (x_1 - \frac{d}{2}))\sin(\beta_n x_3)A_n$$

$$u_1^P = \sum_{n=1}^{m}\sum_{i=1}^{2} R_{ni}^P g_{ni}^P \sin(h_{ni}^P (x_1 - \frac{d}{2}))\cos(\beta_n x_3)A_n + CR_0^P \sin(h_{01}^P (x_1 - \frac{d}{2})) \qquad (19)$$

$$\Phi^P = \sum_{n=1}^{m} C_n^P \cosh(\beta_n (x_1 - \frac{d}{2}))\sin(\beta_n x_3)A_n + Cx_3$$

where R_{n1}^C, R_{n2}^C, R_{n3}^C, R_{n1}^P, R_{n2}^P and C_n^P are determined in eq. (16), β_n, h_{ni}^C and h_{ni}^P are the wave vector components of the nth mode in the x_3- and x_1-directions where the superscripts c and p stand for the ceramic and polymer, respectively. h_{01}^C and h_{01}^P are related to the mode in which β is equal to zero: $h_{01}^C = \sqrt{\frac{\rho^C}{c_{11}^E}}\omega$ and $h_{01}^P = \sqrt{\frac{\rho^P}{c_{11}^P}}\omega$. R_0^c and R_0^p are determined by eq. (16) in which β is set to zero. The mode with β=0 is generated due to the fact that the velocity of the electromagnetic wave is much faster than that of the elastic waves and the composite plate is clamped in the x_3-direction (S_3 = 0). A_n and C are the coefficients which will be determined by the boundary conditions which are traction free and $\Phi = \pm V/2$ (here $\exp(-j\omega t)$ is omitted) at $x_3 = \pm t/2$.

The stresses T_3, T_5 and electric displacement D_3 are expressed as:

$$T_3^C = \sum_{n=1}^{m}\sum_{i=1}^{3} T_{33}^C(n,i)\cos(h_{ni}^C x_1)\cos(\beta_n x_3)A_n + (e_{33} + T_0^C \cos(h_{01}^C x_1))C \qquad (20a)$$

$$T_5^C = \sum_{n=1}^{m}\sum_{i=1}^{3} T_{13}^C(n,i)\sin(h_{ni}^C x_1)\sin(\beta_n x_3)A_n \qquad (20b)$$

$$D_3^C = \sum_{n=1}^{m}\sum_{i=1}^{3} D_3^C(n,i)\cos(h_{ni}^C x_1)\cos(\beta_n x_3)A_n + (-\varepsilon_{33}^S + D_0^C \cos(h_{01}^C x_1))C \qquad (20c)$$

$$T_3^P = \sum_{n=1}^{m}\sum_{i=1}^{2} T_{33}^P(n,i)\cos(h_{ni}^P (x_1 - \frac{d}{2}))\cos(\beta_n x_3)A_n + T_0^P \cos(h_{01}^P (x_1 - \frac{d}{2}))C \qquad (20d)$$

$$T_5^P = \sum_{n=1}^{m}\sum_{i=1}^{2} T_{13}^P(n,i)\sin(h_{ni}^p(x_1 - \frac{d}{2}))\sin(\beta_n x_3)A_n \qquad (20e)$$

$$D_3^P = \sum_{n=1}^{m}\sum_{i=1}^{2} D_3^P(n,i)\cos(h_{ni}^p(x_1 - \frac{d}{2}))\cos(\beta_n x_3)A_n - \varepsilon_{11}^P C \qquad (20f)$$

Where $T_{33}^C(n,i)$, $T_{13}^C(n,i)$, $D_3^C(n,i)$, $T_{33}^P(n,i)$, $T_{13}^P(n,i)$ and $D_3^P(n,i)$ are the same as $T_{33}^C(i)$, $T_{31}^C(i)$, $D_3^C(i)$, $T_{33}^P(i)$, $T_{31}^P(i)$, and $D_3^P(i)$ in equations (11) to (14) if the subscript i there is replaced by n and i for i-th partial wave of n-th mode here. And

$T_0^C = c_{13}^E h_{01}^C R_0^C$, $T_0^P = c_{12}^P h_{01}^P R_0^P$, $D_0^C = e_{31} h_{01}^C R_0^C$.

The number of the eigenfunctions, m, required in the expansion is determined by the accuracy needed for the solution. For the problem treated here, we found that it is adequate to use eight eigen-modes in the expansion. In the frequency range studied (fd<2 MHz•mm), there are two branches having real β and the other branches having either imaginary or complex β, which corresponds to the modes confined at the surface of $x_3=\pm t/2$.

For the problem treated here, all the stress components in air are zero and for the sake of simplicity, D in air is also assumed to be zero since the dielectric permittivity of the composite is much higher than air. Under these conditions, the variational formula takes the following form:

$$\int_V \left[(T_{kl,k} - \rho \ddot{u}_l)\delta u_l^* + D_{k,k}\delta\Phi^*\right]dV + \int_S \left[(-T_{kl})\delta u_l^* + (\Phi - \overline{\Phi})\delta D_k^*\right]dS = 0 \qquad (21)$$

where the integration over time has been performed to take into account of the complex notations for the quantities in the integrands.[19,21] The * represents the complex conjugate of the corresponding quantity. The first integral is over the volume of the 2-2 composite plate and it can be shown that it is equal to zero since all the quantities in the integrand satisfy eq. (1). The second integral is over the surfaces of the composite plate at $x_3=\pm t/2$ where $\overline{\Phi}=\pm V/2$ at $x_3=\pm t/2$ where V is the applied voltage. The periodic condition of the composite in the x_1-direction and the symmetric condition of the solutions and the boundary conditions about the plane of $x_3 = 0$ allow the second integration to be performed over one unit cell at $x_3 = t/2$.

Substituting T_3, T_5, u_1,u_3, Φ and D_3 into equation (21) yields the following linear algebraic equation:

$$(M_{ij})(A_j) = (V_i) \qquad (22)$$

where (M_{ij}) is a 9×9 matrix, $(A_j)=(A_1,A_2,A_3,A_4,A_5,A_6,A_7,A_8,C)^T$, (V_i) is a 9×1 matrix whose elements depend only on V, the applied voltage. For a given frequency f, one can solve eq. (22) to obtain A_j

and C. From A_j and C, eqs. (18), (19), and (20) yield all the characteristic properties related to the vibration of a 2-2 composite plate with different thickness and different ceramic volume fraction such as the electrical impedance, surface displacement distribution, resonant modes, electromechanical coupling coefficient, etc.

For the composite plate treated here, the electrical impedance for a single repeating unit can be found from:

$$Z = \frac{V}{I} \tag{23}$$

where I is the current which is equal to $I = \frac{dQ}{dt} = -j\omega Q = -j2\omega b \int_0^{d/2} D_3 dx_1$, where Q and b are the electric charge and the length in the x_2-direction of the plate respectively. To compare with the experimental result, the current I should be multiplied by N, the number of repeating unit in a composite plate.

Shown in figure 6(a) is the electric impedance curve calculated from eqs. (22) and (23) for a composite plate with t/d=4.5 and the ceramic volume fraction v=44%. The electric impedance measured experimentally from the same composite plate is shown in figure 6(b) and clearly the theoretical impedance curve reproduces the experimental data quite well. The difference in the sharpness of the resonant peaks between the experimental data and the theoretical curve is due to the fact that in the theoretical analysis, the electrical and mechanical losses of the ceramic and polymer phases were not included.

In figure 6(c), the peak positions from the experimental data are compared with the dispersion curves for this composite which shows excellent agreement between the two. In order to elucidate the nature of these modes, the spatial distribution of u_3 at each mode at the composite surface is presented in figure 7 which are evaluated based on eqs. (18) and (19). Apparently, f_{L1} is the fundamental thickness resonance and f_{t1} is the first lateral mode as revealed by the fact that the ceramic and polymer vibrate 180° out of phase at this mode, as predicted in the earlier theoretical work.[7,8] The frequency position and the distribution of u_3 along the x_3 axis indicate that f_{L3} is the third harmonic of the thickness mode. However, the appearance of f_{t2} is not expected from the earlier theoretical works in which the ceramic and polymer vibrate in phase. By examining the equations of the boundary conditions at $x_3=\pm t/2$, it can be deduced that a resonance will occur whenever $\beta = (1+2n)\pi/t$, i.e., $\cos(\beta t/2) = 0$. Hence, the dispersion curves of real β, as shown in figure 6(c), reveal that the fundamental thickness resonance and the first lateral resonance occur at $\beta = \pi/t$ (f_{L1} and f_{t1}). Similarly, when $\beta = 3\pi/t$, the third harmonic of the thickness mode will occur at f_{L3}. In addition, a mode f_{t2} will also show

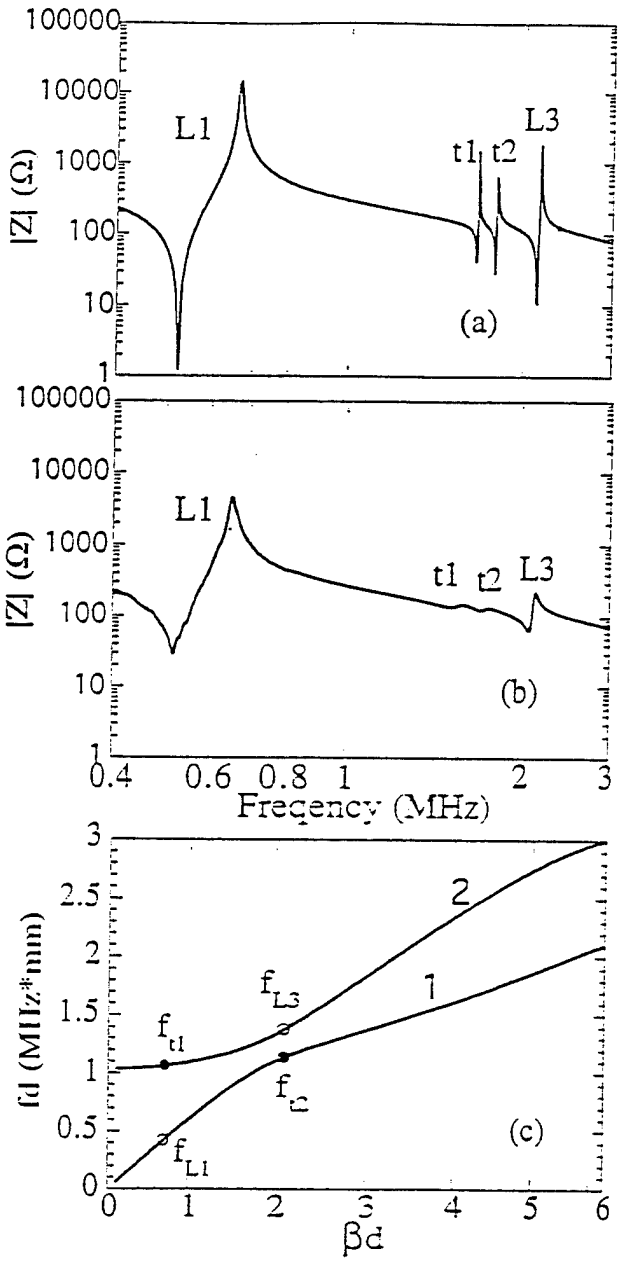

Figure 6. The electric impedance curve for a 2-2 composite plate with PZT-5H and Spurr epoxy (44% ceramic) measured in air: (a) the theoretical curve and (b) the experimental curve. The thickness t of the composite is t/d = 4.5 and d=0.635 mm. f_{L1} and f_{L3} are the fundamental and third harmonic of the thickness mode and t1 and t2 are the modes arose from the periodicity of the composite. (c) The dispersion curves elucidating the origin of the resonant modes f_{t1} and f_{t2}. In general, any modes on the dispersion curves will show up whenever $\beta d = (2n+1)/2$, n=0,1,2, ... is satisfied, where $\beta=2\pi/\lambda$ and $\lambda = 2t$.

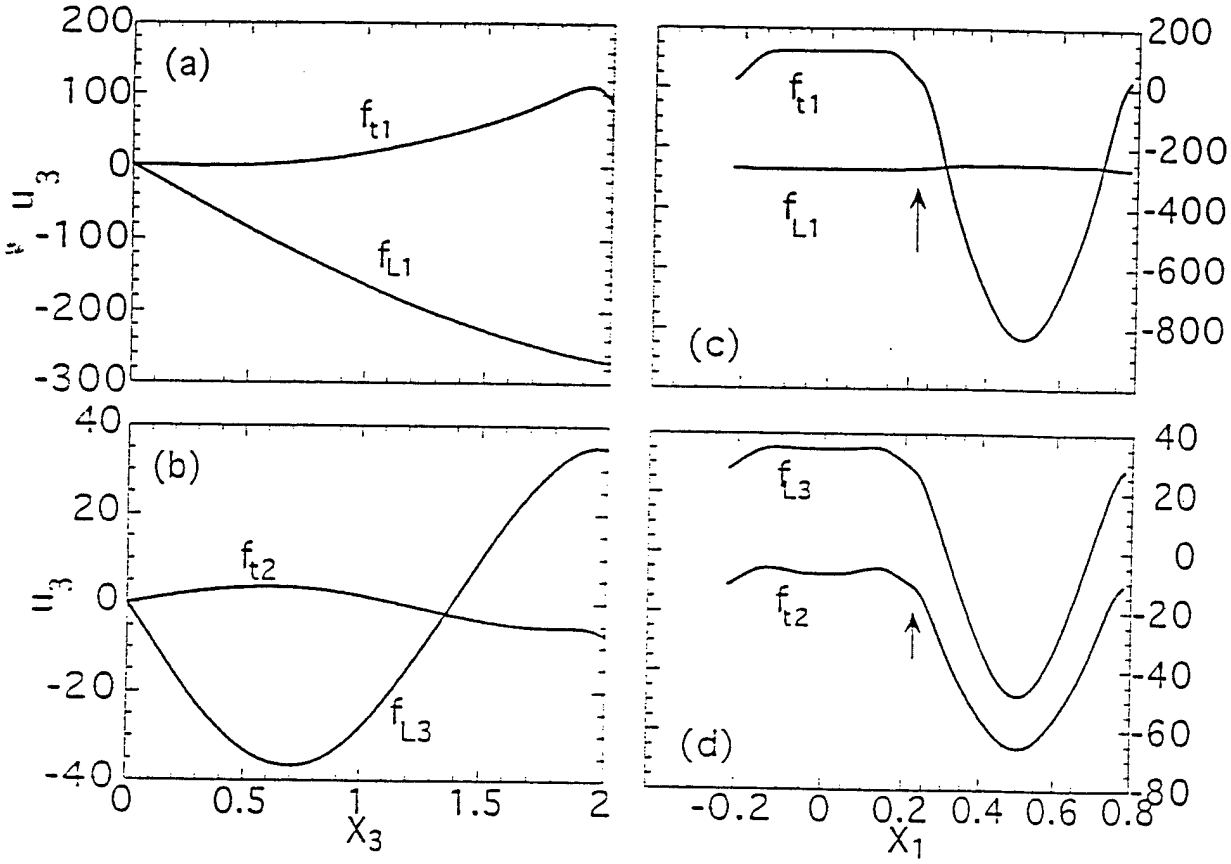

Figure 7. The distribution of the elastic displacement u_3 for f_{L1}, f_{L3}, f_{t1}, and f_{t2} of a 2-2 composite with t/d=4, where (a) and (b) are the distributions along the x_3-direction when x_1=0 (at the center line of the ceramic plate, figure 1(b)), x_3=0 is at the center and x_3=2 is at the ceramic surface; (c) and (d) are surface vibration profiles at x_3=2, x_1=0 corresponds to the center of the ceramic plate and x_1=0.5 is at the center of the polymer plate.

up at the branch 1 which is at a frequency near and above f_{t1}. By the same argument, it would be expected that f_{L5}, f_{t3}, etc. may also be observed, depending on the electromechanical coupling factors of these modes. As shown later, the effective coupling factor for the modes in the first branch will decrease with increasing βd, i.e., reducing thickness, and on the other hand, the effective coupling factor for the modes in the second branch will increase with β. As the ratio of t/d decreases, the frequency of the thickness mode will gradually move towards the first lateral mode which will become stronger (coupling factor increases), and the second lateral mode (f_{t2}) becomes weaker and finally it will disappear. These features are summarized in figure 8 which provide understanding on the earlier experimental observations on how various modes change with temperature (which causes reduction of the shear velocity of the polymer phase) and the composite thickness.[5]

Both the experimental results and the theoretical data indicate that the ceramic and polymer vibrate in phase for all the modes on the first branch and out of phase for modes on the second branch.

The electromechanical coupling factor for the thickness resonance can be evaluated based on the definition of IEEE:[20]

$$k_t^2 = \frac{\pi}{2}\frac{f_s}{f_p}\tan\left(\frac{\pi}{2}\frac{f_p - f_s}{f_p}\right) \qquad (24)$$

where k_t is the thickness mode coupling factor, f_s and f_p are the series and parallel resonance frequencies, respectively. Eq. (24) is used here to calculate the coupling factor for the modes in both the first and second branches. Shown in figure 9 is the results for a 2-2 composite plate with 44% ceramic volume content for different d/t, where both theoretical and experimental results are presented. As the ratio of d/t increases, the coupling factor of the mode (thickness mode) in the first branch gradually decreases, while the coupling factor of the mode in the second branch gradually increases due to the modes coupling. As d/t increases further, the thickness mode will jump to the second branch when the coupling factor in the second branch surpasses that of the first branch. Although in this region the coupling factor for the thickness mode can still be quite high, the distribution of u_3 is not uniform on the composite surface and the ceramic and polymer vibrate 180° out of phase which is not desirable since the polymer phase will not be able to perform properly the function of transferring the acoustic energy between the ceramic plates and the external medium.

For a composite plate to work effectively as an electromechanical transduction material, it is required that the ceramic and the polymer plates in the composite vibrate in phase with nearly the same amplitude in the x_3-direction. The evolution of the vibration pattern in the two phases with frequency and the effect of the aspect ratio t/d of a composite plate on this distribution are investigated. Shown in figure 10(a) is the variation of the ratio u_3^P / u_3^C at the surface of the composite plate, where u_3^P and u_3^C

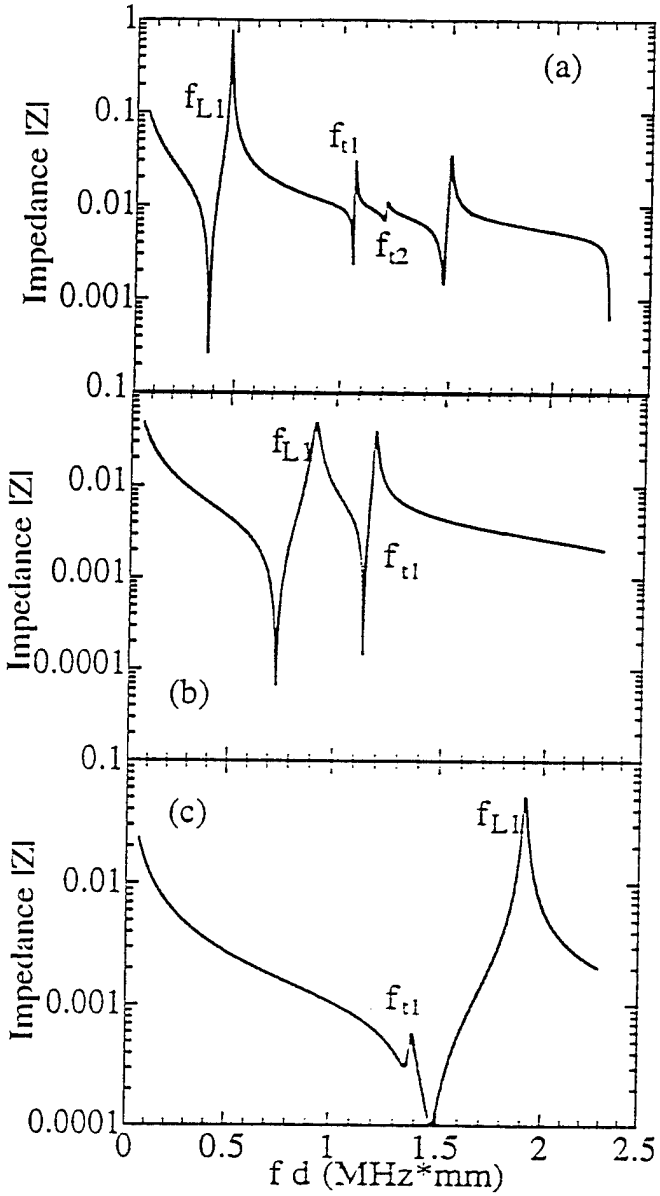

Figure 8. The evolution of various modes in a 2-2 composite made of PZT-5H (44% ceramic) and Spurr epoxy with the thickness t of composite plate: (a) t/d = 4, (b) t/d = 2, and (c) t/d = 1. There is already substantial coupling between the thickness and lateral modes at t/d = 2 for this composite. At low t/d values (thin samples), the lateral mode will disappear.

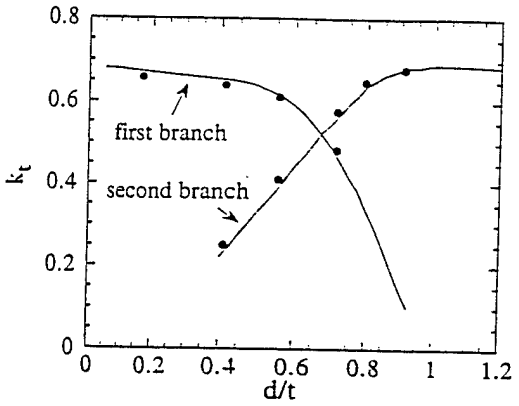

Figure 9. The evolution of the coupling factor for the modes on the first and second branches of the dispersion curves with the composite thickness d/t for a composite made of PZT-5H and Spurr epoxy with 44% ceramic content.

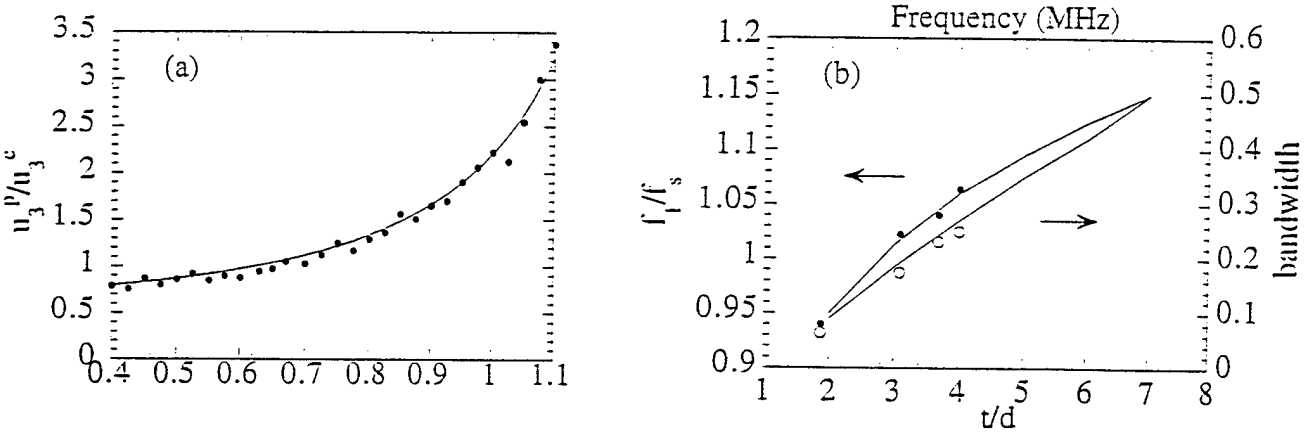

Figure 10. (a) The ratio of u_3^p/u_3^c vs. frequency for a composite made of PZT-5H and Spurr epoxy (44% ceramic content) at a thickness of t/d = 4 (d=0.635 mm) measured in air. u_3^p and u_3^c are the surface displacements at the centers of the polymer plate and ceramic plate, respectively. The black dots are the experimental data measured using a laser dilatometer and the solid line is derived from the model.

(b) The ratio f_1/f_s as a function of the ratio d/t of the composite plate, where f_1 is the frequency at which $u_3^p/u_3^c=1$ and f_s is the series resonant frequency for the thickness mode. The black dots are experimental data and the solid lines are derived from the model calculation.

(c) The bandwidth as a function of the ratio d/t of the composite plate. The black dots are experimental data and the solid lines are derived from the model calculation.

are u_3 at the centers of the polymer (x_1=d/2) and the ceramic plates (x_1=0), respectively, with frequency for the composite plate of t/d=4 where both the experimental results and theoretically calculated curve are presented. The experimental data were acquired using a laser dilatometer.[24] Hence, at frequencies far below any resonant mode, u_3^P / u_3^C is always less than one, which is true as long as the composite is driven electrically. For a given frequency, as t/d increases, this ratio increases and approaches one. These are consistent with the results of the earlier theoretical work on the static properties of composites.[25] As frequency increases, the ratio u_3^P / u_3^C increases towards one. At a frequency f_1 which is near f_s of the thickness mode, $u_3^P / u_3^C = 1$. This ratio will surpass one as the frequency is further increased. This is true as long as $f_{L1} < f_{t1}$. In figure 10(b), the change of f_1/f_s vs. the ratio of d/t is presented. Clearly, f_1/f_s is close to but larger than one except for composite plates with a small aspect ratio. Hence, the aspect ratio t/d does not have a significant effect on the ratio of u_3^P / u_3^C at frequencies very near f_s of the thickness mode, where u_3^P / u_3^C is always near one if the thickness mode is below the first lateral mode frequency. However, it will affect the bandwidth in which u_3^P / u_3^C is near one. For example, the bandwidth $\Delta f/f_1$, where Δf is defined here as the frequency width in which $0.9 < u_3^P / u_3^C < 1.1$, increases as the ratio of d/t decreases, which is shown in figure 10(b). The experimental data points are also presented in figure 10(b) and the agreement between the two is quite good.

2.4. Forced Vibration of a Piezocomposite Plate in a Fluid Medium:

Following a similar procedure as outlined in the preceding section, the vibration problem of a composite plate in a fluid medium can also be analyzed which are more relevant to the practical design and application of a composite transducer. The fluid medium chosen for the study is water and two situations will be investigated: the composite plate as a transmitter, i.e., under a harmonic electric field, and the composite as a receiver, i.e., under a harmonic acoustic pressure in water.

(2.4.1) Forced Vibration of a Composite Plate in Water under an AC Electric Field

For the sake of convenience, we will treat the system as a symmetric one in which the composite plate is loaded by water on both surfaces, hence, the boundary conditions at the composite-water interface are:

$$T_3^{Cm} = T_3^W, \quad T_5^{Cm} = 0, \quad u_3^{Cm} = u_3^W \quad \text{and} \quad \Phi = \pm\frac{V}{2} \quad \text{at } x_3 = \pm\frac{t}{2} \qquad (25)$$

where superscripts Cm and W denote the quantities in the composite and water, and the factor $e^{-j\omega t}$ is omitted in electric potential Φ. The variational formula for this problem can be derived as

$$\int_{S^{\pm}} \frac{1}{2}\Big[(T_3^W - T_3^{Cm})(\delta(u_3^W)^* + \delta(u_3^{Cm})^*) + (u_3^{Cm} - u_3^W)(\delta(T_3^W)^* + \delta(T_3^{Cm})^*)\Big]dS$$

$$+\int_{S^{\pm}}\Big[(\Phi^{Cm} - \overline{\Phi})\delta(D_3^{Cm})^* - T_5^{Cm}\delta(u_1^{Cm})^*\ \Big]dS = 0 \qquad (26)$$

where $S^{\pm}$ indicates that the integration is over the two composite-water interfaces (at $x_3 = \pm t/2$), and the integration over the volume has been omitted since it is equal to zero.

Here, the expressions for the elastic displacement vectors and the electrical potential Φ in the composite are those in eq. (18) and (19). Because of the periodic nature of the composite plate in the x_1-direction, the solutions in water have the form:

$$u_1^W = j\sum_{n=0}^{J} h_n^W \sin(h_n^W x_1)\exp(\pm j\beta_n^W x_3)R_n^W$$

$$u_3^W = \sum_{n=0}^{J} \beta_n^W \cos(h_n^W x_1)\exp(\pm j\beta_n^W x_3)R_n^W \qquad (27)$$

$$T_3^W = jT_0^W \sum_{n=0}^{J} \cos(h_n^W x_1)\exp(\pm j\beta_n^W x_3)R_n^W$$

where $h_n^W = \frac{2n\pi}{d}$, $\beta_n^W = \sqrt{\frac{\omega^2}{(V^W)^2} - (h_n^W)^2}$, $T_0^W = c^W(\beta_0^W)^2$, $\beta_0^W = \frac{\omega}{V^W}$, $V^W = \sqrt{\frac{c^W}{\rho^W}}$ is the longitudinal wave velocity of water, c^W is the bulk modulus of water. $\pm$ correspond to the solutions in $x_3 > 0$ region and $x_3 < 0$ region, respectively. h and β are the wave vector components in the x_1- and x_3-directions in water. R_n^W is determined by the boundary conditions through the variational principle formula eq. (26).

Substituting equations (18), (19) and (27) into equation (26) yields a set of linear algebraic equations:

$$(M_{ij})(A_j)=(V_i) \qquad (28)$$

where (M_{ij}) is a matrix in which its elements are related to the parameters of water, ceramic and polymer and the geometrical parameters ν and d, as well as ω, β and h. $(A_j)=(A_1, \ldots, A_m, C, R_0^W, \ldots, R_J^W)$, where m and J are the numbers of the eigenfunctions used in the expansions for the quantities in the composite and in water, respectively, and how many eigenfunctions should be used in the expansion depends on the accuracy desired. In this calculation, m=8 and J=6. Hence, (V_i) is a 16×1 matrix which elements depend on the applied voltage V. Equation (28) is solved numerically.

Shown in figure 11(a) is a theoretical electrical impedance curve for a 2-2 composite plate of 44% ceramic volume content and the aspect ratio t/d = 3.8 loaded with water. For the comparison, the experimental curve for the same composite plate is shown in figure 11(b). The agreement between the

experimental result and the theoretical one is quite good. The relatively sharp resonant peaks in the theoretical curve compared with the experimental one are due to the fact that in the theoretical calculation, the elastic and dielectric losses of the composite plate are not included. Comparison between figure 11 with figure 6, which is the electrical impedance for a similar composite plate in air, reveals that the resonance is severely damped in water as shown by the marked broadening of the resonant peaks in the impedance curve. For the lateral modes (modes 1 and 2 in figure 11) which is mainly determined by the shear resonance of the polymer phase in the 2-2 composite investigated, because the acoustic impedance between the polymer and water is very close, the change in the amplitude is quite significant. One interesting feature of the influence of the water loading on a composite plate is the appearance of a mode which is labeled 3 in the figure. It can be shown that the resonant frequency for this mode does not change very much as the thickness of the composite plate changes. From the stress distribution pattern in the water, it is not difficult to show that this mode is related to the coupling between the composite and water and its frequency is determined by the periodicity d and the acoustic wave velocity of water ($f = V^w/d$). And it corresponds to the local oscillation of water within one unit cell.

In analogous to the situation in air, it is also found that in water, at frequencies far below any resonant mode, the ratio of u_3^P / u_3^C is always less than one and will approach one as the aspect ratio t/d increases. As the frequency increases towards the thickness resonant frequency, u_3^P / u_3^C increases towards one. At a frequency f_1 near the thickness resonant frequency f_s, this ratio becomes one and above that, this ratio is larger than one (figure 12(a)). Figure 12(b) presents f_1/f_s and $\Delta f/f_1$ vs. the ratio of d/t for a composite with 44% ceramic content. Clearly, the effect of the aspect ratio t/d on the surface uniformity of a composite plate is to change the frequency position f_1 with respect to the thickness resonance and the frequency width Δf in which u_3^P / u_3^C is near one which are very similar to that found in air. However, the bandwidth $\Delta f/f_1$ in water is larger than that in air, indicating that the surface distribution of the displacement of the two phases is much flatter in water than in air which is quite understandable. Because of the water loading, the vibration amplitude of the polymer phase is significantly reduced. Figure 12(a) shows how the ratio of u_3^P/u_3^c at the composite surface varies with frequency (t/d=4). One noticeable change between the surface profiles in air and in water is that in water, even at the lateral mode frequency, this ratio does not become very large (not shown in the figure since the lateral mode frequency is at about 1.5 MHz).

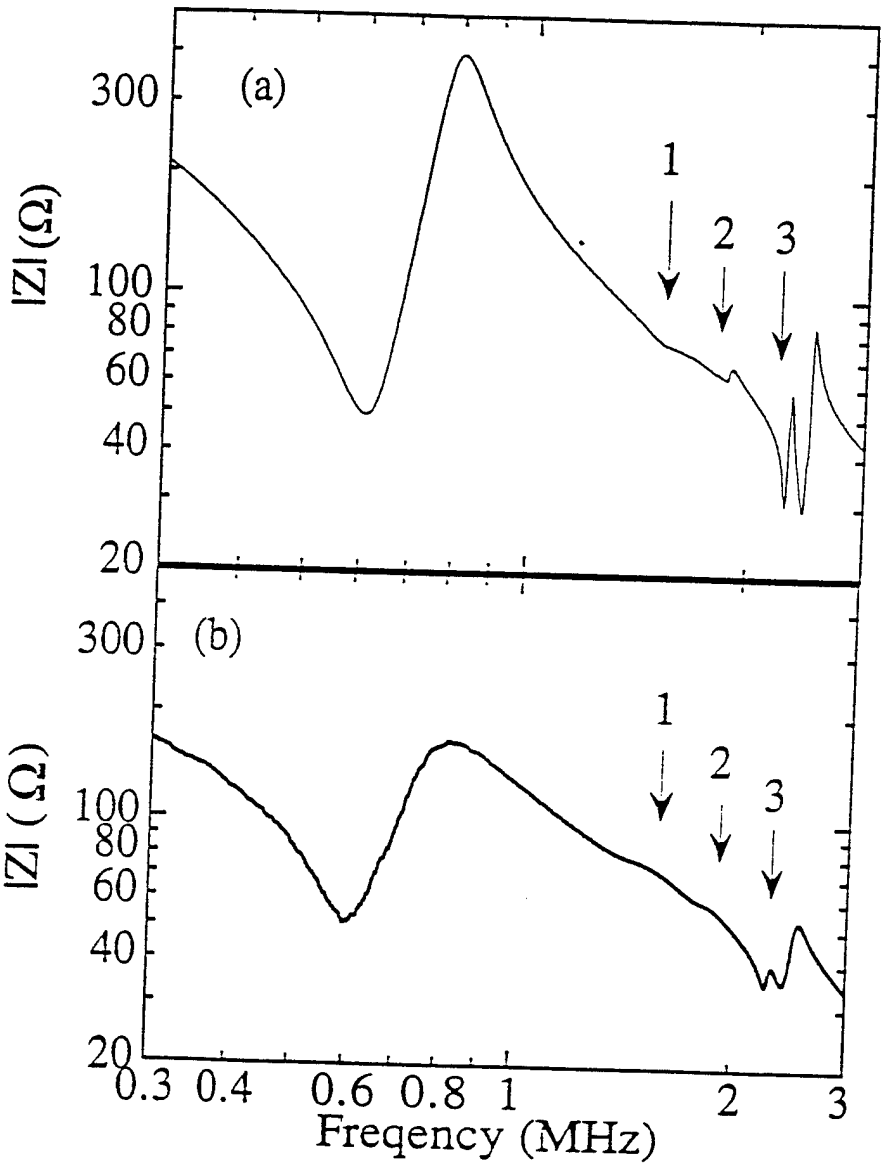

Figure 11. The electrical impedance magnitude for a 2-2 composite of PZT-5H and Spurr epoxy with 44% ceramic content measured in water. The thickness of the composite is t/d=3.8 and d=0.635 mm. (a) is derived from the model and (b) is the experimental results. The modes 1 and 2 are the lateral modes (f_{t1} and f_{t2} in figure 6(c)) and mode 3 arises from the coupling of water to the periodic structure of the composite surface.

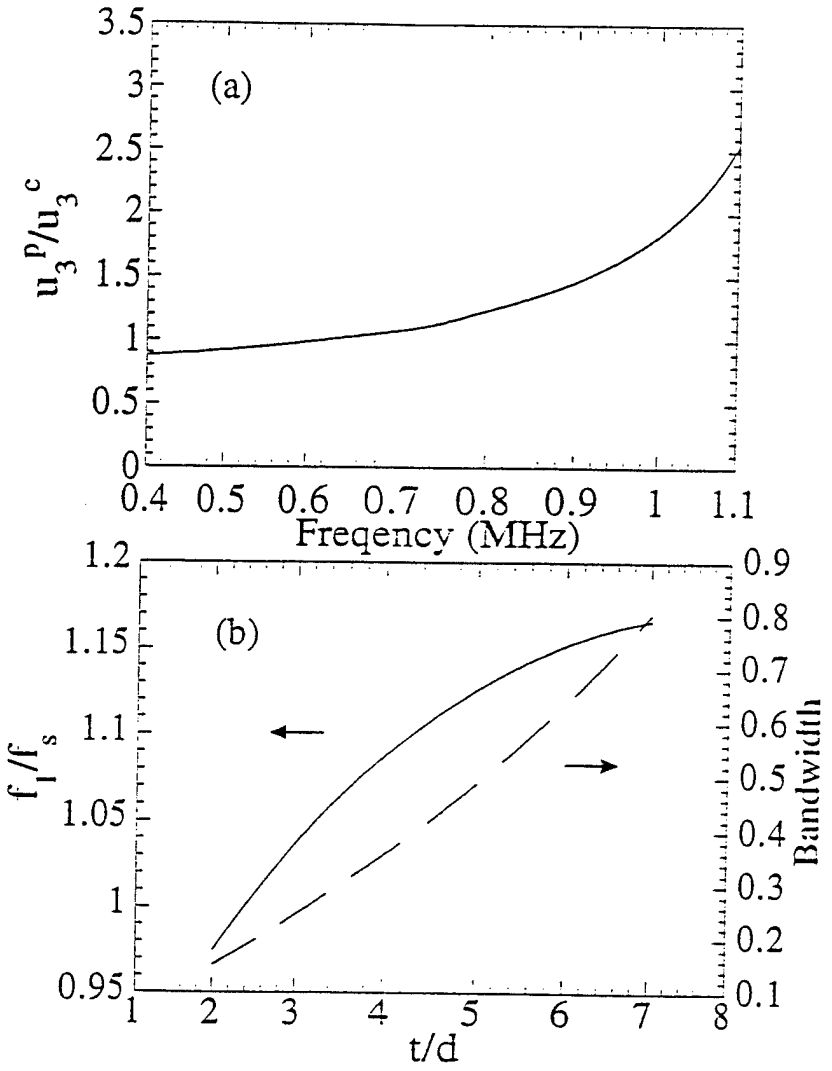

Figure 12. (a) The ratio of u_3^p/u_3^c vs. frequency for a composite made of PZT-5H and Spurr epoxy (44% ceramic content) at a thickness of t/d = 4 (d=0.635 mm) measured in water. u_3^p and u_3^c are the surface displacements at the centers of the polymer plate and ceramic plate, respectively. The results are derived from the model.

(b) The ratio f_l/f_s as a function of d/t of the composite plate, where f_l is the frequency at which $u_3^p/u_3^c=1$ and f_s is the series resonant frequency for the thickness mode. The results are derived from the model.

(c) The bandwidth as a function of d/t of the composite plate. The results here can be compared with those in figure 10 and apparently, and the water loading improves the uniformity of the vibration profile at the composite surface. The results are derived from the model.

(2.4.2) Forced Vibration of a Composite Plate in Water under Harmonic Acoustic Pressure

Now we turn to investigate the vibration behavior of a composite plate in water under harmonic acoustic pressure, that is, to study issues related to the receiving sensitivity of a simple 2-2 composite transducer. For simplicity, we shall restrict the treatment to the symmetric system. In this case, as sketched in figure 13, the incident acoustic waves impinge normally on the two surfaces of the composite plate from opposite directions and the boundary conditions for this problem are:

$$T_3^{Cm} = T_3^W, \quad T_5^{Cm} = 0, \quad u_3^{Cm} = u_3^W \text{ and } D_3^{Cm} = 0 \quad \text{at } x_3 = \pm\frac{t}{2} \tag{29}$$

The appropriate variational formula is

$$\int_{S^=} \frac{1}{2}\left[(T_3^W - T_3^{Cm})(\delta(u_3^W)^* + \delta(u_3^{Cm})^*) + (u_3^{Cm} - u_3^W)(\delta(T_3^W)^* + \delta(T_3^{Cm})^*)\right] dS$$
$$-\int_{S^\pm}\left[D_3^{Cm}\delta(\Phi^{Cm})^* + T_5^{Cm}\delta(u_1^{Cm})^*\right] dS = 0 \tag{30}$$

The expressions of the displacements and electrical potential in the composite plate are those in equations (18) and (19) except now the mode of β=0 should not be included since there is no externally applied electric field. To account for the incident wave in water, equation (27) is modified and the solutions in the $x_3 > 0$ region are:

$$u_1^W = j\sum_{n=0}^{J} h_n^W \sin(h_n^W x_1)\exp(j\beta_n^W x_3)R_n^W$$
$$u_3^W = -\beta_0 \exp(-j\beta_0 x_3) + \sum_{n=0}^{J} \beta_n^W \cos(h_n^W x_1)\exp(j\beta_n^W x_3)R_n^W \tag{31}$$
$$T_3^W = jT_0^W\left[\exp(-j\beta_0 x_3) + \sum_{n=0}^{J}\cos(h_n^W x_1)\exp(j\beta_n^W x_3)R_n^W\right]$$

where the term of $-\beta_0 \exp(-j\beta_0 x_3)$ corresponds to the incident plane wave. By substituting equations (18), (19) and (31) into (30), we obtain a set of linear algebraic equations:

$$(M_{ij})(A_j)=(V_i) \tag{32}$$

where (M_{ij}) is a 15x15 matrix, $(A_j)=(A_1,\ldots, A_m, R_0^W, \ldots, R^W)$ with m=8 and J=6, and (V_i) is a 15×1 matrix related to the incident wave. By solving equation (32) one can obtain all of the properties related to the behaviors of a composite plate under a harmonic acoustic pressure.

Shown in figure 14 is the open circuit voltage receiving sensitivity V/p, where V is the voltage output and p is the pressure of the incident wave, for a 44% 2-2 composite plate at the thickness resonance vs. d/t for the thickness resonance mode where the cross over region (point B in figure 2) is at d/t = 0.65.[26] That is, at d/t < 0.65, the thickness mode is in the first branch of the dispersion curves and above that, the thickness resonance is at the second branch of the dispersion curves where the polymer and ceramic vibrate out of phase. Since the problems treated in this paper are related only to

the piezo-materials, the open-circuit receiving sensitivity is used here which, as pointed out by Kojima, is a system independent parameter.[26] The bandwidth is defined as the 3dB width about the peak frequency (f_p for the receiving mode). For a single phase material, it can be derived from the KLM model that the sensitivity here should be proportional to t, the thickness of the transducer. Hence, in figure 14, the V/p vs. d/t curve for a single phase material should fall off as t (solid line in the figure) while the bandwidth should stay constant. The results show that the sensitivity of the thickness mode for a 2-2 composite decreases slowly as d/t becomes larger than 0.4, but the bandwidth increases gradually. The increase in the bandwidth is due to the merger of the two resonant modes in water. After that, there are anomalous changes in both the bandwidth and the sensitivity in the cross-over region. At higher values of d/t (thin composite plates), both the sensitivity and the bandwidth fall much below the values of single phase material (solid line). If we define the figure of merit (FOM) here as the product of sensitivity and bandwidth, as shown in figure 14(b), at $d/t < 0.5$, the FOM falls off with t. At $d/t > 0.5$, the FOM drops to much smaller value. Therefore, in order to gain a high receiving sensitivity and a broad bandwidth of a 2-2 composite transducer, it is desirable to have d/t less than 0.5. The results here can be compared with what shown in figures 2, 8, 9, and 12. At d/t above 0.5, the coupling factor shows a precipitous drop (figure 9) and the thickness mode frequency also shows an apparent deviation from the extrapolated value (the dashed line in figure 2). Figure 8 also shows that there is a significant coupling between the two modes. Although the results presented are for a composite with 44% ceramic content, it is approximately true for composites with other volume fractions.

In general, the maximum transmitting voltage sensitivity of a transducer is at a frequency near f_s and the maximum open circuit receiving sensitivity is near f_p of the thickness mode ($f_p > f_s$), and hence it is expected that the influence of the lateral mode (hence, the aspect ratio t/d) will be more severe on the receiving sensitivity. From the data analysis, it is shown that when an FOM which is the product of the sensitivity and the bandwidth is introduced as the criterion of the performance of a composite transducer as a receiver, the performance deteriorates when $d/t > 0.5$ for the composite discussed here. Experimental results confirm this finding where as shown in figure 15, the insertion loss of a 2-2 piezocomposite shows large increases at d/t near and above 0.5.[27]

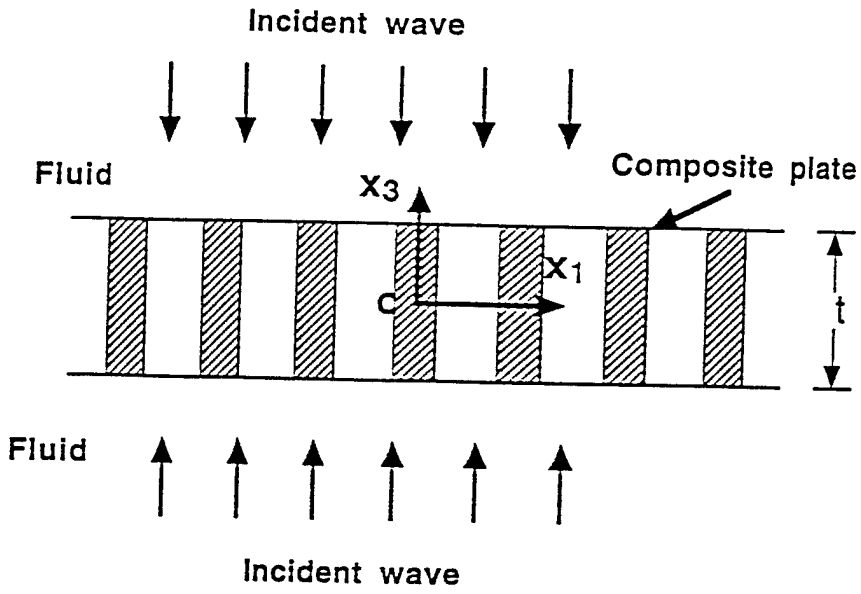

Figure 13. Schematic drawing of a 2-2 composite plate under normal incident of a pressure wave from the water.

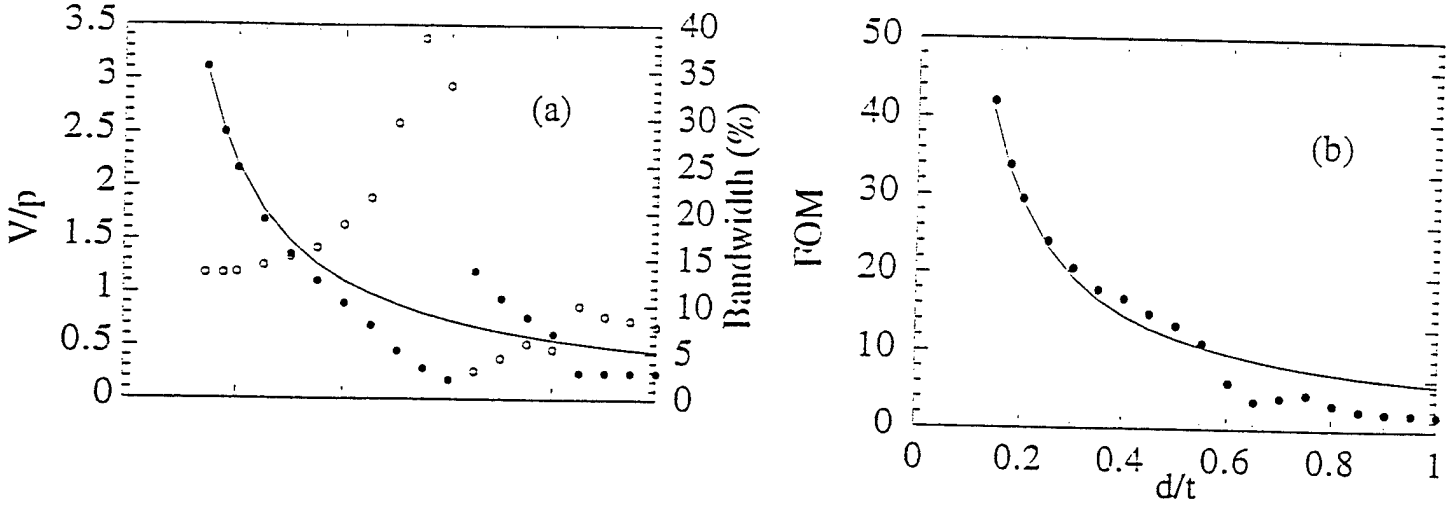

Figure 14. (a) The influence of the unit cell dimension ratio of d/t on the open circuit voltage sensitivity of a 2-2 composite with 44% PZT-5H and Spurr epoxy matrix. Solid dots are V/p at the peak frequency (f_p) and the solid line is the sensitivity of a single phase material with the effective properties of the composite. The results are derived from the model.

(b) The 3 dB bandwidth as a function of d/t for a composite transducer derived from the model.

(c) FOM (solid dots, the product of the sensitivity and the bandwidth) for the 2-2 composite in (a) as a function of d/t. The solid line is FOM for a single phase material with the effective properties of the composite. At d/t > 0.5, FOM drops much below the single phase material value. The results are derived from the model.

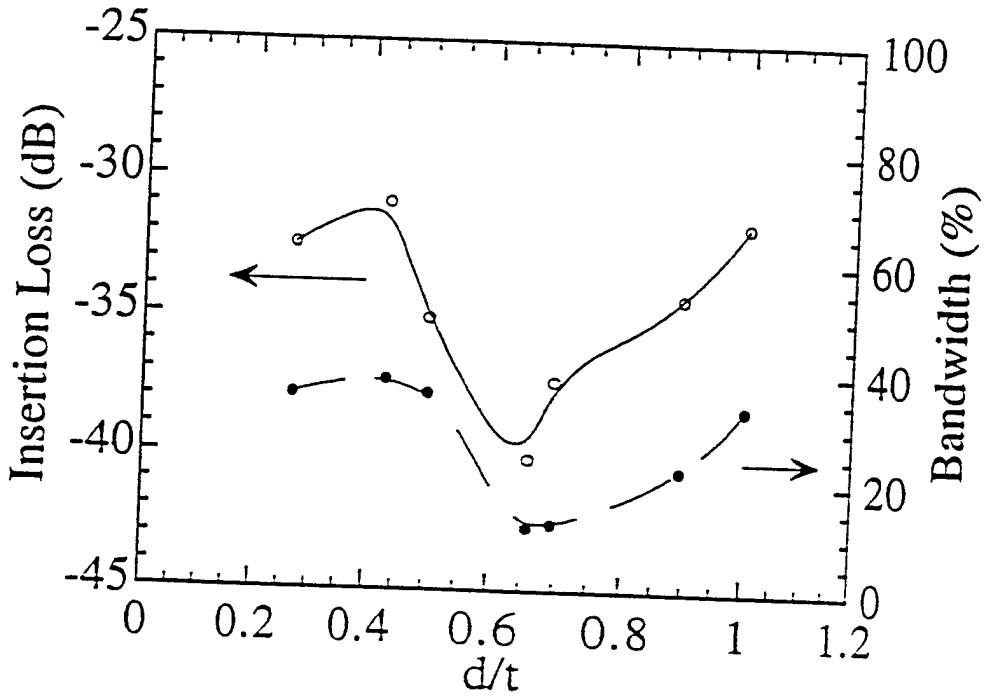

Figure 15. The experimental data on the insertion loss (open circles) and 6 dB bandwidth (solid dots) of 2-2 composites with 44% volume content of PZT-5H and Spurr epoxy polymer matrix measured by the pulse echo method for different ratio of d/t (d=0.635 mm). The solid lines are drawn to guide eyes.

III. Plane Wave Propagation at an Interface of a Medium-2-2 Piezocomposite and the Effective Impedance of the Composite[28,29]

In this section, the piezoceramic polymer composites used in the model calculations and in experiments are those made of PZT-5H piezoceramic and Spurrs epoxy polymer matrix (see Table I).

3.1. Plane acoustic wave propagation at a fluid-2-2 composite interface:

(3.1.1) Eigen-modes and eigen-functions in the 2-2 composite and fluid medium

When a plane acoustic wave encounters a boundary between two media, energy is reflected and transmitted from and across the boundary. In this section, we shall derive the former formula used to treat the plane wave transmission and reflection at the interface between a fluid and a piezoceramic polymer composite of 2-2 connectivity. The schematic of the interface system is shown in figure 16 where a plane acoustic wave is normally incident upon the boundary between a fluid and a 2-2 piezocomposite. The coordinate system is chosen such that the x_3-axis is perpendicular to the interface, the x_1-axis is parallel to the interface as shown in the figure, and the x_2-axis is perpendicular to both the x_1 and x_3 axes (pointing out of the paper). The fluid occupies the space of $x_3 < 0$ and the 2-2 composite is in $x_3 > 0$. To the problems treated, apparently, the periodic lamina structure of the composite in the x_1-direction causes variations of the acoustic and

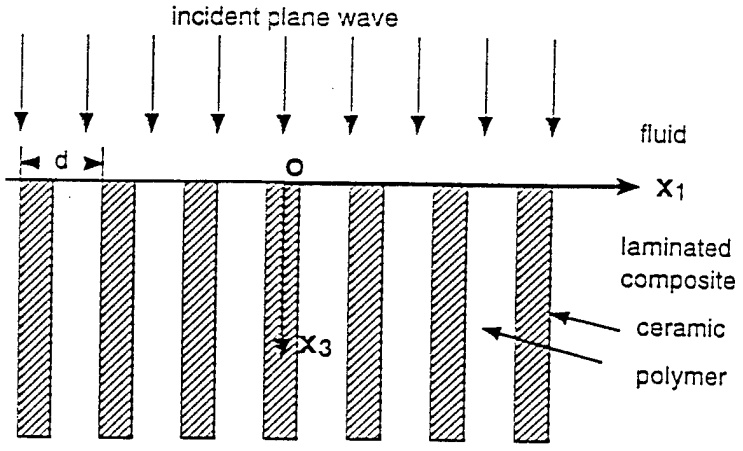

Figure 16. Schematic of an interface between a fluid and a 2-2 piezocomposite where a plane acoustic wave normally incidents to the interface from the fluid medium. The composite occupies the semi-infinite space $x_3 > 0$.

electric fields in that direction and the interface between the composite and fluid introduces variations of these fields in the x_3-direction.

The eigenmodes and eigen-functions for a 2-2 piezocomposite have been derived in the section 2.1 and section 2.2.

The boundary conditions at the fluid-2-2 composite interface for the problem are

$$T_{33}^{Cm} = T_{33}^{W},\ T_{13}^{Cm} = 0, u_3^{Cm} = u_3^{W}$$
$$\Phi^{Cm} = \Phi^{W},\ D_3^{Cm} = D_3^{W} \qquad \text{at } x_3=0 \qquad (33)$$

The superscripts Cm and W represent the 2-2 composite and the fluid. And Φ is the electric potential.

In the fluid medium, the constitutive relation has the form

$$T_{11} = T_{33} = \lambda^{W}\left(\frac{\partial u_1}{\partial x_1} + \frac{\partial u_3}{\partial x_3}\right) \qquad (34)$$

where λ^W is the bulk modulus of the fluid. The periodic condition in the x_1-direction due to the composite structure also imposes the constraints on the solutions in the fluid region:

$$u_1^{W} = jh_n^{W}\sin(h_n^{W}x_1)\exp(j\beta_n^{W}x_3)R_n^{W}$$
$$u_3^{W} = \beta_n^{W}\cos(h_n^{W}x_1)\exp(j\beta_n^{W}x_3)R_n^{W} \qquad (35)$$

where $h_n^W = \frac{2n\pi}{d}$ and $\beta_n^W = \sqrt{\frac{\omega^2}{(V^W)^2} - (h_n^W)^2}$ (n=0,1,2,3...) are the wave vector components in the x_1- and x_3-directions in the fluid region, $V^W = \sqrt{\frac{\lambda^W}{\rho^W}}$ is the longitudinal wave velocity of fluid, and the superscript W denotes the quantities in the fluid medium. In eq. (35), R_n^W is an undetermined constant.

(3.1.2) Variational formula on the boundary problem at the composite-fluid interface

In order to satisfy the boundary conditions at the composite-fluid interface, the elastic and electric fields in the two regions are expanded in terms of the eigenfunctions obtained. The coefficient of each mode is determined by the variational method as briefly outlined in this section. The variational formula for the problem here is:

$$\int_S \frac{1}{2}[(T_{33}^{W} - T_{33}^{Cm})(\delta u_3^{W} + \delta u_3^{Cm})^* - 2T_{13}^{Cm}(\delta u_1^{Cm})^*$$
$$+ (u_3^{Cm} - u_3^{W})(\delta T_{33}^{Cm} + \delta T_{33}^{W})^* + (D_3^{W} - D_3^{Cm})(\delta\Phi^{W} + \delta\Phi^{Cm})^* \qquad (36)$$
$$+ (\Phi^{W} - \Phi^{Cm})(\delta D_3^{W} + \delta D_3^{Cm})^*]dS = 0$$

where the surface integral is performed at x_3=0 over one unit cell ($-\frac{d}{2} \le x_1 \le \frac{d}{2}$), W and Cm refer to the fluid and composite, respectively, and * denotes the complex conjugate.

For the situation considered here, in the fluid medium, there are incident wave and reflected wave, therefore, in terms of the eigenfunctions in the fluid medium, the elastic displacement and electric potential in the fluid can be expressed as

$$
\begin{aligned}
u_1^W &= j \sum_{n=0}^{G} h_n^W \sin(h_n^W x_1)\exp(-j\beta_n^W x_3) R_n^W \\
u_3^W &= \beta_0^W \exp(j\beta_0^W x_3) - \sum_{n=0}^{G} \beta_n^W \cos(h_n^W x_1)\exp(-j\beta_n^W x_3) R_n^W \\
\Phi^W &= \sum_{n=0}^{G} \cos(h_n^W x_1)\exp(h_n^W x_3) R_n^W
\end{aligned}
\tag{37}
$$

where $\beta_0^W = \frac{\omega}{V^W}$ and $\beta_0^W \exp(j\beta_0^W x_3)$corresponds to the incident wave normal to the interface. R_n^W are the coefficients determined by equation (36).

In the composite region, only the transmitted wave exists. However, the expressions for the elastic and electric variables in the ceramic phase and in the polymer phase are different. In the ceramic phase, the elastic displacements and the electric potential are

$$
\begin{aligned}
u_3^C &= \sum_{n=1}^{m}\sum_{i=1}^{3} R_{ni}^C f_{ni}^C \cos(h_{ni}^C x_1)\exp(j\beta_n x_3) A_n \\
u_1^C &= j \sum_{n=1}^{m}\sum_{i=1}^{3} R_{ni}^C g_{ni}^C \sin(h_{ni}^C x_1)\exp(j\beta_n x_3) A_n \\
\Phi^C &= \sum_{n=1}^{m}\sum_{i=1}^{3} R_{ni}^C t_{ni}^C \cos(h_{ni}^C x_1)\exp(j\beta_n x_3) A_n
\end{aligned}
\tag{38}
$$

and in the polymer phase, they are

$$
\begin{aligned}
u_3^P &= \sum_{n=1}^{m}\sum_{i=1}^{2} R_{ni}^P f_{ni}^P \cos(h_{ni}^P (x_1 - \frac{d}{2}))\exp(j\beta_n x_3) A_n \\
u_1^P &= j \sum_{n=1}^{m}\sum_{i=1}^{2} R_{ni}^P g_{ni}^P \sin(h_{ni}^P (x_1 - \frac{d}{2}))\exp(j\beta_n x_3) A_n \\
\Phi^C &= \sum_{n=1}^{m} C_n^P \cosh(\beta_n (x_1 - \frac{d}{2}))\exp(j\beta_n x_3) A_n
\end{aligned}
\tag{39}
$$

where A_n are coefficients to be determined from eq. (36). In the expansions (37), (38) and (39), the number of modes used are determined by the accuracy needed. Making use of the constitutive equations in the ceramic and polymer phases, the stress and electric displacement in the composite

region can be obtained. Substituting these quantities into eq. (36) yields the following algebraic equation:

$$(M_{ij})(R_j) = (V_i) \tag{40}$$

where $(R_j)=(R_0, R_1,\ldots R_G, A_1,\ldots A_m)^T$, (M_{ij}) is a (G+m+1)×(G+m+1) matrix, and (V_j) is a (G+m+1)×1 matrix. In the problem treated, G=7 and m=9 are used. From eq. (40), the coefficients R_j and A_j are determined.

(3.1.3) Reflection coefficient and input acoustic impedance

For an acoustic transducer to function effectively, it is highly desirable that nearly all of the acoustic energy arriving at the interface be transmitted across the boundary, which implies a minimum in the reflected wave. In this section, we will first derive the reflection coefficient for a composite in contact with water based on the results derived in the preceding sections. As we have pointed out, in the expression (37), $\beta_0^w \exp(j\beta_0^w x_3)$is the incident wave and other terms are from the reflected wave. The zeroth order reflected wave, i.e., n=0 and $h_0{}^w=0$, represents the normal reflection. For $n\neq 0$, in the frequency of interest, i.e., below the first lateral mode frequency, it can be shown that $\beta_n{}^w$ is nearly equal to $j\,(2n\pi/d)$ which implies that the amplitude of these waves will decay as $\exp(-2n\pi x_3/d)$ as the waves depart from the interface and hence they are evanescent waves which are important only in the boundary region. In this sense, the reflection coefficient which can be measured experimentally is equal to $-R_0$.

Figure 17(a) shows the reflection coefficient derived for a plane acoustic wave on the boundary between water and a 2-2 composite in which the volume fraction of ceramic phase is 44%. At lower frequencies where the periodicity d of the 2-2 composite in the x_1-direction is much smaller than the wavelength of the incident wave, the 2-2 composite behaves like an effective homogeneous medium, and the reflection coefficient is real and can be fully characterized by the acoustic impedance of the two materials, i.e., the effective acoustic impedance of the composite derived based on effective medium theory and the characteristic impedance of water.[3.30] As the frequency increases, however, the vibrational displacement at the surface of the 2-2 composite becomes nonuniform, which implies that it could no longer be regarded as a homogeneous medium. Hence, the reflection coefficient at the water and composite interface will be dispersive and become a complex number as shown in figure 17(a) where the magnitude of the reflection coefficient decreases gradually and meanwhile, the phase of the reflection coefficient becomes larger than 180° and increases with frequency. To verify the result, an experiment was conducted to measure the reflection coefficient from the interface between water and a 2-2 composite of 44% ceramic. The schematic of the experimental set-up is shown in figure 18, where

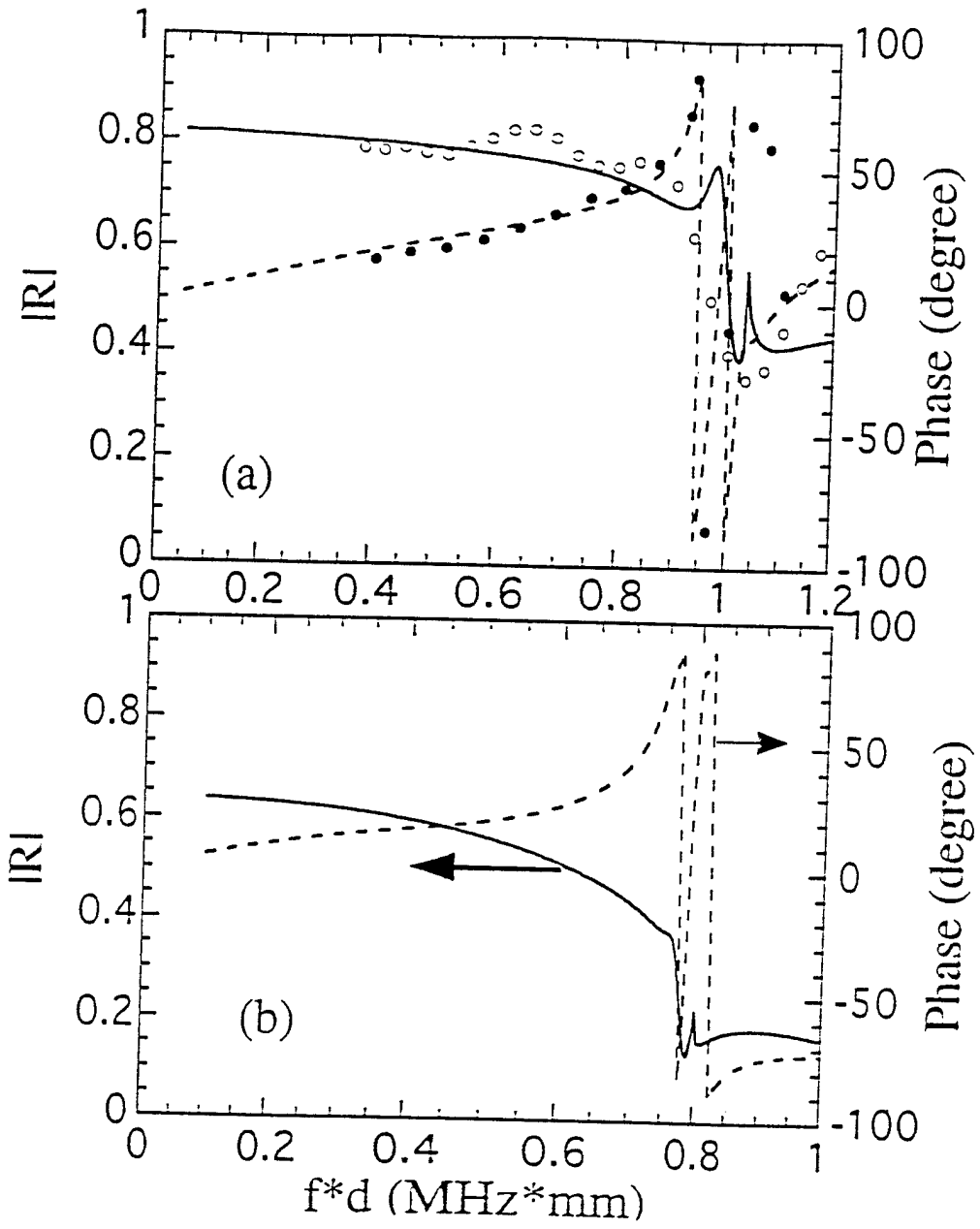

Figure 17. The reflection coefficient (both the amplitude and phase) as a function of frequency for 2-2 composites with (a) 44% ceramic and (b) 15% ceramic content. The anomalous changes at fd = 1 in (a) and fd = 0.8 in (b) are related to the lateral resonant mode in these composites, respectively. The experimental data are shown in (a) where the open circles are the amplitude and solid circles are the phase of the measured reflection coefficient.

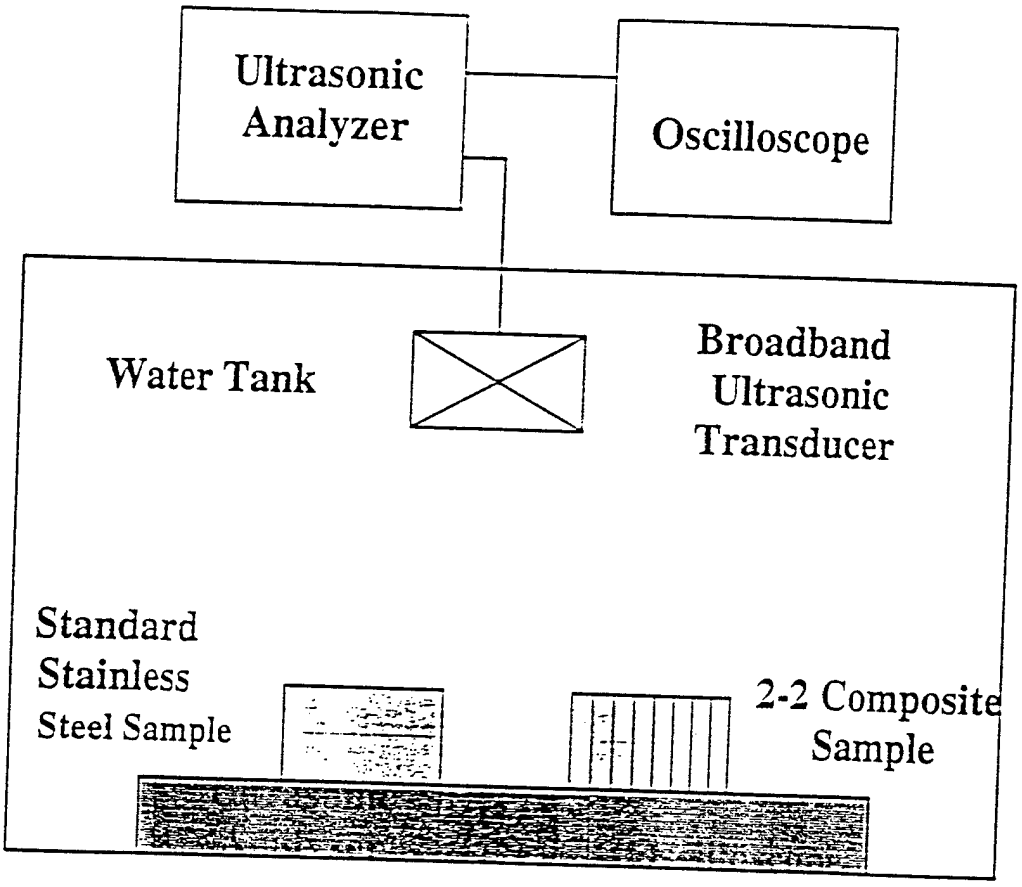

Figure 18. Schematic of the set-up used to measure the reflection coefficient of 2-2 composites. In order to obtain phase information of the reflection coefficient, the distance between the probe transducer and the 2-2 composite is maintained the same as that between the probe and the stainless steel standard.

the reflected signals, both the amplitude and time delay, from a 2-2 composite of 44% ceramic volume and a standard reflector made of a stainless steel rod, were compared. Since the acoustic impedance of the stainless steel standard is know, the reflection coefficient from the water-composite interface can be determined. To approximate the plane wave condition, the distance between the transducer and the water-composite interface is smaller than the radius of the transducer. The result thus obtained is shown in figure 17(a). The agreement between the model result and experimental result is quite good.

In figure 17(b), the reflection coefficient for a 2-2 composite with 15% ceramic content is presented. Clearly, the trend is quite similar to that in figure 17(a), although the magnitude and the phase of the reflection coefficient are more sensitive to the frequency of incident wave which is apparently due to the small volume content of the ceramic phase in the composite and lower lateral mode frequency (fd -- 0.8 Mhz*mm).

One important parameter related closely to the reflection and transmission of an acoustic wave at an interface is the acoustic impedance of the media at the two sides of the boundary which also depends on the nature of the wave such as plane wave or spherical wave.[2,13] For homogeneous isotropic materials, the acoustic impedance for a plane wave is the characteristic acoustic impedance which is simply the product of the mass density ρ and the wave (longitudinal wave or shear wave) velocity V.[19,31,32] For nonuniform materials (such as piezocomposite materials), on the other hand, no characteristic impedance can be defined in such a simple manner due to the dispersive nature of the properties as has been shown. However, the acoustic impedance of a material can still be found, for example, from the reflection coefficient or other methods. It should be pointed out that although there exist several definitions for determining the acoustic impedance at an interface (input acoustic impedance), and for a heterogeneous material, the results obtained by using different definitions may not be the same.[33,34] However, since the input acoustic impedance is not a direct physical quantity but rather a parameter introduced for the convenience of the analysis, a situation in analogy to the complex notation introduced in many engineering fields, which definition is more appropriate really depends on the situation where it is used. In dealing with the energy transfer across an interface, one might have to use the formula derived under energy flow consideration. On the other hand, in designing matching layers and dealing with the reflection and transmission of acoustic waves in a multilayer medium, the amplitude and phase of the wave components are crucial which may not be included in the coefficients related to the transmission and reflection of the acoustic energy. In the discussion here, we will adopt the definition related to the wave reflection and transmission problems.[30,33]

From the reflection coefficient R, the input acoustic impedance of the composite at the interface can be found as

$$Z_{in} = \frac{1-R}{1+R} Z^{W} \tag{41}$$

where Z_{in} is the effective input impedance of the 2-2 composite, Z^{W} is the characteristic impedance of water. Using the results in figure 17, the effective input acoustic impedance of 2-2 composites with 44% and 15% ceramic volume content is evaluated and presented in figures 19(a) and 19(b). Apparently, there is a large change of the magnitude and phase of the input acoustic impedance as the frequency increases. For the comparison, the acoustic impedance is also evaluated from eq. (41) where only the magnitude of the reflection coefficient is used and shown in figure 19. Clearly, the results show how erroneous it can be if the phase information in the reflection coefficient is ignored.[35]

In analogy to the electrical impedance, the specific impedance at the interface can also be found from the ratio of the stress (in analogy to the voltage) to the displacement velocity (in analogy to the current):

$$Z(x_1, 0) = \frac{T_3^{Cm}(x_1, 0)}{v_3^{Cm}(x_1, 0)} \tag{42}$$

where v_3^{Cm} is the particle displacement velocity in the 2-2 composite. Eq. (42) is used widely in the equivalent circuit model of transducers.[36-38] Apparently, for a 2-2 composite considered, Z from eq. (42) is a function of x_1 due to the variation of T_3 and v_3 in that direction. To eliminate this variation, the approach taken by Miller and Pursey is adopted here.[33] That is, the averaged T_3 and averaged v_3 in the x_1-direction are used:

$$Z_{in} = \frac{\int T_3^{Cm}(x_1,0)dx_1}{\int v_3^{Cm}(x_1,0)dx_1} \tag{43}$$

where the integration is taken in one unit cell. This expression seems physically meaningful since it reflects an averaged mechanical impedance of the composite at the interface. Z_{in} calculated from eq. (43) for composites with 44% and 15% ceramic contents is shown in figure 20 which is quite close to those in figure 19. In the following discussion, eq. (43) is used to calculate Z_{in} in the composite.

One interesting question one might ask is whether the acoustic impedance of the fluid phase will affect the effective input impedance of the composite at the interface. To answer this question, the effective input impedance of the composite at the interface is evaluated for fluid phases with different acoustic impedance (by varying the bulk modulus) and the results are presented in figure 21. Clearly, the effective acoustic impedance of a 2-2 composite is independent of the acoustic impedance of the fluid at the interface.

In order to shed light on the large change of the input acoustic impedance with frequency, the surface displacement u_3 is evaluated at the center of the ceramic plate (x_1=0) and polymer plate (x_1=d/2)

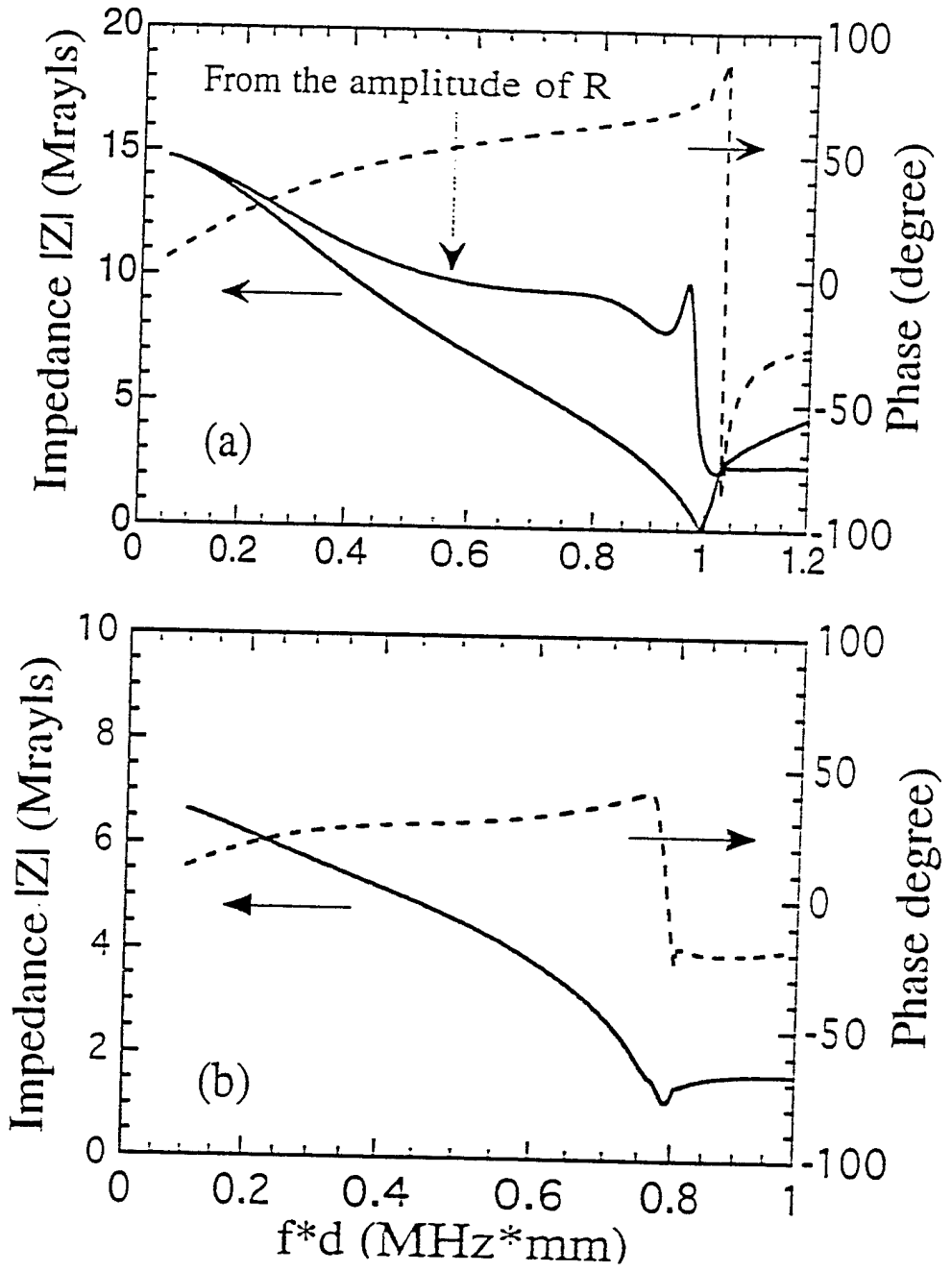

Figure 19. (a) The effective input acoustic impedance Zin of the 2-2 composite with 44% ceramic content calculated from the data in figure 3 (the reflection coefficient). For the comparison, Zin calculated from eq. (14) where only the amplitude of R is used. The results demonstrate the importance of the phase information which (b) Zin for the 2-2 composite with 15% ceramic volume content.

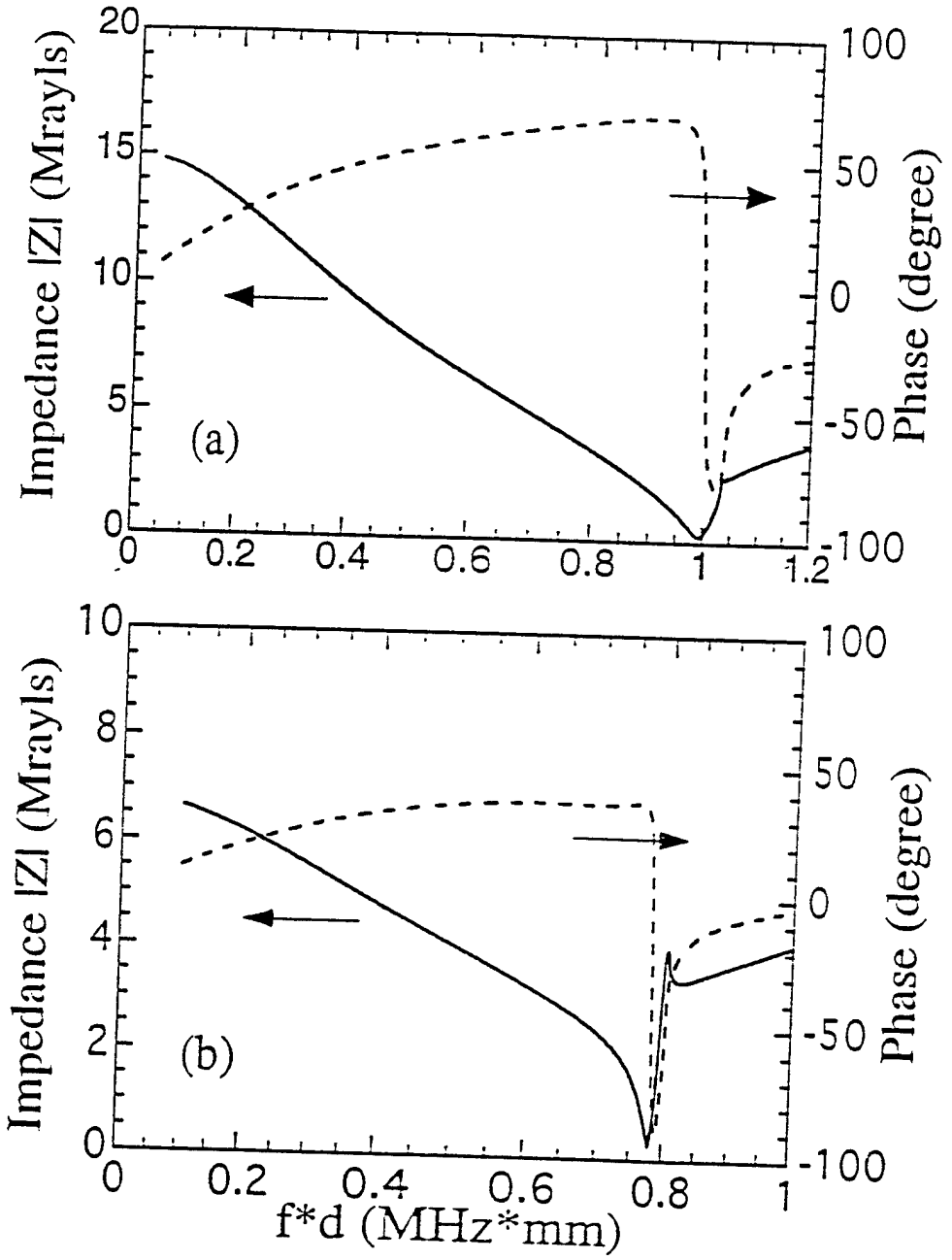

Figure 20. The effective input impedance Z_{in} calculated from eq. (16) for (a) the composite of 44% ceramic volume content and (b) the composite of 15% ceramic content. The results here are nearly the same as those in figure 5 except at frequencies above the first lateral mode.

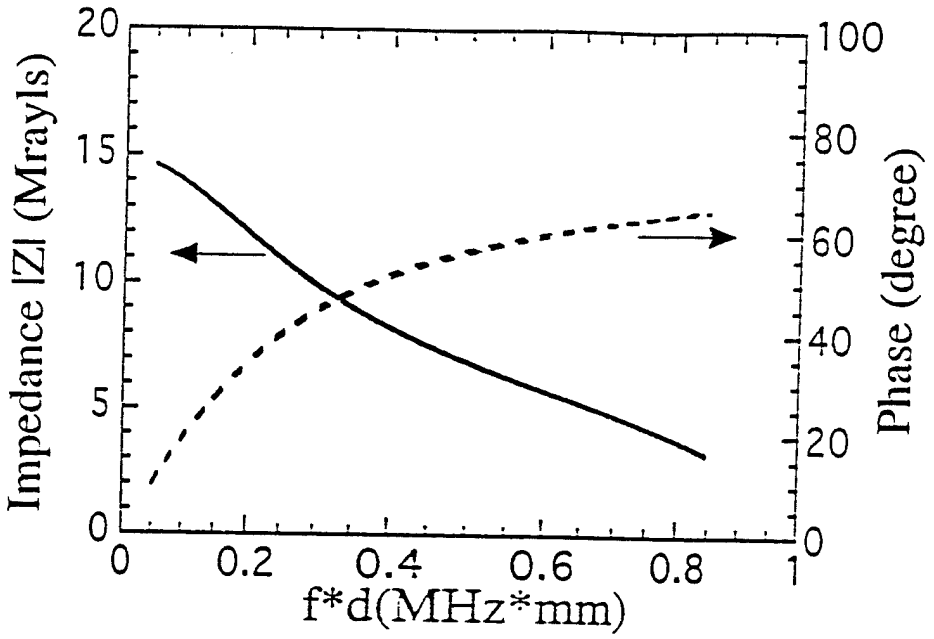

Figure 21. Z_{in} of the composite of 44% volume content derived from the reflection coefficient for fluid media with different acoustic impedance: Z_1 = 1.48 Mrayls (water), and Z_2= 2.09 Mrayls. Apparently, Z_{in} of the composite for the two cases overlaps with each other indicating that it does not change with the acoustic impedance of the fluid medium.

and the results are presented in figure 22(a). At low frequencies, the surface displacements in the polymer and ceramic regions are in unison which indicate that the isostrain model used in many earlier modelings on ultrasonic composite transducers is valid in this frequency region.[3,30] As the frequency increases, even at frequencies still far below the first lateral mode (at fd near 1), the surface vibration amplitudes in the two regions become quite different. At the frequency near the first lateral mode, the vibrations in the polymer and ceramic regions are 180 out of phase and in this frequency region, the effective input acoustic impedance of the composite is very near that of water and the reflection coefficient exhibits a minimum as shown in figure 17.

As we have pointed out in the introduction, for an ultrasonic piezoceramic polymer composite, one of the most important factors in determining the performance is the effective acoustic energy exchange between the ceramic and the external medium. As we have seen in figure 17 and 19 where at frequencies near the lateral mode, the input acoustic impedance of the composite is close to that of water and the reflection coefficient reaches a minimum, the question is how much of that energy enters into the ceramic plates. Figure 22(b) shows how the total acoustic powers entering into the ceramic region and polymer region vary with frequency. Clearly, at the high frequency region, in spite of the

fact that the effective transmission coefficient of the composite increases, the amount entering into the ceramic plate actually decreases.

It is also interesting to examine how this acoustic energy distribution in the polymer and ceramic regions changes along the x_3-direction since the interaction between the ceramic and polymer through the joint region will cause the acoustic energy transfer between the two. In figure 23, the acoustic energy distribution along the x_3-direction at three frequencies ($f << f_t$, $f -- f_t/2$, and $f -- f_t$, where f_t is the first lateral mode frequency) is shown. In all the cases, there is a redistribution of the acoustic energy along the x_3-axis and the acoustic energy in the polymer is gradually transferred to the ceramic plate. However, at low frequencies, the transition region is much shorter than that at high frequencies (with respect to the wave length at that frequency). For instance, in figure 23(a), the reduced length x_3/λ is about 0.01 for the acoustic power in the ceramic to reach 90% of the final value, while in figure 23(b), this region increases to about 0.1, and in figure 23(c), it becomes near 0.2. It should be reminded that in a thickness mode transducer, the thickness of the piezocomposite is $\lambda/2$.

In figure 24, the change of the displacement u_3 in the polymer and ceramic regions along the x_3-direction at the three frequencies is presented and it shows that at high frequencies, the displacement amplitude in the polymer and ceramic regions is no longer the same even deep inside the composite.

The change of the input acoustic impedance from eq. (43) along the x_3-direction in the composite is also evaluated. Figure 25 are the results of the 2-2 composite with 44% ceramic content at different frequencies. Apparently, at high frequencies there is a large change of the effective acoustic impedance from the surface into the interior of the composites and even in the interior of the composite, the effective impedance is not the same as that derived from the effective medium theory.[3,30]

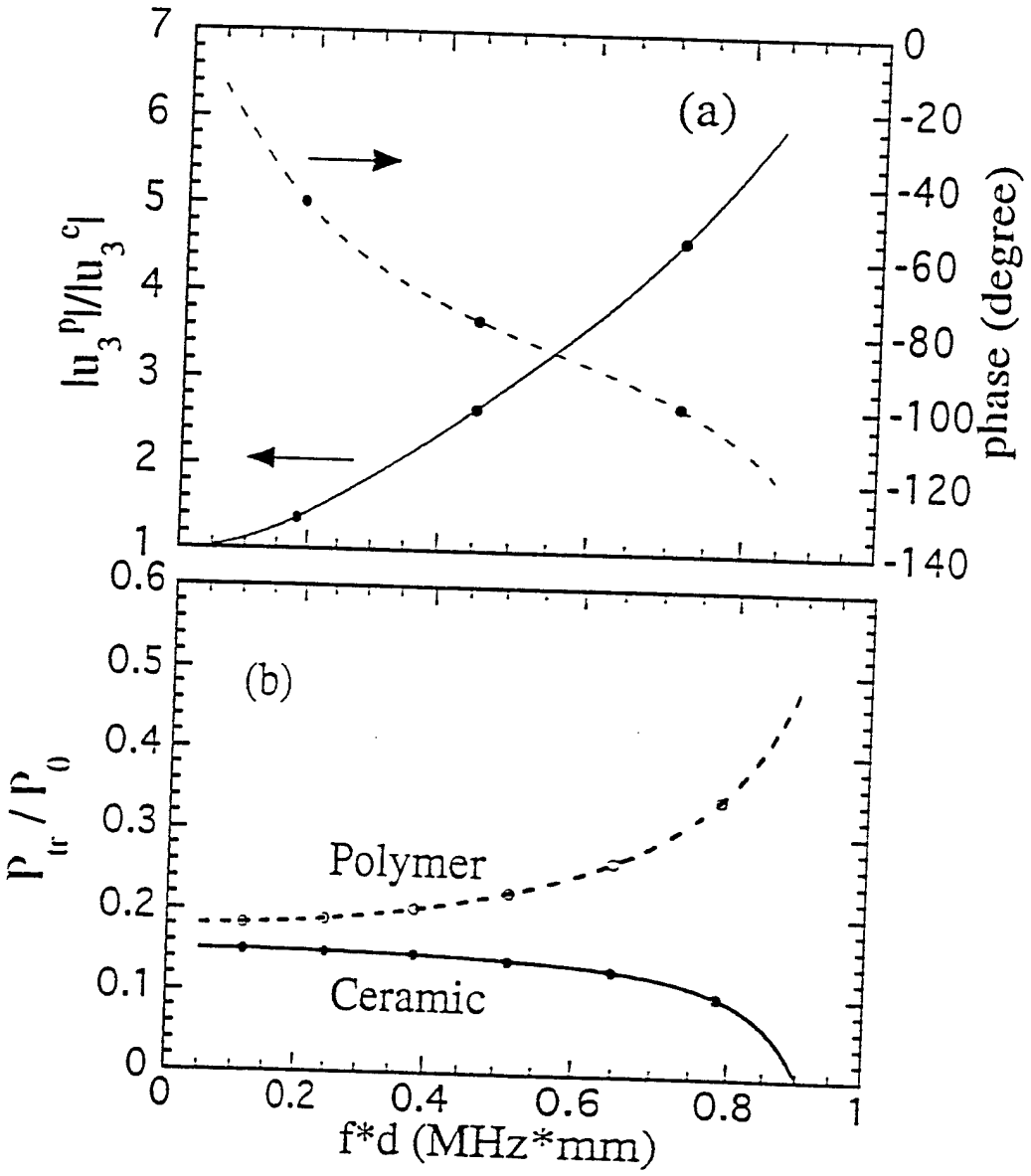

Figure 22. (a) The surface vibration distribution as a function of frequency for the 2-2 composite with 44% ceramic content at the interface with water and under an acoustic field. u_3^p and u_3^c are the displacement at the center of the polymer plate (x_1=d/2) and ceramic plate (x_1=0). (b) The acoustic energy (in reduced units) entering the ceramic and polymer regions as a function of frequency evaluated at the interface (x_3=0) where P_0 the total energy in the incident wave.

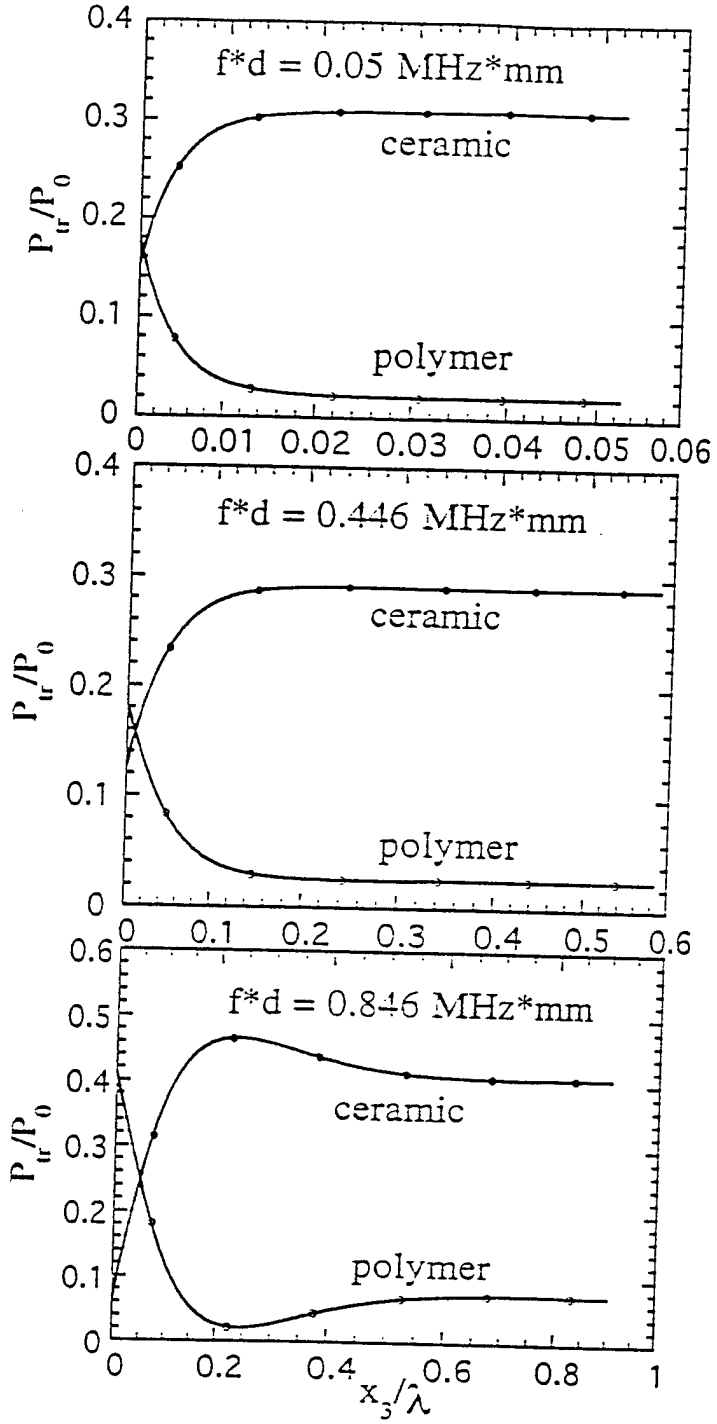

Figure 23. The energy redistribution inside the composite along the x_3-direction where x_3=0 is the interface. There is an energy transfer from the polymer to the ceramic inside the composite. As shown in the figures, the width of the transition region increases as the frequency increases (in reduced length unit).

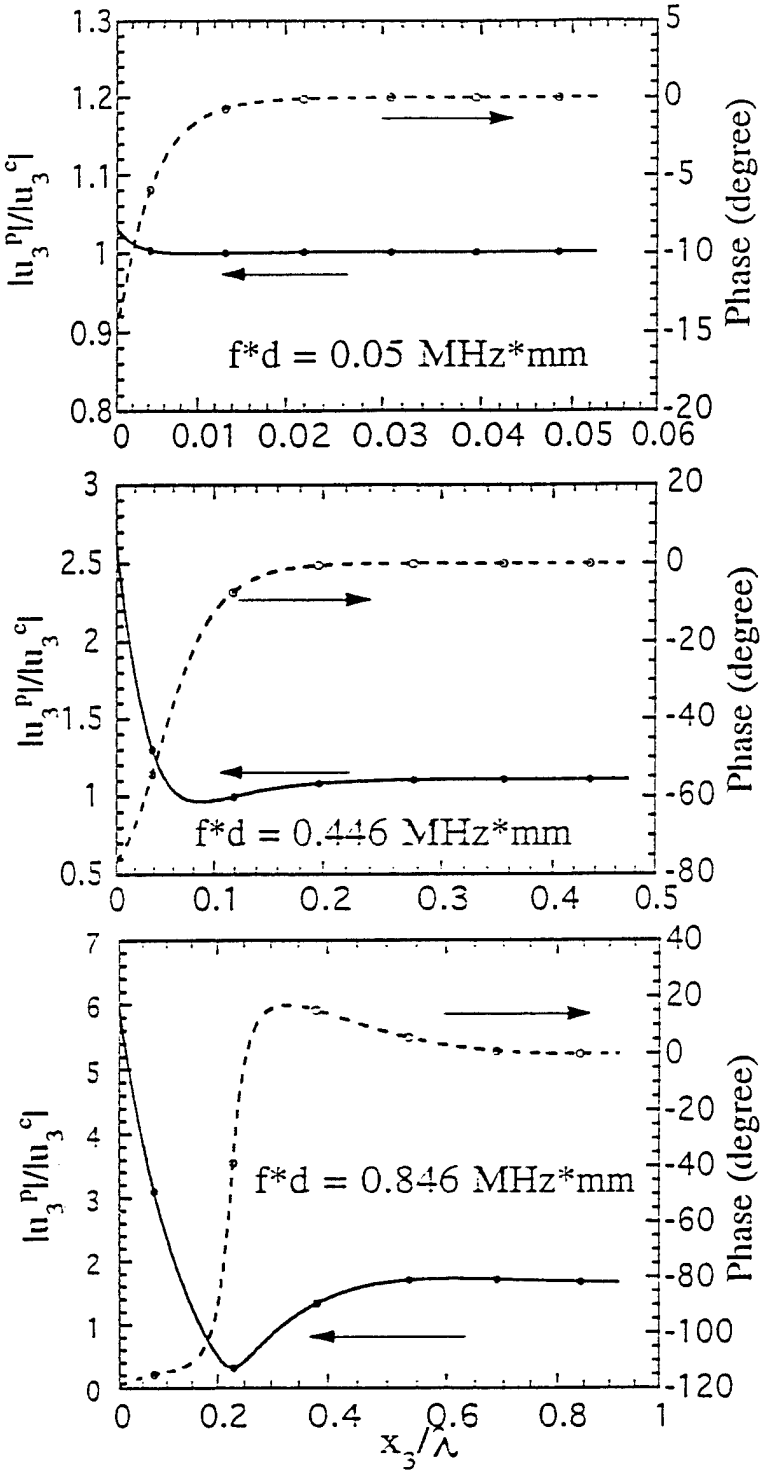

Figure 24. The vibration profile as a function of the distance from the interface with water (x_3=0) where u_3^p and u_3^c are the displacement at the center of the polymer plate (x_1=d/2) and ceramic plate (x_1=0). At low frequencies, the polymer and ceramic vibrate with the same amplitude and phase while at high frequencies, even far away from the interface, the vibration amplitude of the two is still not the same while the phase becomes the same.

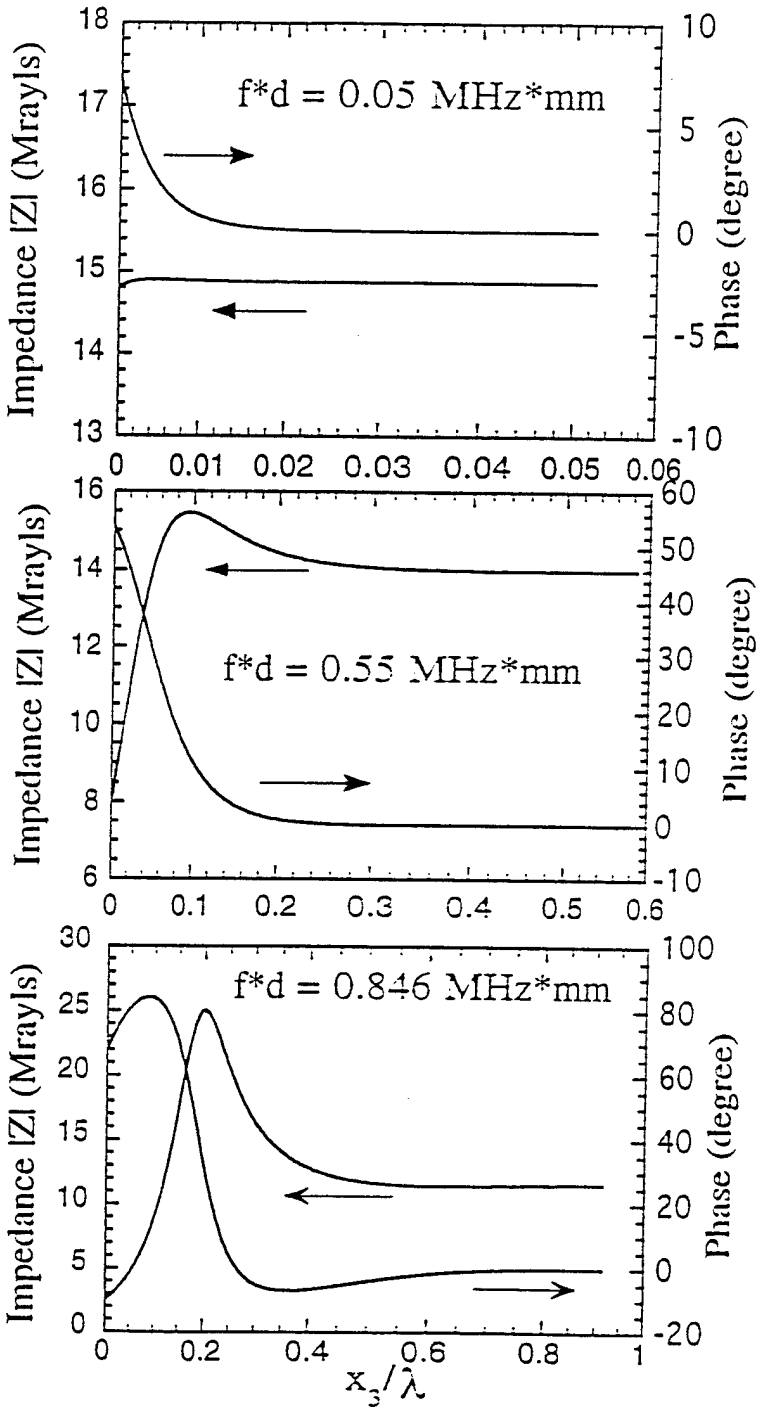

Figure 25. The effective input impedance from eq. (16) as a function of the distance from the interface with water (x_3=0) at three typical frequencies: far below the lateral mode, at about the half of the lateral mode frequency, and near the lateral mode frequency.

3.2. Wave reflection and transmission at solid-2-2 composite interfaces:

In general, a piezoelectric ultrasonic transducer has a multilayer structure in which there are one or two quarter wavelength impedance matching layers in front of the piezoelectric element and a backing material in the back. The piezoelectric element in the transducer does not contact directly with fluid medium. Therefore, the investigation of the interaction between a 2-2 composite and solid medium has practical importance for composite transducers.

The issues investigated in this section are quite similar to those studied in the preceding section. The difference is that a solid medium can support shear waves while a fluid cannot. Due to this difference, the boundary conditions (3) must be modified to:

$$\begin{aligned} &T_{33}^{Cm} = T_{33}^{S},\ T_{13}^{Cm} = T_{13}^{S}, u_3^{Cm} = u_3^{S}, u_1^{Cm} = u_1^{S} \\ &\Phi^{Cm} = \Phi^{S},\ D_3^{Cm} = D_3^{S}, \end{aligned} \tag{44}$$

where the superscript S refers to the variables in the solid medium. Hence, the variational formula for the problem becomes

$$\begin{aligned} &\int_S \frac{1}{2}[(T_{33}^{S} - T_{33}^{Cm})(\delta u_3^{S} + \delta u_3^{Cm})^* + (T_{13}^{S} - T_{13}^{Cm})(\delta u_1^{Cm} + \delta u_1^{S})^* \\ &+ (u_3^{Cm} - u_3^{S})(\delta T_{33}^{Cm} + \delta T_{33}^{S})^* + (u_1^{Cm} - u_1^{S})(\delta T_{13}^{Cm} + \delta T_{13}^{S})^* \\ &+ (D_3^{S} - D_3^{Cm})(\delta\Phi^{S} + \delta\Phi^{Cm})^* + (\Phi^{S} - \Phi^{Cm})(\delta D_3^{S} + \delta D_3^{Cm})^*]dS. = 0 \end{aligned} \tag{45}$$

where the surface integral is performed at x_3=0 over one repeat unit in the x_1-direction of the composite. The elastic displacement u_1^S, u_3^S, and the electrical potential Φ^S in the solid medium are expanded in terms of the eigenfuntions:

$$\begin{aligned} u_1^{S} &= j\sum_n \sum_{i=1}^{2} g_{ni}^{S} \sin(h_n^{S} x_1) \exp(-j\beta_{ni}^{S} x_3) R_n^{S} \\ u_3^{S} &= \beta_0^{S} \exp(j\beta_0^{S} x_3) - j\sum_n \sum_{i=1}^{2} f_{ni}^{S} \cos(h_n^{S} x_1) \exp(-j\beta_{ni}^{S} x_3) R_n^{S} \\ \Phi^{S} &= \sum_n \cos(h_n^{S} x_1) \exp(h_n^{S} x_3) R_n^{S} \end{aligned} \tag{46}$$

where $\beta_0^S \exp(j\beta_0^S x_3)$ is the incident wave and other terms are from the reflected waves in which both the longitudinal and shear components exist except the one with n=0 where the reflected wave is a pure longitudinal one. Substituting the elastic and electrical variables in the 2-2 composite and eq. (46) into equation (45), the coefficients of the expansions can be obtained.

Figure 26 presents the dispersion curve of the reflection coefficient at the interface for 2-2 piezocomposites with 44% ceramic volume content and the acoustic impedance calculated from eq. (41) where the characteristic impedance of the solid medium is Z=2.4 Mrayls.

By comparing the results in figure 26 and figure 19, it can be found that the input acoustic impedance of 2-2 composites calculated here is different from that in the fluid case. In addition, it is also found that at a solid medium-2-2 composite interface, the input acoustic impedance also depends on the characteristic impedance of the solid medium at the interface, which seems to be quite different from the fluid medium interface.

To understand this phenomenon, we notice that the difference between a solid medium and a fluid one is that a solid medium has a non-zero shear stiffness constant. Therefore, Z_{in} for a 2-2 composite (44% ceramic content) in contact with solid medium is evaluated where ρ (mass density) and c_{11} are kept as constant and c_{44} is varied and the results are presented in figure 27(a). Similarly, Z_{in} for a 2-2 composite in contact with solid medium is also evaluated where ρ and c_{44} are kept constant and c_{11} is varied and the results are shown in figure 27(b). The results demonstrate that for a plane incident wave, even if the characteristic longitudinal impedance of the solid medium is kept constant, the effective input impedance of a composite and, hence, the reflection coefficient from the interface will change if the shear stiffness coefficient of the solid medium changes. On the other hand, if the shear stiffness constant is kept constant and the characteristic longitudinal impedance is varied in the solid medium, the effective input acoustic impedance of a composite will not have much change. This phenomenon is directly related to the surface uniformity of the composite and as has been shown earlier, the enhanced stress transfer between the ceramic and polymer regions is through the shear action.[39]

To illustrate this, the surface vibration distribution in the ceramic and polymer regions is also evaluated for the 2-2 composite in contact with solid media of different c_{11} and c_{44} and the results are presented in figure 28. There is very little difference in the surface vibration profile for solid media with the same c_{44} and different c_{11}. In contrast, the surface vibration profile will change as c_{44} is changed.

Figure 29 illustrates the input acoustic impedance of a composite as a function of x_3 for different solid media at the interface. It shows the length of the transition region in the composite where the evanescent waves are important decreases as the acoustic impedance of the medium, especially the shear modulus, increases.

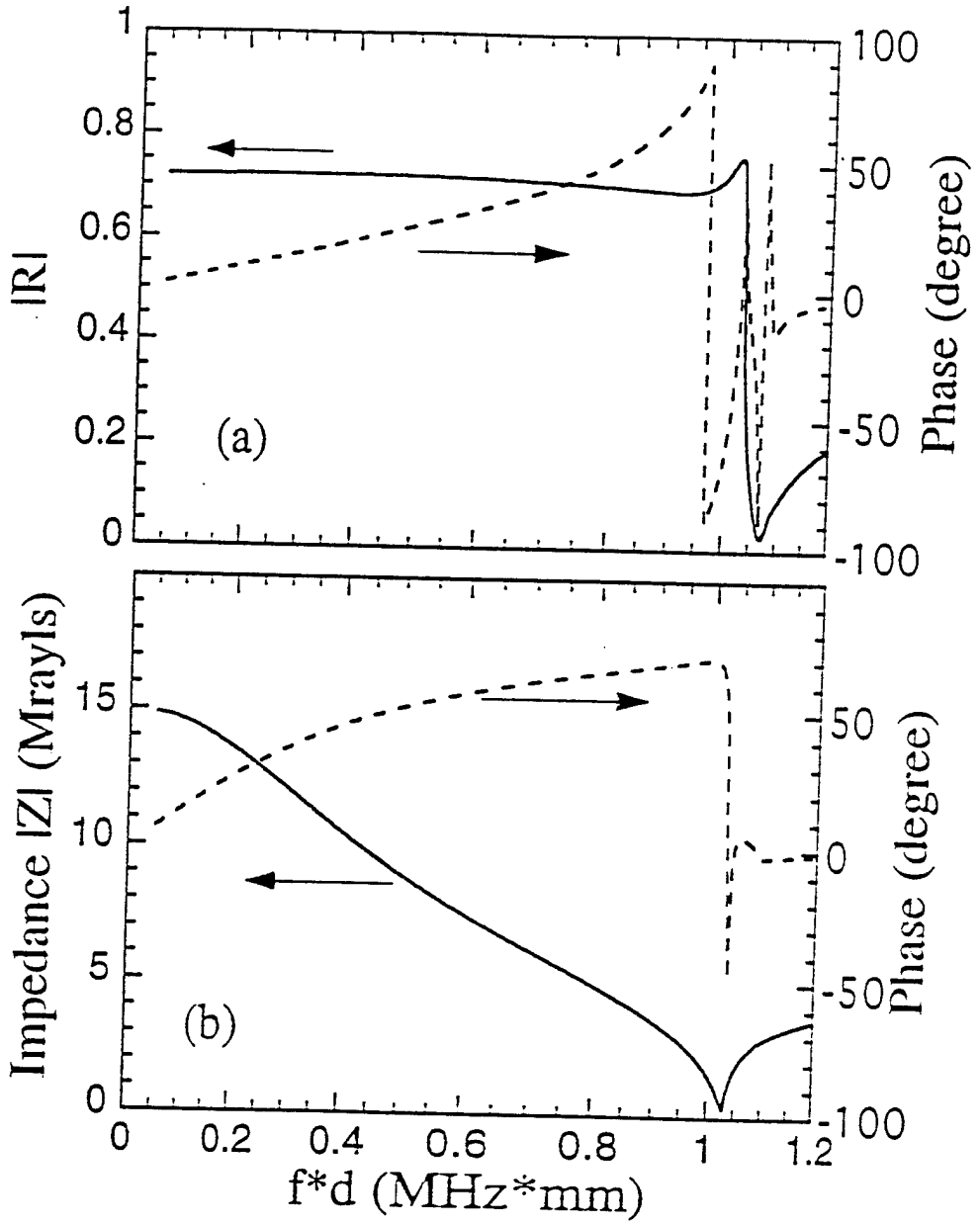

Figure 26. (a) The reflection coefficient at a interface between a solid medium (ρ= , c_{11}= c_{44}=) and a 2-2 composite of 44% ceramic volume content as a function of frequency. (b) The effective input acoustic imepdance of a 2-2 composite of 44% ceramic volume content as a function of frequency. Z_{in} is calculated from the reflection coefficient.

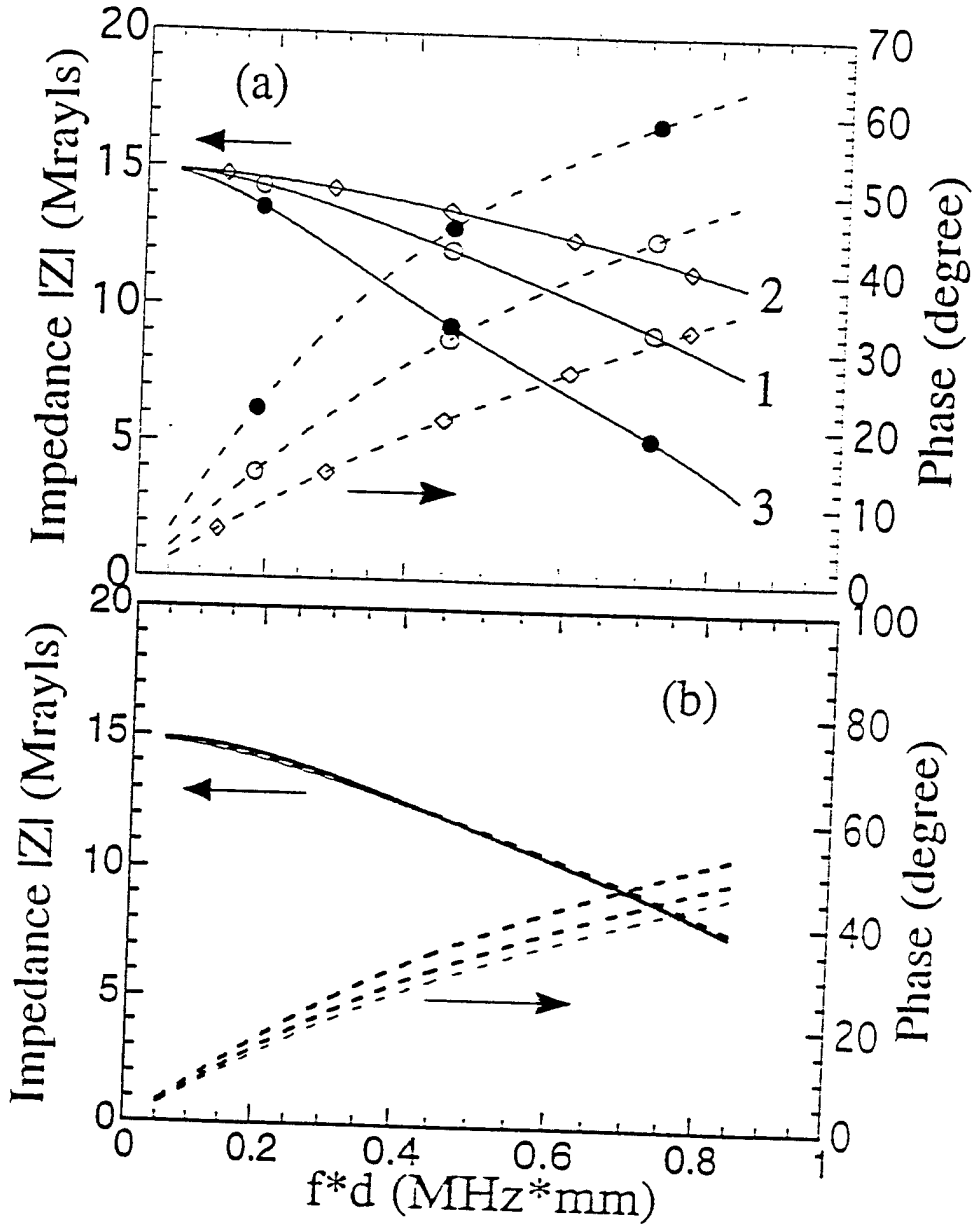

Figure 27. Data illustrate the dependence of the input acoustic impedance of a composite on the elastic properties of the solid medium at the interface. (a) The solid medium for the curve 1 is ρ=1.61 g/cm^3, c_{11} = 1.36*10^{10} N/m^2, and c_{44} = 3.43*10^9 N/m^2, and for the curve 2 and curve 3, both ρ and c_{11} are kept constant and c_{44} = 6.86*10^9 N/m^2 and c_{44} = 1.72*10^9 N/m^2. (b) Here both ρ and c_{44} are kept constant, and c_{11}= 0.68 *10^{10}, c_{11}= 1.36 *10^{10}, and c_{11}= 2.72 *10^{10} N/m^2. The amplitude of Z_{in} does not change much with c_{11} except a small change in the phase.

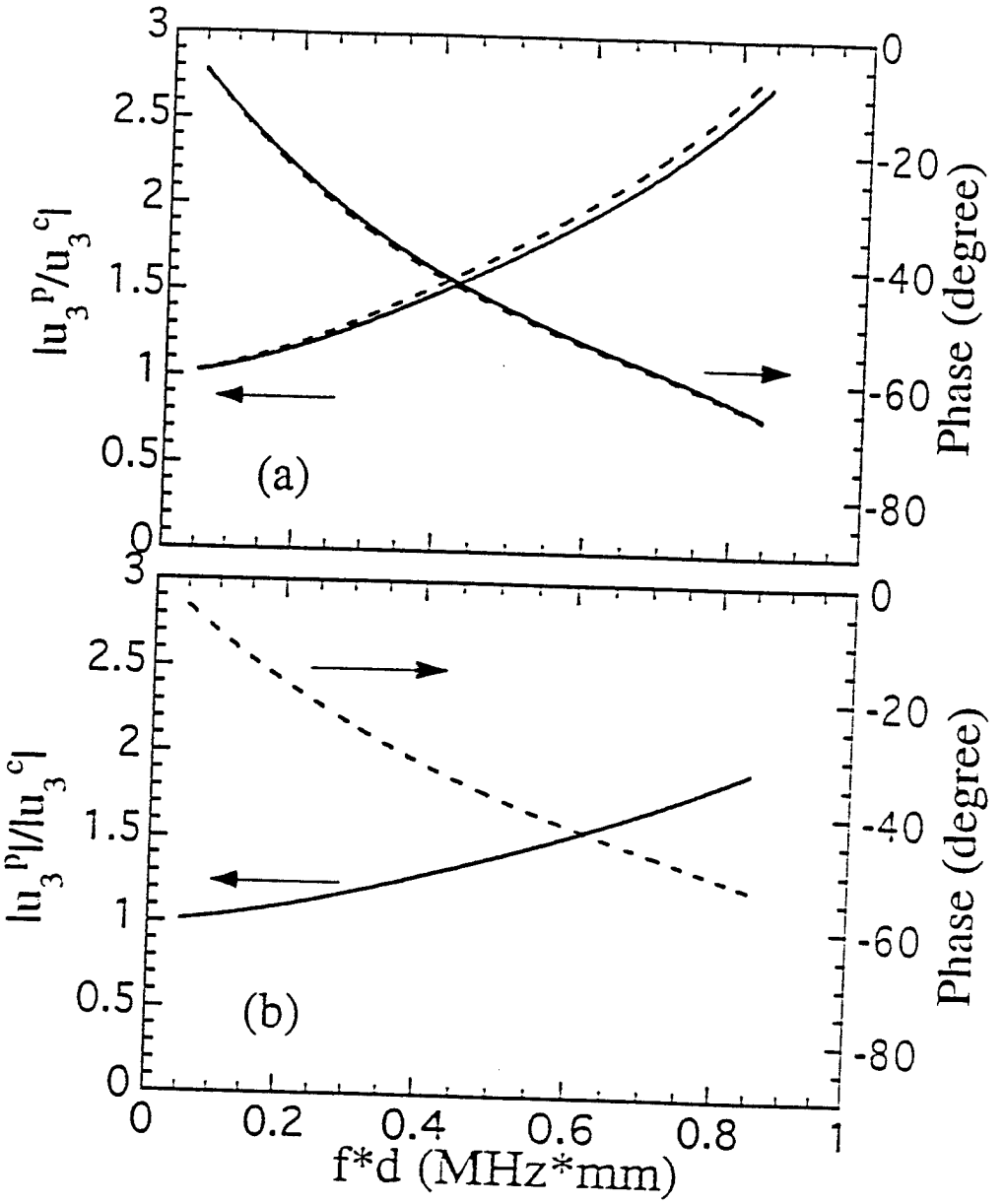

Figure 28. The figures illustrate the effect of c_{11} and c_{44} of the solid medium on the surface vibration profile of the composite. (a) The parameters of the solid medium for the data of dashed curve is ρ=1.61 g/cm^3, c_{11} = 1.36*10^{10} N/m^2, and c_{44} = 3.43*10^9 N/m^2, and for the solid curve, both ρ, c_{44} are the same except c_{11}=2.72*10^{10} N/m^2. (b) The parameters for the solid medium is ρ=1.61 g/cm^3, c_{11} = 1.36*10^{10} N/m^2, and c_{44} = 6.86*10^9 N/m^2. Notice the effect of c_{44} on the surface vibration profile of the composite.

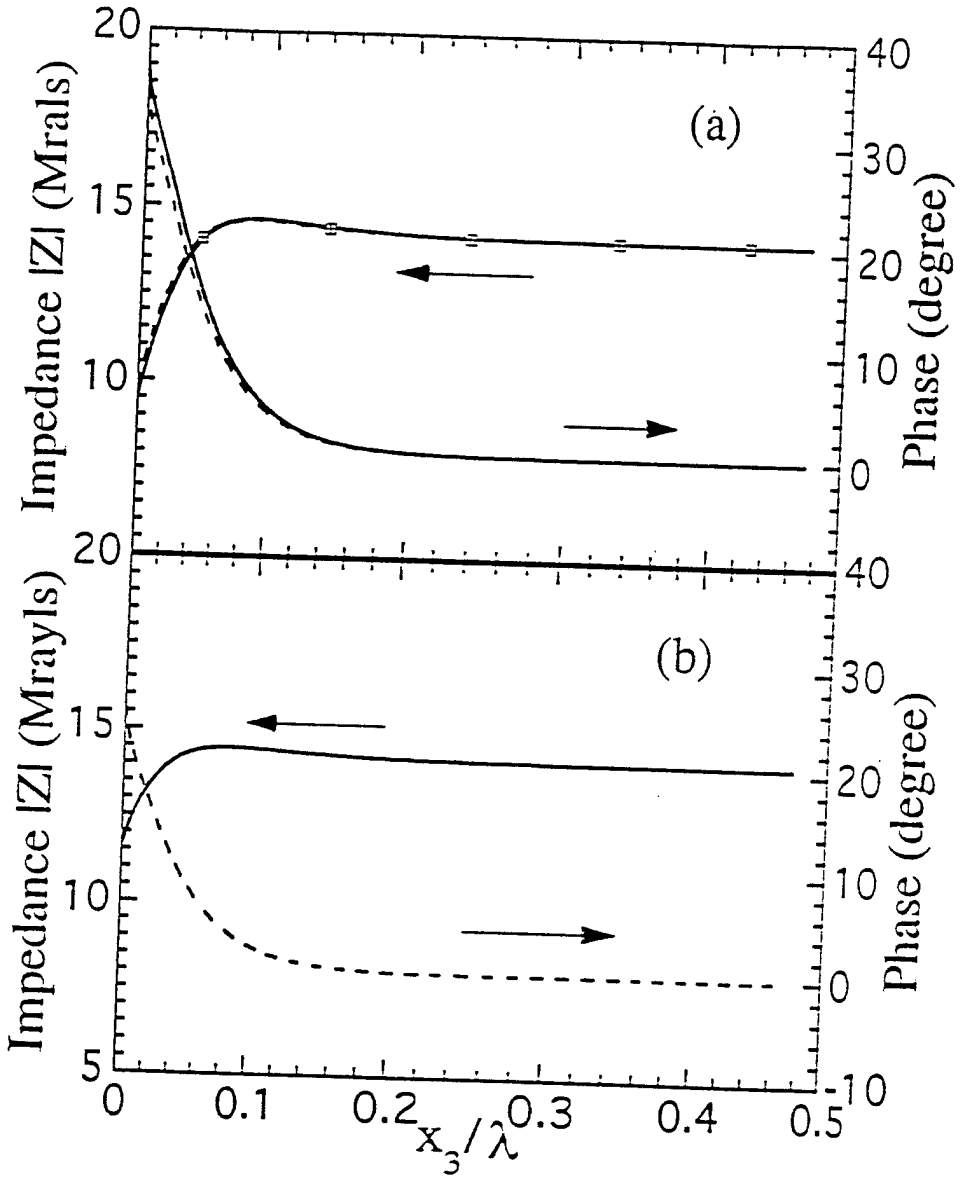

Figure 29. The figures illustrate the effect of the elastic properties of the solid medium at the interface on the effective input impedance distribution along the x_3-axis at a frequency f*d = 0.446 Mhz*mm where x_3=0 is the interface. (a) The dashed line: ρ=1.16 g/cm^3, c_{11}= 7.72*10^9 N/m^2, and c_{44} =1.588*10^9 N/m^2. The solid line: ρ=1.1 g/cm^3, c_{11} = 5.41*10^9 N/m^2, and c_{44} = 1.307*10^9 N/m^2 (Spurrs epoxy). (b) The parameters for the solid medium is: ρ=1.61 g/cm^3, c_{11} = 1.36*10^{10} N/m^2, and c_{44} = 3.43*10^9 N/m^2.

3.3. Reflection and transmission from the boundary between fluid and acoustic impedance matching layer:

We now proceed to investigate how the various effects observed in the preceding sections affect the selection of anti-reflection matching layers at the interface. Figure 30 is a schematic of an acoustic system which consists of a fluid medium, a matching layer and a 2-2 composite. In this case, there are two interfaces with different boundary conditions to be treated. One of the interfaces is

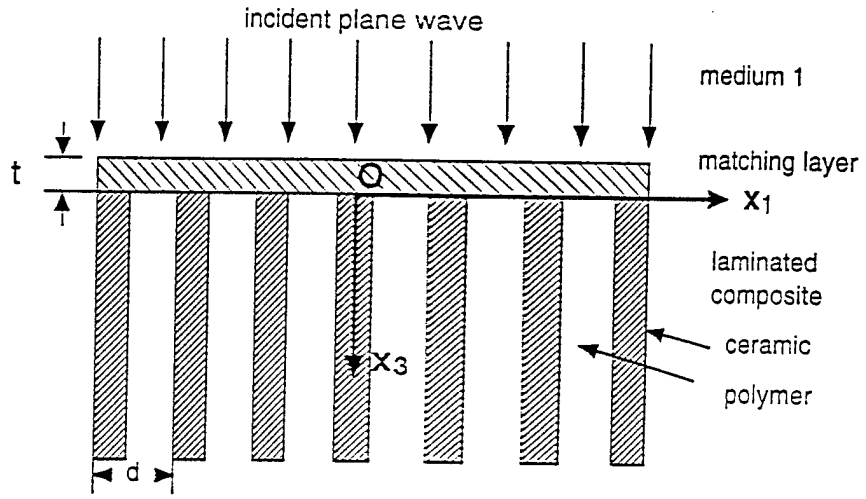

Figure 30. Schematic of an interface system consisting of a fluid medium (medium 1) matching layer, and a 2-2 composite. The thickness of the matching layer is t and the period of the composite is d.

between the 2-2 composite and matching layer where the boundary conditions are those of equation (44). Another one is the fluid and matching layer interface where the boundary conditions are:

$$T_{33}^S = T_{33}^W,\ T_{13}^S = 0,\ u_3^S = u_3^W,\ \Phi^S = \Phi^W,\ D_3^S = D_3^W \quad \text{at } x_3\text{=-t} \tag{47}$$

where t is the thickness of the matching layer and the other notations are the same as before. The variational formula for this problem can be derived:

$$\begin{aligned}
&\int_{S_1} \frac{1}{2}[(T_{33}^S - T_{33}^{Cm})(\delta u_3^S + \delta u_3^{Cm})^* + (T_{13}^S - T_{13}^{Cm})(\delta u_1^{Cm} + \delta u_1^S)^* \\
&+(u_3^{Cm} - u_3^S)(\delta T_{33}^{Cm} + \delta T_{33}^S)^* + (u_1^{Cm} - u_1^S)(\delta T_{13}^{Cm} + \delta T_{13}^S)^* \\
&+(D_3^S - D_3^{Cm})(\delta\Phi^S + \delta\Phi^{Cm})^* + (\Phi^S - \Phi^{Cm})(\delta D_3^S + \delta D_3^{Cm})^*]dS \\
&+\int_{S_2} \frac{1}{2}[(T_{33}^W - T_{33}^S)(\delta u_3^S + \delta u_3^W)^* + 2T_{13}^S(\delta u_1^S)^* + (u_3^S - u_3^W)(\delta T_{33}^S + \delta T_{33}^W)^* \\
&+(D_3^W - D_3^S)(\delta\Phi^S + \delta\Phi^W)^* + (\Phi^W - \Phi^S)(\delta D_3^S + \delta D_3^W)^*]dS = 0
\end{aligned} \tag{48}$$

where the surface integrals S_1 and S_2 are performed at x_3=0 and x_3=-t planes, respectively, from x_1=0 to x_1=d/2.

In the matching layer region, there are waves which propagate in both the $+x_3$ and $-x_3$ directions due to the two interfaces at x_3=0 and x_3=t. Hence, the expressions for the elastic and electrical variables become:

$$u_1^S = j\sum_n \sum_{i=1}^{2} g_{ni}^S(\beta_{ni}^S)\sin(h_n^S x_1)[-\exp(-j\beta_{ni}^S x_3)R_n^1 + \exp(j\beta_{ni}^S x_3)R_n^2]$$

$$u_3^S = \sum_n \sum_{i=1}^{2} f_{ni}^S(\beta_{ni}^S)\cos(h_n^S x_1)[-\exp(-j\beta_{ni}^S x_3)R_n^1 + \exp(j\beta_{ni}^S x_3)R_n^2] \qquad (49)$$

$$\Phi^S = \sum_n \cos(h_n^S x_1)[-\exp(-h_n^S x_3)R_n^1 + \exp(h_n^S x_3)R_n^2]$$

The solutions in the composite and in the fluid medium are those of eqs. (37), (38) and (39). Substituting those expressions into equation (48), the undetermined coefficients in these equations can be found and various quantities in different regions can be evaluated.

In general, for homogeneous materials, the reflection coefficient from the boundary between a fluid and a matching layer will be zero when the thickness of the matching layer is quarter wavelength and its acoustic impedance Z^M is

$$Z^M = \sqrt{Z^W Z^S} \qquad (50)$$

where Z^W and Z^S are the acoustic impedance of the media on the two sides of the matching layer, respectively.[19,31]

For a composite material, from the results obtained in the preceding sections, it is expected that the parameters of the anti-reflection matching layer will be modified. Figure 31 illustrates the derived reflection coefficient from the boundary between the fluid and matching layer for different matching layer materials where the thickness of the matching layer is chose so that the frequency of the reflection coefficient minimum is at fd=0.335 MHz*mm. From results, it is found that the acoustic impedance of the matching layer from which the reflection coefficient becomes zero satisfies approximately equation (50) if Z^S is replaced by the effective input acoustic impedance of the 2-2 composite at the low frequency. However, the thickness of the matching layer is no longer quarter wavelength and in fact, it is shorter than $\lambda/4$. These results are summarized in figure 32. The data in figure 32(a) is the acoustic impedance of the matching layer in order for the reflection coefficient to be zero as a function of frequency. In figure 32(b), the change of the matching layer thickness as a function of frequency is presented where t=1 corresponds to the thickness of $\lambda/4$ at that frequency. Therefore, as the frequency

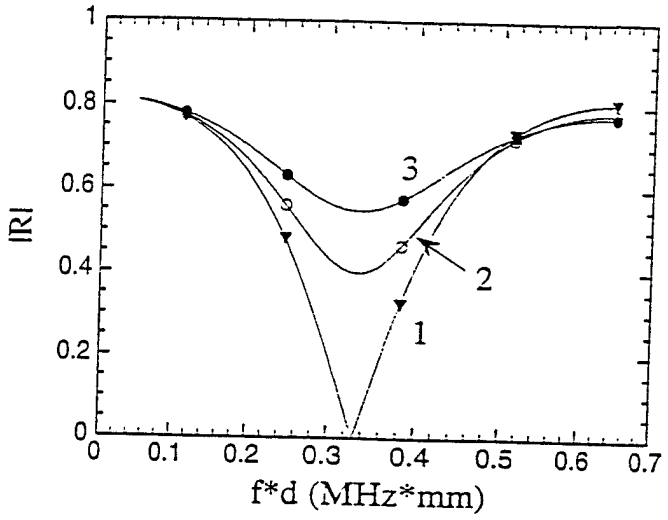

Figure 31. The reflection coefficient from the matching layer system where the total transmission occurs at f*d = 0.334 MHz*mm for the matching layer with t = 2.02*d = 0.91*(λ/4) (at f*d = 0.334 MHz*mm) and Z^M=4.68 Mrayls (ρ=1.61 g/cm^3, c_{11} = 1.36*10^{10} N/m^2, and c_{44} = 3.43*10^9 N/m^2) (the curve 1). For the comparison, the reflection coefficient from the matching layers with other parameters is also shown here: for the curve 2, Z^M = 3.0 Mrayls and t = 1.85*d, and for the curve 3, Z^M = 2.44 Mrayls and t = 1.58*d.

increases, both the acoustic impedance and the thickness of the matching layer decrease. For example, when the frequency changes from 0.05 MHz*mm to 0.5 MHz*mm, the acoustic impedance of the matching layer changes from 4.70 Mrayls to 4.42 Mrayls and the thickness t changes from about λ/4 to 0.86*λ/4. The reduction in the matching layer thickness is a direct result of the fact that the incident plane wave suffers more than 180° phase loss upon the reflection from the interface.

From the fact that in the frequency range of interesting, the evanescent waves at the interface will decay approximately as exp(-2nπx$_3$/d), the effect of the interface of x_3=t, where t is approximately λ/4, to the surface vibration distribution at the composite-matching layer interface will be quite small. Therefore, the reflection coefficient introduced in the section III between the composite and a solid medium can be used to approximate the reflection at the matching layer-composite interface. Hence, the reflection coefficient R from the system in figure 30 can be approximated as:

$$R = \frac{R_{12} + R_{23}e^{2j\beta_0^s t}}{1 + R_{12}R_{23}e^{2j\beta_0^s t}} \qquad (51)$$

where R_{12} and R_{23} are the reflection coefficients at the fluid-matching layer interface and matching layer-2-2 composite interface, respectively. In eq. (51), R_{12} is the reflection coefficient from the

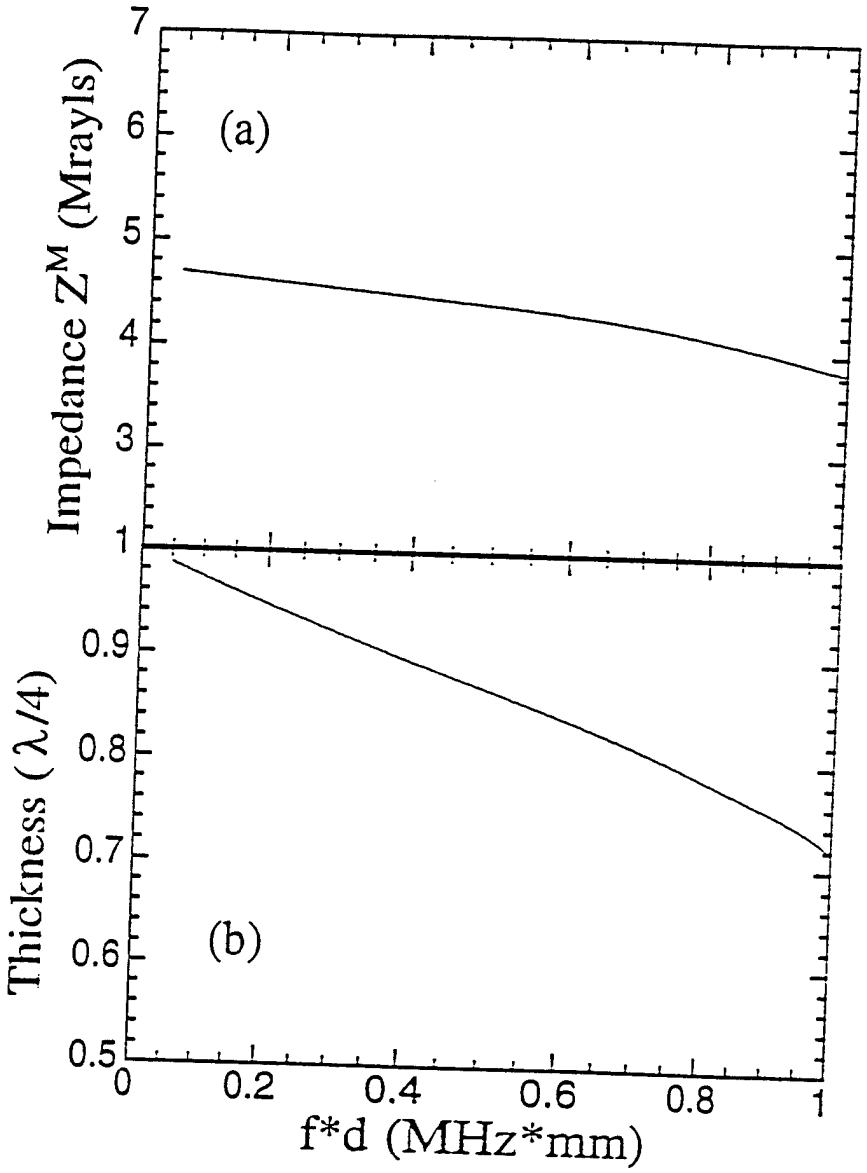

Figure 32. The required parameters for (a) Z^M and (b) t of the matching layer to have total transmission as a function of frequency for a water-2-2 composite (44% ceramic volume content) interface.

interface of two semi-infinite media of the fluid and solid, and R_{23} is that derived in the section III (the reflection coefficient from the solid medium-composite interface). From equation (51), the requirements to the matching layer to achieve the total transmission (R=0) can be derived. The acoustic impedance of the matching layer is

$$Z^M = \sqrt{Z^W \left|Z^{Cm}\right| \frac{\left|Z^{Cm}\right| - Z^W \cos(\theta)}{\left|Z^{Cm}\right| \cos(\theta) - Z^W}} \tag{52}$$

where θ is the phase angle of the acoustic impedance of the 2-2 composite. The thickness of the matching layer is

$$t = \frac{\lambda}{4}\{1 - \frac{1}{\pi}\arctan(\frac{2Z^M \left|Z^{Cm}\right| \sin(\vartheta)}{\left|Z^{Cm}\right|^2 - (Z^M)^2})\} \tag{53}$$

As shown in figure 32, in the frequency range of interest, the results from eqs. (52) and (53) are almost identical to those derived from the numerical calculation.

IV. Modeling and Experimental Study of 1-3 Piezocomposites:

Both analytical modeling and experimental investigation of 1-3 composites are currently underway. As a first step to model a 1-3 composite, a concentric unit cell as schematically shown in figure 33 is adopted. This unit cell is an approximation to a 1-3 composite with the ceramic rods arranged in a hexagonal lattice. In the analysis here, the elastic loss in the polymer phase is included. The other losses such as the dielectric loss in the ceramic phase can also be included. However, compared with the elastic loss in the polymer phase, these other loss mechanisms may not be significant. The wave equation and the boundary conditions can be expressed as

$$\begin{aligned} \rho \ddot{u}_r &= T_{rr,r} + T_{rz,z} + \frac{T_{rr} - T_{\theta\theta}}{r} \\ \rho \ddot{u}_z &= T_{rz,r} + \frac{T_{rz}}{r} + T_{zz.z} \\ D_{r,r} &+ \frac{D_r}{r} + D_{z,z} = 0 \end{aligned} \tag{54}$$

and

$$\begin{aligned} & T_{rr}^C = T_{rr}^P, T_{rz}^C = T_{rz}^P, \Phi^C = \Phi^P, \\ & u_r^C = u_r^P, u_z^C = u_z^P, D_r^C = D_r^P, \qquad \text{at } r=r_1 \\ & D_r^P = 0, u_r^P = 0, T_{rz}^P = 0, \qquad \text{at } r=r_2 \end{aligned} \tag{55}$$

The constitutive relations for ceramic phase are

$$T_{rr}^C = c_{11}^E u_{r,r}^C + c_{12}^E \frac{u_r^C}{r} + c_{13}^E u_{z,z}^C - e_{31} E_z^C$$

$$T_{\theta\theta}^C = c_{12}^E u_{r,r}^C + c_{11}^E \frac{u_r^C}{r} + c_{13}^E u_{z,z}^C - e_{31} E_z^C$$

$$T_{zz}^C = c_{13}^E (u_{r,r}^C + \frac{u_r^C}{r}) + c_{33}^E u_{z,z}^C - e_{33} E_z^C \qquad (56)$$

$$T_{rz}^C = c_{44}^E (u_{r,z}^C + u_{z,r}^C) - e_{15} E_r^C$$

$$D_r^C = e_{15} (u_{r,z}^C + u_{z,r}^C) + \varepsilon_{11}^S E_r^C$$

$$D_z^C = e_{31} (u_{r,r}^C + \frac{u_r^C}{r}) + e_{33} u_{z,z}^C + \varepsilon_{33}^S E_z^C$$

The constitutive relations of the polymer phase are obtained by setting the piezoelectric coeficients e_{31},e_{33}, and e_{15} zero in eq. (39). The superscripts C and P denote the ceramic and polymer phases, respectively.

From the symmetry consideration, the solutions to the equation (54) are

$$u_r^C = AJ_1(h^C r)\cos(\beta z)\exp(j\omega t)$$

$$u_z^C = BJ_0(h^C r)\sin(\beta z)\exp(j\omega t) \qquad (57)$$

$$\Phi^C = CJ_0(h^C r)\sin(\beta z)\exp(j\omega t)$$

where A, B, and C are constants, J_0 and J_1 are zeroth and the first order Bessel functions respectively. h^C and β are wave vectors along the radial and the axial directions, respectively.

Substitude Eq. (56) and (57) into Eq. (54) yields three homogenieous equations which, for a given ω and β, yield three h^C, corresponding to the quasi-longitudinal, quasi-shear, and quasi-electromagnetic waves in the ceramic phase. Hence, the general solutions in ceramic phase can be expressed as

$$u_r^C = \sum_{i=1}^{3} C_i g_i J_1(h_i^C r)\cos(\beta z)$$

$$u_z^C = \sum_{i=1}^{3} C_i f_i J_0(h_i^C r)\sin(\beta z)$$
$$\Phi^C = \sum_{i=1}^{3} C_i t_i J_0(h_i^C r)\sin(\beta z) \qquad (58)$$

For the polymer phase, the solutions are

$$u_r^P = \sum_{i=1}^{2} [A_i g_i^P J_1(h_i^P r) + B_i g_i^P Y_1(h_i^P r)]\cos(\beta z)$$
$$u_z^P = \sum_{i=1}^{2} [A_i f_i^P J_0(h_i^P r) + B_i f_i^P Y_0(h_i^P r)]\sin(\beta z) \qquad (59)$$
$$\Phi^P = [D_1 J_0(h_3^P r) + D_2 Y_0(h_3^P r)]\sin(\beta z)$$

where Y_0 and Y_1 are modified zeroth and the first order Bessel functions and h^P are

$$h_1^P = \sqrt{\frac{\omega^2}{v_s^2} - \beta^2}, \quad v_s^2 = \frac{c_{44}^P}{\rho^P}$$
$$h_2^P = \sqrt{\frac{\omega^2}{v_l^2} - \beta^2}, \quad v_l^2 = \frac{c_{11}^P}{\rho^P}$$
$$h_3^P = j\,\beta$$

The elastic stiffness of polymer can be expressed as

$$c_{11}^P = c_{11} - j\,\eta_{11}\omega$$
$$c_{44}^P = c_{44} - j\,\eta_{44}\omega$$

where η_{11}, η_{44} are the viscosity constants. by the boundary conditions (eq. (55)).

Substituting Eq. (58) and Eq. (59) into the boundary conditions (55) yields 9 homogenieous equations from which the relations among the coefficients A_i, B_i, D_i, and C_i can be determined which are functions of ω, β and the material parameters of both ceramic and polymer phases:

$$(K_{ij})\,(A_j) = 0$$

where (Kij) is a 9x9 matrix and (Aj) a 1x9 matrix in which the elements are C_1, C_2, C_3, A_1, A_2, B_1, B_2, D_1, D_2. The condition for a non-trivial solution to these equation is

$$|K_{ij}| = 0,$$

from which, the relation between β and ω, i.e., the dispersion curves for the guided waves in a composite, can be determined. These procedures are exactly parallel to those in a 2-2 composite.

Shown in figure 34 are the dispersion curves for a 1-3 composite with 44% ceramic volume content where the loss in the polymer phase is assumed zero (PZT-5H and Spur epoxy). However, the dispersion curves, especially the ones related to the periodic structure in the lateral direction, show changes with the elastic loss. As presented in figures 35 and 36, the cut-off frequency for the dispersion cuver for the second branch (the lateral mode) becomes zero as βd approaches zero when the elastic loss in introduced. On the other hand, the imaginary part of the wave vector increases rapidly as $\beta d \rightarrow 0$, indicating that in the limit $\beta d \rightarrow 0$ the second mode (the lateral mode) becomes non-propagational.

Experimentally, it was observed that the behavior of the lateral modes in a 1-3 composite is quite different from the prediction based on the stop-band edge resonance and seems to be much more complicated than that in a 2-2 composite. These results will be presented in the future.

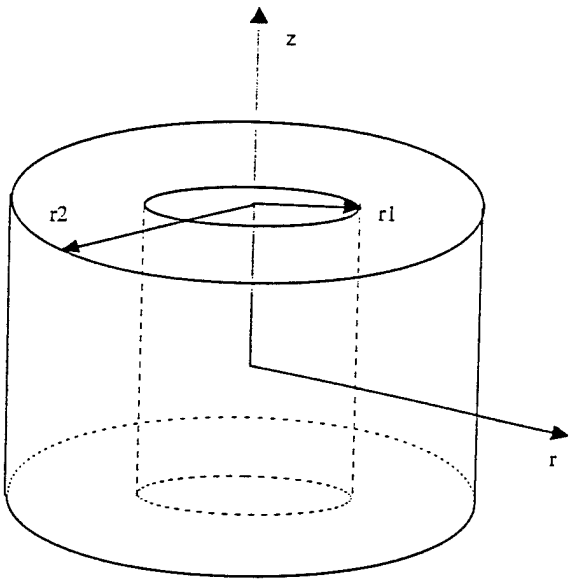

Figure 33. Schematic of a 1-3 composite which approximates the unit cell of a 1-3 composite with a hexagonal lattice.

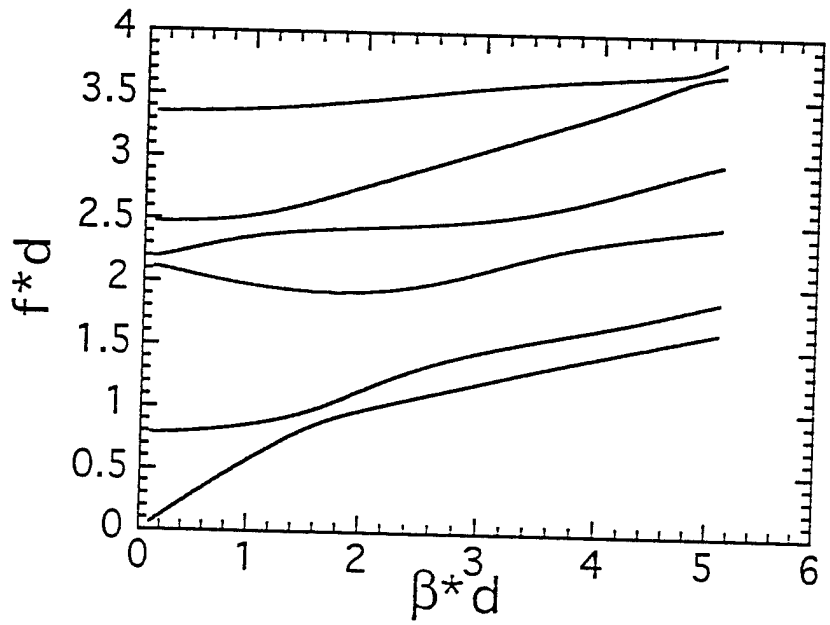

Figure 34. The dispersion curves for a 1-3 composite made of PZT-5H and Spur epoxy (no elastic loss is included).

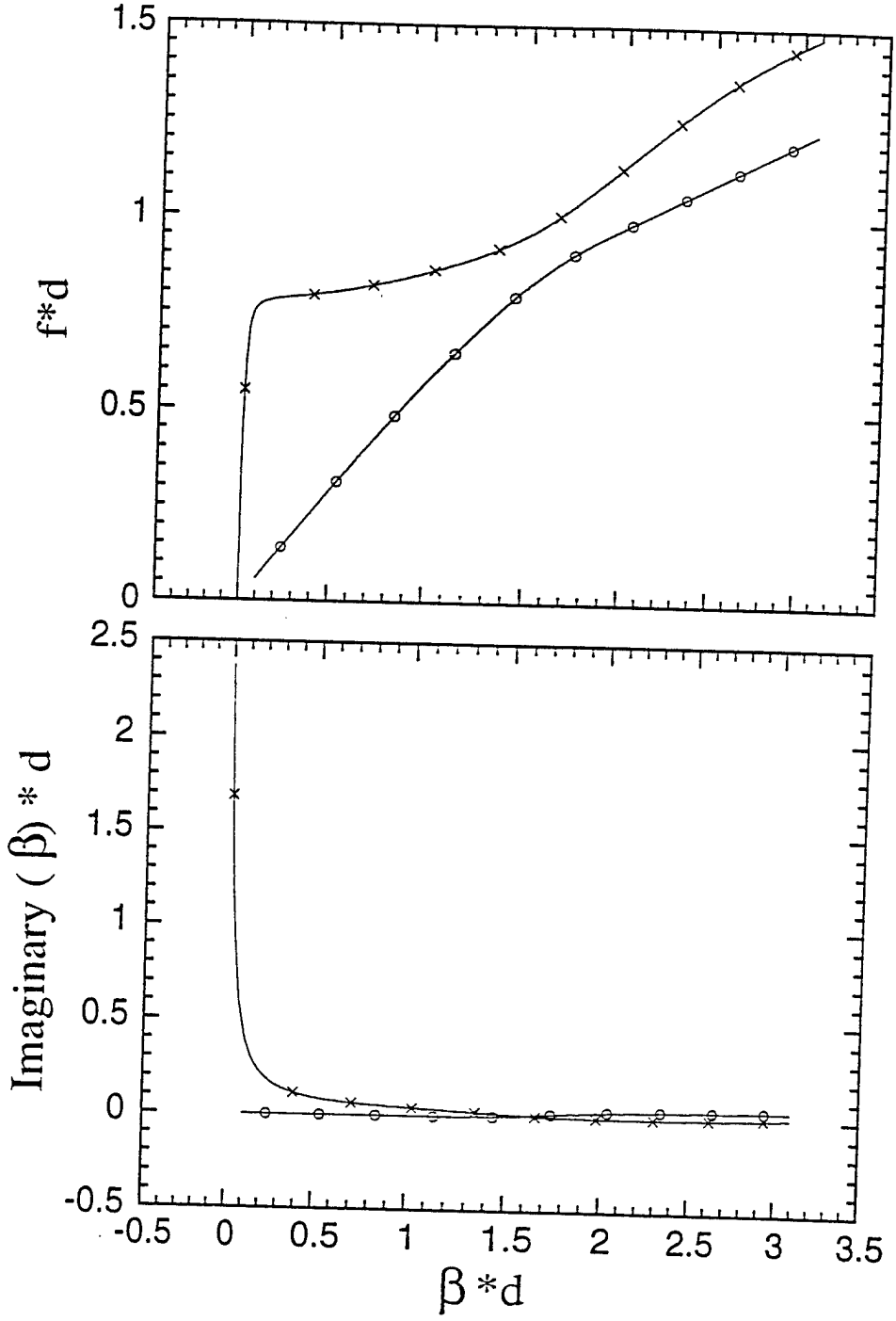

Figure 35. The effect of the elastic loss in the polymer phase on the dispersion curve of a 1-3 composite (PZT-5H) where the parameters for the polymer phase are those of Spur epoxy (the elastic loss is included): ρ=1100 kg/m3, c_{11}= 5.41x10^9 N/m^2, c_{44}= 1.037x10^9 N/m^2, η_{11}= 12.64 N s/m^2, η_{44}= 4.5 N s/m^2.

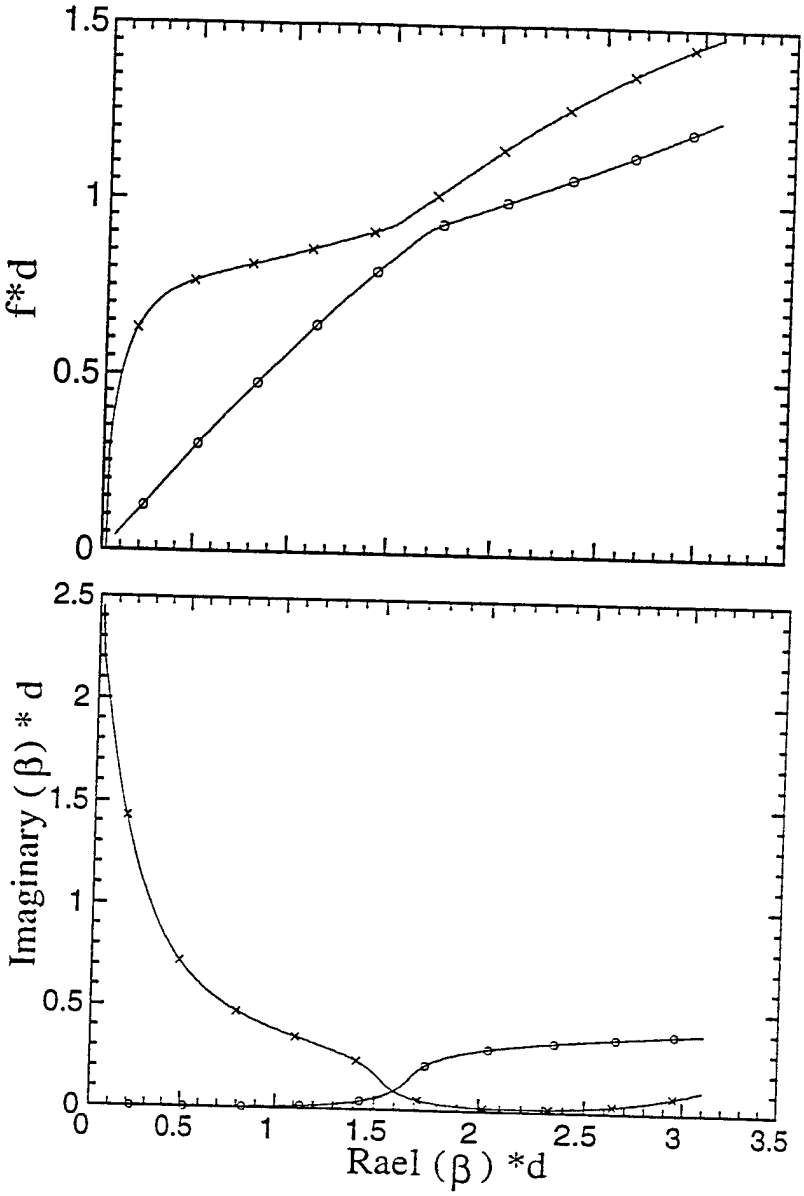

Figure 36. The effect of increased elastic loss (compared with figure 35) in the polymer phase on the dispersion curves where the parameters for the polymer phase are: ρ=1100 kg/m3, c_{11}= 5.41x10^9 N/m^2, c_{44}= 1.037x10^9 N/m^2, η_{11}= 101.12 N s/m^2, η_{44}= 36 N s/m^2 .

V. Summary:

A dynamic model on piezoceramic polymer composites with laminar periodic structure are presented. The result shows that the various resonant modes in a composite structure can be traced back to the modes in either an isolated ceramic plate or polymer plate with appropriate boundary conditions (stress free for the ceramic plate and strain free for the polymer plate). It also shows that there exist a series of modes associated with the periodic structure of a composite, which is beyond the stop-band edge resonance prediction. One of the main concerns in designing a composite transducer is how the surface vibration profile changes with frequency and how this is influenced by the aspect ratio t/d. It was predicted and verified by experiment that as long as the thickness resonance is below the first lateral mode frequency, there is always a frequency f_1 which is near the thickness resonance and at which the polymer and ceramic vibrate in unison. The effect of t/d is to change the position of f_1 with respect to the thickness resonance frequency and the bandwidth in which polymer and ceramic have nearly the same vibration amplitude and phase. It is also predicted that when operated in a fluid medium such as water, there will be a resonance mode whose frequency is determined by the velocity of the fluid medium and the unit cell length d and is associated with the oscillation of the fluid, causing the polymer and ceramic to vibrate 180° out of phase. The difference in the surface vibration profiles between in air and in water indicates the need to characterize the vibration pattern of a composite in a fluid medium since it is much closer to the real application environment.

The reflection and transmission of a plane acoustic wave at a medium-composite interface and the issues related to the design of matching layer for a composite are analyzed based on the model developed. It has been shown that the reflection coefficient from the interface is a complex and the reflected wave suffers a more than 180° phase change. The effective input acoustic impedance Z_{in} of the composite at the interface was evaluated and both the amplitude and phase show a strong frequency dependence. For a fluid medium, it was found that Z_{in} does not change with the acoustic impedance of the medium. However, for a solid medium, Z_{in} will change if the shear stiffness constant of the medium changes. It was demonstrated that this difference originates from the non-uniformity of the surface vibration distribution of the composite at the interface which depends crucially on the shear stiffness constant of the medium.

Since for a piezoceramic polymer composite, it is the ceramic phase which performs the energy conversion between the acoustic and electric forms, how much acoustic energy can enter the ceramic region is one of the most important parameters in a composite transducer design. In the paper, we show that even though the effective transmission coefficient increases as the frequency is increased, the amount of acoustic energy entering the ceramic region actually decreases. Therefore, there may be

a trade-off between the bandwidth, which is related to the transmission coefficient, and the sensitivity in the composite transducer design.

From the fact that there is more than 180° phase change in the reflection from the medium-composite interface, it is shown that the matching layer thickness is no longer equal to the quarter wavelength but smaller than that. In addition, the acoustic impedance of the matching layer will also be affected by the phase of Z_{in} of the composite.

1-3 piezocomposite was also modeled in which the elastic loss of the polymer phase is included. It was observed that at small βd limit, the cut-off frequency of the second branch which is related to the lateral mode approaches zero and the imaginary part of the wave vector increases rapidly. Experimentally, it was observed that the modes related to the periodic structure of a 1-3 composite seems to be much more complicated than the prediction of the stop-band edge resonance.

VI. References:

1. W. A. Smith, " The application of 1-3 piezocomposites in acoustic transducers," Proc. 1990 IEEE ISAF7 (Urbana, Illinois 1990) pp. 145-152, 1990.
2. T. R. Gururaja, A. Safari, R. E. Newnham, and L. E. Cross, " Piezoelectric ceramic-polymer composites for transducer applications," in Electronic Ceramics, ed. L. M. Levinson, pp. 92-128, Marcel Dekker, New York, 1987.
3. W. A. Smith and B. A. Auld, " Modeling 1-3 composite piezoelectrics: Thickness-mode oscillations," IEEE Trans. UFFC Vol. 38, pp. 40-47, 1988.
4. K. Y. Hashimoto and M. Yamaguchi, "Elastic, piezoelectric and dielectric properties of composite materials," Proc. 1986 IEEE Ultrasonics Symp. (Williamsburg, VA), pp.697-702, 1986.
5. T. R. Gururaja, W. A. Schulze, L. E. Cross, R. E. Newnham, B. A. Auld, and J. Wang, "Piezoelectric Composite Materials for Ultrasonic Transducer Applications. Part I: Resonant Modes of Vibration of PZT-Rod-Polymer Composites," IEEE Trans. Sonics and Ultrasonics, Vol. SU 32, pp 481-498, 1985.
6. R. E. Newnham, D. P. Skinner, and L. E. Cross, "Connectivity and piezoelectric-pyroelectric composites," Mater. Res. Bull. Vol.13, pp. 525-536, 1984.
7. B. A. Auld, H. Kunkel, Y. A. Shui, and Y. Wang, "Dynamic behavior of periodic piezoelectric composites," Proc. 1983 IEEE Ultrasonics Symp. (Atlanta, GA), pp. 554-558, 1983.
8. B. A. Auld, Y. A. Shui, and Y. Wang, "Elastic wave propagation in three-dimentional periodic composite materials," Journal de Physique, Vol. 45, pp. 159-163, 1984.

9. Y. Wang, E. Schmidt, and B. A. Auld, "Acoustic wave transmission through one-dimensional PZT-epoxy composites," Proc. 1986 IEEE Ultrasonics Symp. (Williamsburg, VA), pp.685-689, 1986.
10. Y. Wang, "Waves and Vibrations in Elastic Superlattice Composites," Ph. D. Thesis, Stanford University, December 1986.
11. F. Craciun, L. Sorba, E. Molinari, and M Pappalardo, "A cooupled-mode theory for periodic piezoelectric composites," IEEE Trans. UFFC Vol. 36, pp. 50-56, 1989.
12. M. Yamaguchi, K. Y. Hashimoto, and H. Makita, "Finite element method analysis of dispersioncharacteristics for the 1-3 type piezoelectric composites," Proc. 1987 IEEE Ultrasonics Symp. (Denver, CO), pp. 657-661, 1987.
13. J. A. Hossack and G. Hayward, "Finite element analysis of 1-3 composite transducers," IEEE Trans. UFFC Vol. 38, pp. 618-629, 1991.
14. Anne-Christine, Hladky-Hennion, and Jean-Noel Decarpigny, "Finite element modeling of active periodic structures: Application to 1-3 piezocomposites," J. Acoust. Soc. Am., Vol. 94, pp. 621-635, 1993.
15. J. Sato, M. Kawabuchi, J. Fukumoto, "Dependence of Electromechanical Coupling Coefficient on the Width to the Thickness Ratio of Plate Shaped Piezoelectric Transducers Used in Electrically Scanned Ultrasonic Diagnostic Systems," J. Acous. Soc. Am., Vol. 66, pp 1609-1611, 1979.
16. Q. M. Zhang and X. Geng, "Dynamic modeling of piezoceramic polymer composite with 2-2 connectivity," J. Appl. Phys. Vol.76, pp. 6014-6016, 1994.
17. Y. A. Shui, X. Geng, and Q. M. Zhang, "Theoretical modeling of resonant modes of composite ultrasonic transducers," IEEE Trans. UFFC Vol.42, pp. 766-773, 1995.
18. X. Geng and Q. M. Zhang, "Dynamic Behavior of Periodic Piezoceramic-Polymer Composite Plates," Appl. Phys. Lett. Vol. 67, pp 3093-3095, 1995.
19. B. A. Auld, Acoustic Fields and Waves in Solid, John Wiley & Sons, N. Y., 1973.
20. IEEE Standard on Piezoelectricity (ANSI/IEEE Standard 176-1987,1988).
21. H. F. Tiersten, Linear Piezoelectric Plate Vibrations, Plennum, New York, 1969.
22. PZT-5H is the trade-mark of Morgan Mattroc Inc. (Beddford, OH 44146) for one of its PZT piezoceramics. Spurr epoxy is the trade-mark of Polysciences, Inc. (Warrington, PA 18976).
23. C. G. Oakley, "Geometric Effects on the Stopband Structures of 2-2 Piezoelectric Composite Plates," Proc. 1991 IEEE Ultrasonics Symp. pp. 657-661, 1991
24. Q. M. Zhang, S. J. Jang, and L. E. Cross, "High-frequency Strain Response in Ferroelectrics and Its Measurement Using a Modified Mach-Zehnder Interferometer," J. Appl. Phys.Vol. 65, 2807-2815, 1989.

25. Q. M. Zhang, W. Cao, J. Zhao, and L. E. Cross, "Piezoelectric performance of piezoceramic-polymer composites with 2-2 connectivity: A combined theoretical and experimental study," IEEE Trans. UFFC Vol. 41, pp. 556-562, 1994.
26. T. Kojima, "A New Method for Estimating the System-Independent Characteristics of an Ultrasonic Piezoelectric Transducer," 1981 IEEE Ultra Symp. pp. 649-654, 1981.
27. Xuecang and Q. M. Zhang, IEEE Trans. UFFC (1997).
28. Q. M. Zhang and Xuecang Geng, J. Appl. Phys. 80, 5503 (1996).
29. Q. M. Zhang and Xuecang Geng, submitted to J. Appl. Phys. (1996).
30. K. Y. Hashimoto and M. Yamaguchi, Proc. 1986 IEEE Ultrasonics Symp. (Williamsburg, VA), 697 (1986).
31. L. M. Berkhovskikh, "Waves in Layered Media" (Academic Press, New York 1980).
32. Donald E. Hall, "Basic Acoustics" (Happer & Row, Publishers, NY 1987).
33. G. F. Miller and H. Pursey, Proc. Royal Soc. of London **223**, 521 (1954).
34. C. S. Desilets, Ph. D. Thesis, Stanford University (1978).
35. A. H. Nayfeh, R. L. Crane, and W. C. Hoppe, J. Appl. Phys. **55**, 685 (1984).
36. G. S. Kino, "Acoustic Waves: Devices, Imaging, & Analog Signal Processing" (Prentice-Hall, Inc. Englewood Cliffs, New Jersey 1987).
37. D. A. Berlincourt, D. R. Curran, and H. Jaffe, in "Physical Acoustics" Vol. I, part A, ed. W. P. Mason (Academic Press, NY 1964).
38. D. Leedom, R. Krimholtz, and G. Matthaei, IEEE Trans. on Sonics and Ultrasonics, SU-18, 128 (1971).
39. Wenwu Cao, Q. M. Zhang, J. Zhao, and L. E. Cross, IEEE Trans. UFFC 42, 37 (1995).